Sediment Accumulation and Diagenesis in the Late Quaternary Equatorial Atlantic Ocean: An Environmental Magnetic and Geochemical Perspective

Dissertation

zur Erlangung des

Doktorgrades der Naturwissenschaften

am Fachbereich Geowissenschaften

der Universität Bremen

vorgelegt von

Jens A. Funk

Bremen 2004

Tag des Kolloquiums:
02. Juli 2004

Gutachter:
Prof. Dr. Ulrich Bleil
PD. Dr. Matthias Zabel

Prüfer:
Prof. Dr. K.-U. Hinrichs
Dr. S. Kasten

Auch hier wird die Natur in neuer Herrlichkeit sichtbar,
und nur der gedankenlose Mensch
wirft die unleserlichen, wunderlich gemischten Worte mit Verachtung weg.

Dankbar legt der Priester diese neue, erhabene Meßkunst auf den Altar
zu der magnetischen Nadel, die sich nie verirrt,
und zahllose Schiffe auf dem pfadlosen Ozean
zu bewohnten Küsten und den Häfen des Vaterlandes zurückführte.

Außer dem Denker giebt es aber noch andre Freunde des Wissens,
die dem Hervorbringen durch Denken nicht vorzüglich zugethan,
und also ohne Beruf zu dieser Kunst, lieber Schüler der Natur werden,
ihre Freude im Lernen, nicht im Lehren,
im Erfahren, nicht im Machen,
im Empfangen, nicht im Geben finden.

Einige sind geschäftig und nehmen im Vertrauen auf die Allgegenwart
und die innige Verwandtschaft der Natur,
mithin auch im voraus von der Unvollständigkeit
und der Continuität alles Einzelnen überzeugt,
irgendeine Erscheinung mit Sorgfalt auf,
und halten den in tausend Gestalten sich verwandelnden Geist derselben
mit stetem Blicke fest,
und gehn dann an diesem Faden durch alle Schlupfwinkel
der geheimen Werkstätte,
um eine vollständige Verzeichnung dieser labyrinthischen Gänge
entwerfen zu können.

Sind sie mit dieser mühseligen Arbeit fertig,
so ist auch unvermerkt ein höherer Geist über sie gekommen,
und es wird ihnen dann leicht, über die vorliegende Karte zu reden
und jedem Suchenden seinen Weg vorzuschreiben.

Unermeßlicher Nutzen segnet ihre mühsame Arbeit,
und der Grundriß ihrer Karte wird auf eine überraschende Weise
mit dem Systeme des Denkers übereinstimmen,
und sie werden diesem zum Trost gleichsam den lebendigen Beweis
seiner abstrakten Sätze unwillkürlich geführt haben.

From VON HARDENBERG F (Novalis), 1798–1799, *Die Lehrlinge zu Sais,* 28. Absatz

Zusammenfassung

In der vorliegenden Arbeit wurden 25 spätquartäre Sedimentabfolgen aus dem zentralen äquatorialen Atlantik gesteinsmagnetisch, geochemisch und stratigrafisch analysiert. Die Untersuchungen erfolgten im Rahmen des Sonderforschungsbereiches 261 „Der Südatlantik im Spätquartär: Rekonstruktion von Stoffflüssen und Stromsystemen“ der Deutschen Forschungsgesellschaft, und dienten dazu primäre und diagenetische Signalanteile voneinander zu unterschieden. Mittels gesteinsmagnetischer Parameter und der Konzentrationsprofile von Karbonat und Eisen, wurden die Sedimente korreliert und datiert. In glazialen Horizonten, insbesondere in den Sauerstoffisotopenstadien 6, 10 und 12, waren erhöhte Konzentrationen an organischem Material, in Verbindung mit einer Vergröberung und partiellen Lösung von Magnetit, zu beobachten. Anreicherungen von nicht-magnetischen und magnetischen Eisenmineralen wurden sowohl an, als auch unterhalb von fossilen und aktiven Fe^{2+}/Fe^{3+} Redox Grenzen gefunden. Mit neu entwickelten, sehr sensitiven Proxies wurde Magnetit Lösung (Fe/κ, χ_{nf}/χ_{tot}) and Neubildung (Fe/κ) quantifiziert und Änderungen in den Redox Bedingungen der Vergangenheit nachgewiesen. Der Vergleich dieser Daten mit den Variationen der Konzentration organischen Kohlenstoffs zeigte, dass gesteinsmagnetische Datensätze, Kohlenstoff- und Karbonatprofile in großen Teilen des äquatorialen Atlantik Erhaltungssignale repräsentieren. Suboxische, reduktive Lösung von Magnetit erwies sich als Indikator für postsedimentäre Oxidation von organischem Kohlenstoff. Die Tiefenlage der aktiven Eisen Redox Grenze korreliert mit dem letzten überlieferten Produktivitätspuls (Stadium 2 bzw. 6) und nicht mit dem rezenten Eintrag organischen Materials. Zwei Kernprofile, die sich jeweils in N-S und in W-E Richtung entlang des Mittelatlantischen Rückens erstrecken, markieren Gebiete und Quellen mit erhöhten kontinentalen und marinen Partikelflüssen. Die Ergebnisse dieser Arbeit werden detailliert in vier publizierten Manuskripten diskutiert.

Contents

Chapter 1

General Introduction to

Sediment Accumulation and Diagenesis in the Late Quaternary Equatorial Atlantic Ocean: An Environmental Magnetic and Geochemical Perspective

Jens A. Funk

Universität Bremen, Fachbereich Geowissenschaften, Postfach 33 04 40, D-28334 Bremen, Germany
(e-mail): funk@uni-bremen.de

Abstract: This thesis investigates 25 Late Quaternary sediment records from the central Equatorial Atlantic by rock magnetic, geochemical and stratigraphical methods. The work was performed in the framework of the Collaborative Research Center 261 'The South Atlantic in the Late Quaternary: Reconstruction of Material Budgets and Current Systems' funded by the Deutsche Forschungsgemeinschaft. The main objective was to analyze and distinguish terrigenous and diagenetic proxy signatures, in particular of rock magnetic parameters. All cores were correlated and dated on basis of their carbonate, iron and rock magnetic records. Magnetite coarsening and partial depletion was observed in glacial organic-rich layers, most intensely during oxygen isotope stages 6, 10 and 12. Non-magnetic and magnetic iron mineral enrichments were found below and at former and active Fe^{2+}/Fe^{3+} redox boundaries. Various new proxies quantifying magnetite reduction (Fe/κ, χ_{nf}/χ_{tot}) and authigenesis (Fe/κ) were established and found to be highly sensitive indicators of past redox conditions. Comparing these signals with the organic carbon records, it was shown, that rock magnetic, carbon and carbonate records in most parts of the Equatorial Atlantic are merely preservation signals. Suboxic reductive magnetite loss can be used to identify burn-down of organic carbon. The depth of the active iron redox boundary correlates with the last preserved productivity pulse (stages 2 or 6) and not with modern productivity. Two composite core profiles span the full WE and NS extension of the Equatorial Atlantic and mark zones and sources of enhanced continental and marine particle fluxes. These and more conclusions of this thesis are discussed in detail within the enclosed four published manuscripts.

1. General Introduction

In paleoceanography marine sediments are traditionally used to reconstruct the history of earth's climate. Variations of data records retrieved from measurements performed on the solid phase of the sediments are used as proxy parameters. They stand in for changes in oceanic and atmospheric circulation, primary productivity or orbitally induced variations in solar insolation. Yet, detritus as deposited on the seafloor ought not to be considered as a homogenous inert mass, because it is subject to various types of alterations. Under certain conditions particles may undergo substantial modification, already at the time of deposition and initial burial. The resulting changes in the fabric and in the element composition alter or even destroy the primary signal. The processes by which the original material is altered are expressed by the idea of '*diagenesis'*. However, there are numerous definitions of this term.

In general, it is used for all the physical and chemical processes that affect sediments from the time they are initially deposited to when they show identifiable signs of the very earliest stages of tectonic metamorphism (anchimetamorphism). In

the course of time, the view of such processes became more differentiate.

For example Dapples (1962) identified three main stages of diagenesis. The first one he called redoxomorphic, after the most outstanding representative of reactions, oxidation and reduction, particularly evident during the stage of early burial, as transitions occur from loose sediment to a lithified aggregate. Accordingly, the redoxomorphic stage is associated with compaction and dewatering in zones that may be either oxidizing or reducing. Chamley (1989) distinguished between diagenetic (= post-sedimentary) and syngenetic (= syn-sedimentary, hydrogenous) effects. Accordingly, the diagenetic history of marine sediments is conventionally considered as starting after the deposit is buried and definitively removed from the influence of the open ocean. In contrast, syngenetic processes are characterized by free exchanges between solid and liquid environments like sediment-water interfaces, sediments reworked by bioturbation and highly porous sediments.

An important cause of early diagenesis is the decomposition of organic matter related with '*redox*' reactions, which are the more intensive the more organic carbon is present. The deposition and burial of organic detritus in deep-sea sediments are controlled by high rates of organic matter production in the surface waters, high sedimentation rates and/or restricted deep-water circulation which leads to oxygen-poor conditions in the bottom waters.

In their important paper, which has influenced subsequent work on this theme, Froelich et al. (1979) considered the effects of organic matter diagenesis on the redox equilibrium of pelagic sediments. They showed that the remineralization of the buried non-oxidized organic matter is performed by microorganisms. After the utilization of the entire dissolved oxygen from the pore water the bacteria resume to take benefit from secondary oxidants. In descending order of free energy gain these secondary oxidants form a sequential series of terminal electron acceptors. Nitrate and phosphate are involved first, followed by manganese - and iron oxides and sulfate, until the stages of fermentation and methanogenesis are finally completed. Their study was carried out in the eastern Equatorial Atlantic, where organic carbon accumulation is sufficiently rapid to allow suboxic and anoxic reactions to be active at shallow subsurface depth in the sediments. Also Berner (1981) classified different early diagenetic environments in marine sediments and separated the different terminal electron acceptor processes into distinct zones. However, according to many studies this concept of redox zonations is of model character and a simplified representation of the true nature. According to Kasten et al. (2004) some of these reactions can occur simultaneously or the zones can even be reversed. Figure 1 displays different stages and zones of early diagenesis and some processes involved.

Concerning the extend of early diagenesis particularly of detrital iron oxides and magnetic minerals, the magnetic properties of the sediment are already significantly affected in case of suboxic conditions (Bloemendal et al. 1992). Fe^{3+} -ions, dissociated from ferrimagnetic iron oxides are not stable under the Eh/pH conditions of the pore waters below the redox boundary and are therefore reduced to ferrous (Fe^{2+}) ions. They diffuse upwards along a concentrational gradient subsequent they are entraped in the sediment column under oxic conditions.

Many detrital magnetic grains are likely to be lost during prolonged diagenesis, whereas new magnetic material can be formed in oxic conditions. Canfield and Berner (1987) demonstrated that due to suboxic diagenesis detritic magnetite grains were affected by reductive dissolution being partly transformed into pyrite (Fig.1.e.). While fine (single-domain) magnetite grains were completely dissolved, coarser (multi-domain) magnetite grains were coated by a crust of pyrite, thus protecting the inner core of pristine magnetite from progressive dissolution. According to Farina et al. (1990) and Mann et al. (1990) dissolved Fe(II) may react with H_2S to form authigenic iron sulphide phases like pyrrhotite and greigite which are stable under reducing conditions (Fig.1.e.).

The active iron redox boundary can be macroscopically identified by a color transition, a characteristic feature of marine sediments (Fig.1, marked by a horizontal, dashed line). This change in color marks the boundary between oxidizing (brown colors) and reducing (grey/green colors) redox

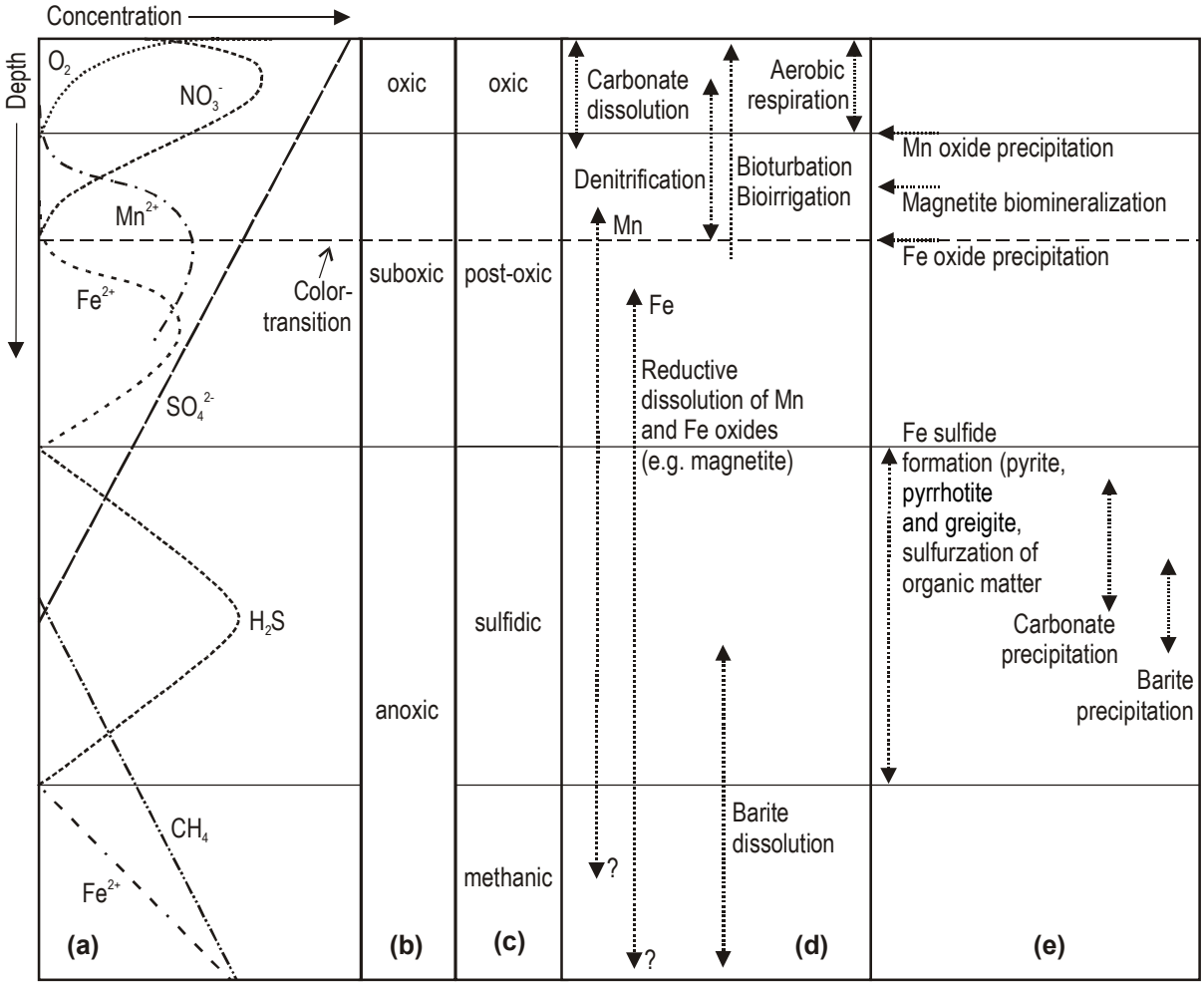

Fig.1. Hypothetical trends in pore water profiles **(a)** predicted by the successive utilization of inorganic compounds as terminal electron acceptors in the decomposition of sedimentary organic matter. The concentration and depth axes are arbitrary. The next two columns display different classifications of redox zonation in marine sediments as given by Froelich et al. (1979) **(b)** and Berner (1981) **(c).** Some processes of early diagenesis which can bias or overprint the primary signal are delineated for dissolution **(d)** and authigenesis **(e)**. Modified from Kasten et al. (2004).

condiltions and represents particularly the position of the in-situ reduction of Fe (III) to Fe (II) in smectites (Lytle 1983, König et al. 1997). The depth of the iron redox boundary is attributed to the supply of organic matter (Lyle 1983, Müller et al. 1988, Tarduno and Wilkison 1996). Hence the higher the C_{org} flux into the sediment, the narrower the depth interval of the above men-tionedl redox zonation is confined and the shallower the iron redox boundary is seated under the sediment surface. A decrease in organic carbon burial will result in an extension of redox zones and a shift of the redox boundary to deeper layers.

Equatorial Atlantic sediments are characterized by cyclic depositional conditions during the Late Quaternary, which bring along intermittent changes of primary productivity within surface waters, organic carbon burial, sedimentation rate, oxygen content of bottom water and redeposition of sediments. The glacial sequences within the sedimentary record contain higher amounts of preserved organic carbon in contrast to interglacial horizons.

The relative abrupt changes disturb the prevailing steady-state depositional conditions where redox zones and redox boundaries remain at relative constant sediment depths. At other locations this has been extensively investigated around sapropels in the sedimentary record of the eastern Mediterranean (Higgs et al. 1994; Thomson et al. 1995; van Santvoort et al. 1996; Passier et al. 1998) and turbiditic sequences from the Maderia Abyssal Plain (Colley et al. 1984; Wilson et al. 1985; Robinson et al. 2000). Consequently, nonsteady-state diagenesis may lead to distinct authigenic enrichments of redox-sensitive elements and redox boundaries fixed at sediment intervals with enhanced C_{org} concentrations. In the Late Quaternary Equatorial Atlantic sedimentary record the strongest early diagenetic overprint of the pristine sediment constituents are detected along transitional sediment intervals like terminations and within glacial sequences.

1.1 Development and Conceptual Formulation of this Study

In a previous study which gave rise to this thesis Late Quarternary marine sediment sequences from the mid ocean ridge of the central Equatorial Atlantic ocean were investigated in order to differentiate and quantify the terrigenous and marine fractions of the total organic matter (Funk 1997). Detritus which may originate from the Saharan dust plume (Sarnthein et al. 1981) has been clearly identified using maceral analysis and fluorescence microscopy. The sediment has proved to have already undergone processes of early diagenesis when authigenic framboidal pyrite has been found in these intervals. The magnetic fraction of the sediments which is also considered to be of terrigenous origin (Bloemendal et al. 1988) has been analysed, since the climatically controlled variations in magnetic mineral concentration and composition often parallel sedimentological and geochemical parameters (Frederichs et al. 1999). However, a direct correlation between the concentrations of organic matter and magnetic minerals could not be observed. The calcium carbonate content and the variations in stable oxygen isotopes ($\delta\,^{18}O$), two proxyparameters for climate changes in paleoceanography, showed only partial agreements with rock magnetic parameters. Obviously the primary signal has been superimposed by a secondary process. This effect was especially interesting, since the primary signal

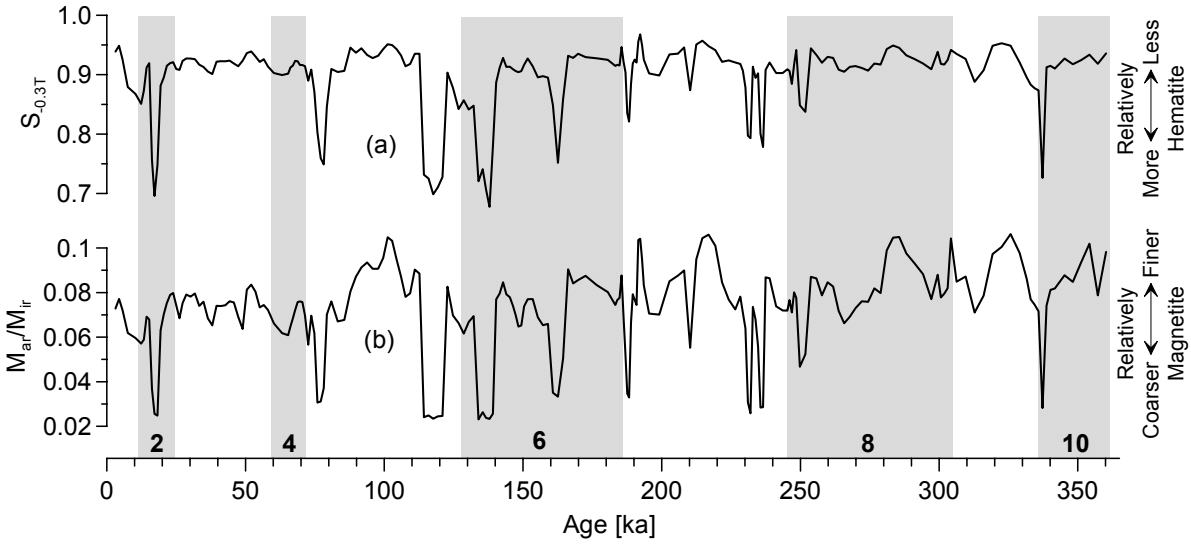

Fig.2. Rock magnetic profiles of gravity core GeoB 2908-7. Background shading indicates glacial periods (marine oxygen isotope stages 2 to 10). **(a)** Hematite/goethite index $S_{-0.3T}$, **(b)** magnetite grain-size index M_{ar}/M_{ir}. Repeatedly disturbance of the pristine signal is clearly documented by the distinct coarsening of magnetite grain-sizes and maxima of relative hematite/goethite contents.

of the unaltered sections could be clearly differentiated from the distorted sequences (Fig2.).

The results of these investigations lead to the present study as part of the Collaborative Research Center 261. The main objective of this thesis is to evaluate the significance of early diagenesis with respect to the interpretation of rock magnetic sedimentary properties. It has long been recognized that dissolution, alteration and authigenesis ought to be considered when extracting primary climate signals from the sedimentary record. However, the high potential use of quantifying early diagenesis of iron minerals and of distinguishing between variations in primary input and post-depositional overprint in interdisciplinary research has not been very popular and should be further emphasized.

1.2 Materials and Methods

In order to gain insights, whether the special character of the post-sedimentary alterations are locally restricted, analyses of 25 gravity cores from the Equatorial Atlantic have been carried out. These cores have been retrieved during several SFB 261 cruises along W-E transects which extend perpendicular to the Mid Atlantic Ridge (Fig.3.).

First of all, magnetic volume susceptibility was measured using an automated, computer controlled measuring bench (Fig.3.a, page 21) on a high resolution scale, sampling every cm. The comparison and correlation of these datasets allow a reliable evaluation of the core material and provide a solid framework for further investigations. Redeposited

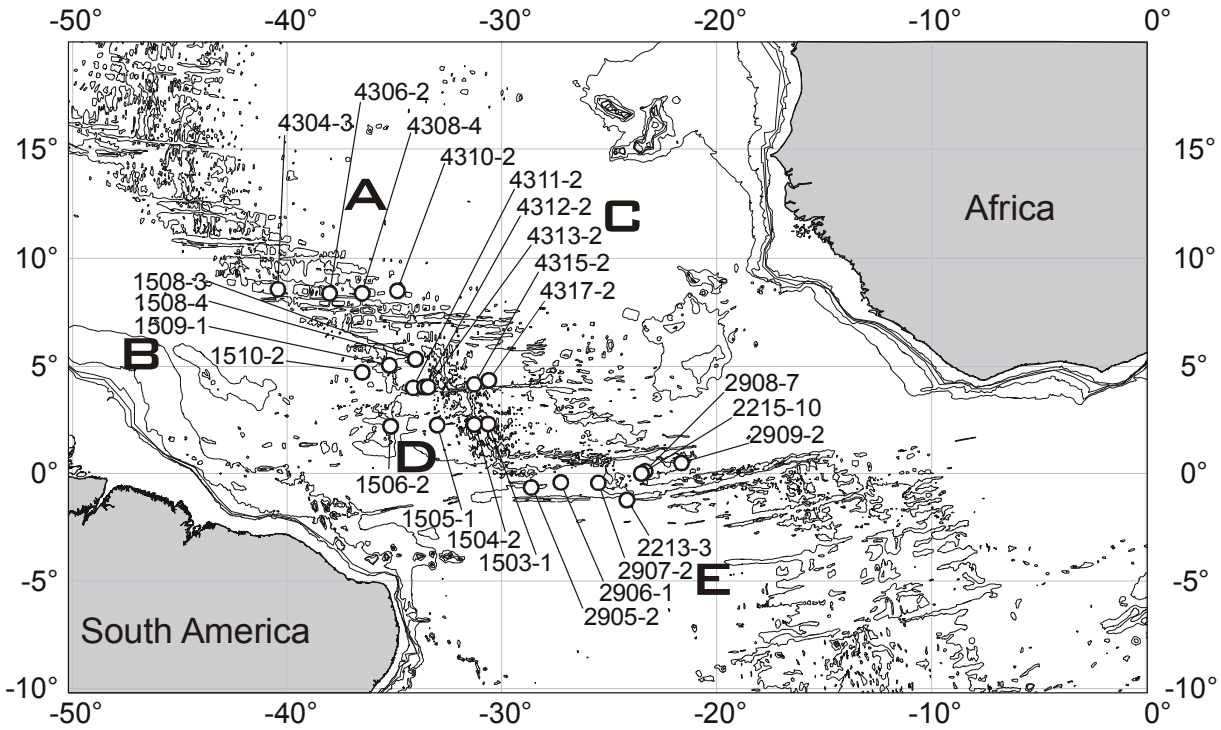

Fig. 3. Study area in the Equatorial Atlantic with sites of 'GeoB'-gravity cores used for magnetic susceptibility (κ) measurements. The cores were retrieved along W-E transects **(A-E)** across the Mid Atlantic Ridge. The susceptibility records are displayed in the following figures. A detailed list of the cores which were used for further investigations is given in the first manuscript (Tab.1, page 43).

sediment, macroscopically not identifiable as turbiditic sequences, as well as coring-induced losses could clearly be detected. The Mid Atlantic Ridge, in particular, rarely exhibits complete stratigraphic sediment series due to its rough topography. However, undisturbed and continous records are preferred for detailed studies. A general view of all magnetic susceptibility profiles derived from this campain is displayed in Figures 4, 5 and 6.

Based on the above mentioned data sets, selected sediment cores have been used for further rock magnetic analyses. These measurements have been performed with a modern cryogenic magnetometer at a 5cm resolution. The deployment of a recently developed autosample robot by technicians of the Marine Geophysics section, Bremen, allowed the essential measuring routines to be carried out during a reasonable period of time. Getting a vast number of data sets new insights on the regional distribution of the studied phenomena could be achieved. Rock magnetic parameters like the M_{ar}/M_{ir} ratio or the so called $S_{-0.3}$-parameter corroborated the first results and even better identified sedimentary alterations than the magnetic susceptibility. Their application is explained in detail in the first manuscript. Likewise, parameters deduced from hysteresis and backfield measurements, which have been performed on two selected cores (GeoB 4317-2 and GeoB 2908-7) using an alternating gradient field magnetometer, clearly indicated the post-depositonal alterations.

In order to obtain information on the geochemical aspects of the observed phenomena, the same sediment sequences have been analysed using an x-ray fluorescence core-scanner (Fig.3.b, page 21). This device allows high-resolution, non-destructive measurements of relative element concentrations like calcium, iron, manganese and titan. By correlating the calcium profiles with $CaCO_3$ records of adjacent already dated sediment cores the required age models have been established. Since both measuring benches, the one for determining the magnetic susceptibility and the XRF core scanner are driven by stepping motors, an exact positioning of the core segments is guaranteed. Consequently, the resulting datasets of both methods can excellently be compared with each other. This multidisciplinary approach (e.g. combining the iron concentration with the magnetic susceptibility) yields new proxy parameters which identify certain early diagenetic processes.

In a further step selected intervals from cores GeoB 4317-2 and GeoB 2908-7 have been analyzed with a standard x-ray fluorescense spectrometer. For this conventional method the time-consuming preparation of powder tablets is required which comprises a multitude of single steps. Due to its complexity it has not been described in great detail in the following manuscripts. However, the workflow is displayed here in a flowchart (Fig.7.). The results have been used for a first overview of the geochemical processes involved and for calibration purposes, since the XRF-core scanner did not provide quantitative results such as weight percent but qualitative element concentrations in ‘counts per seconds’. Apart from that a broader spectrum of elements is identified by the conventional method.

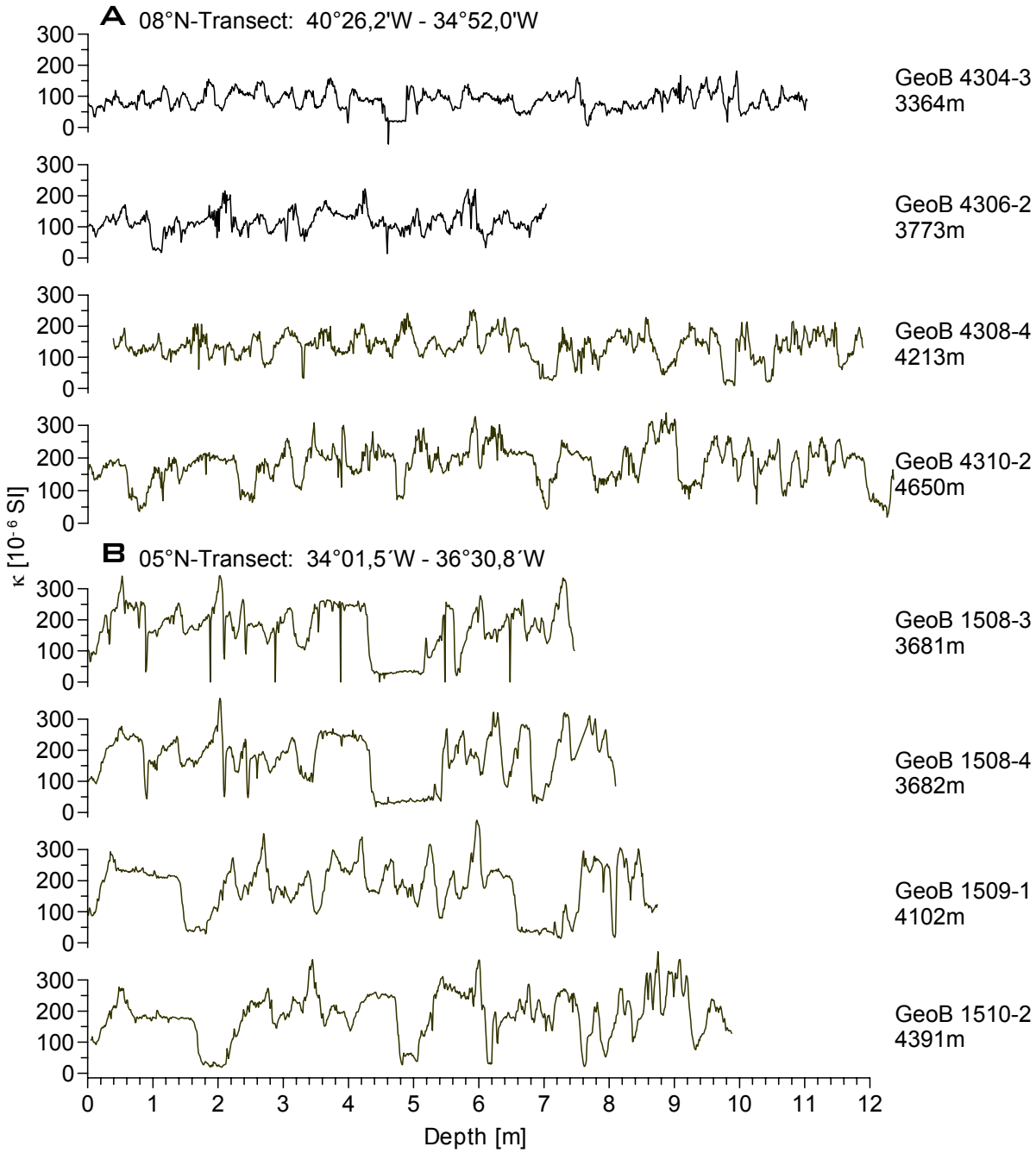

Fig. 4. Magnetic susceptibility (κ) records of the northernmost transect at about 8°N **(A)** and along 5°N **(B)**. Disturbances by redeposited sediments identified by plateau shaped signal sequences and distinct sharp minima. None of these cores were used for further investigations.

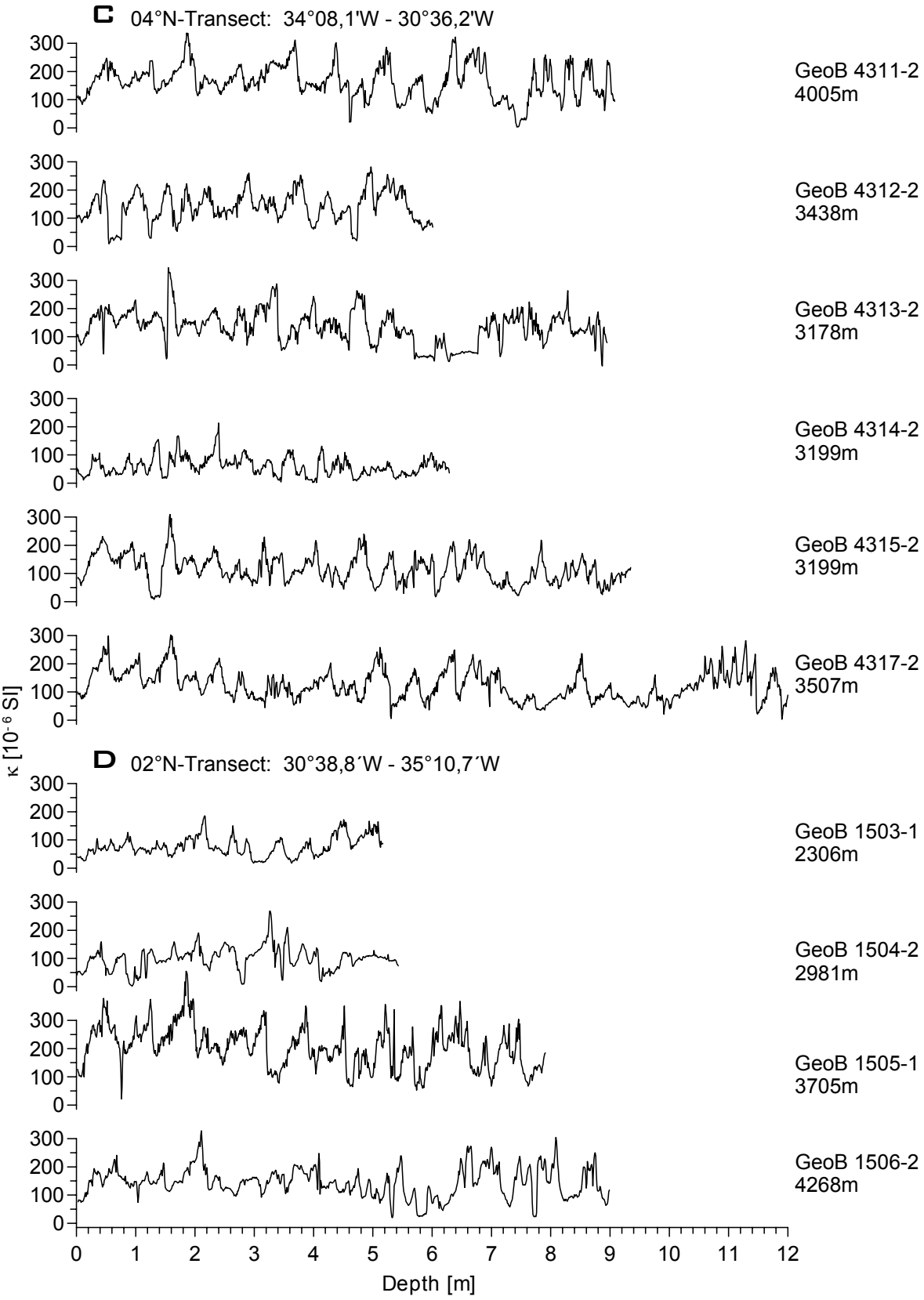
C 04°N-Transect: 34°08,1'W - 30°36,2'W
GeoB 4311-2
4005m
GeoB 4312-2
3438m
GeoB 4313-2
3178m
GeoB 4314-2
3199m
GeoB 4315-2
3199m
GeoB 4317-2
3507m
D 02°N-Transect: 30°38,8´W - 35°10,7´W
GeoB 1503-1
2306m
GeoB 1504-2
2981m
GeoB 1505-1
3705m
GeoB 1506-2
4268m
κ [10-6 SI]
Depth [m]

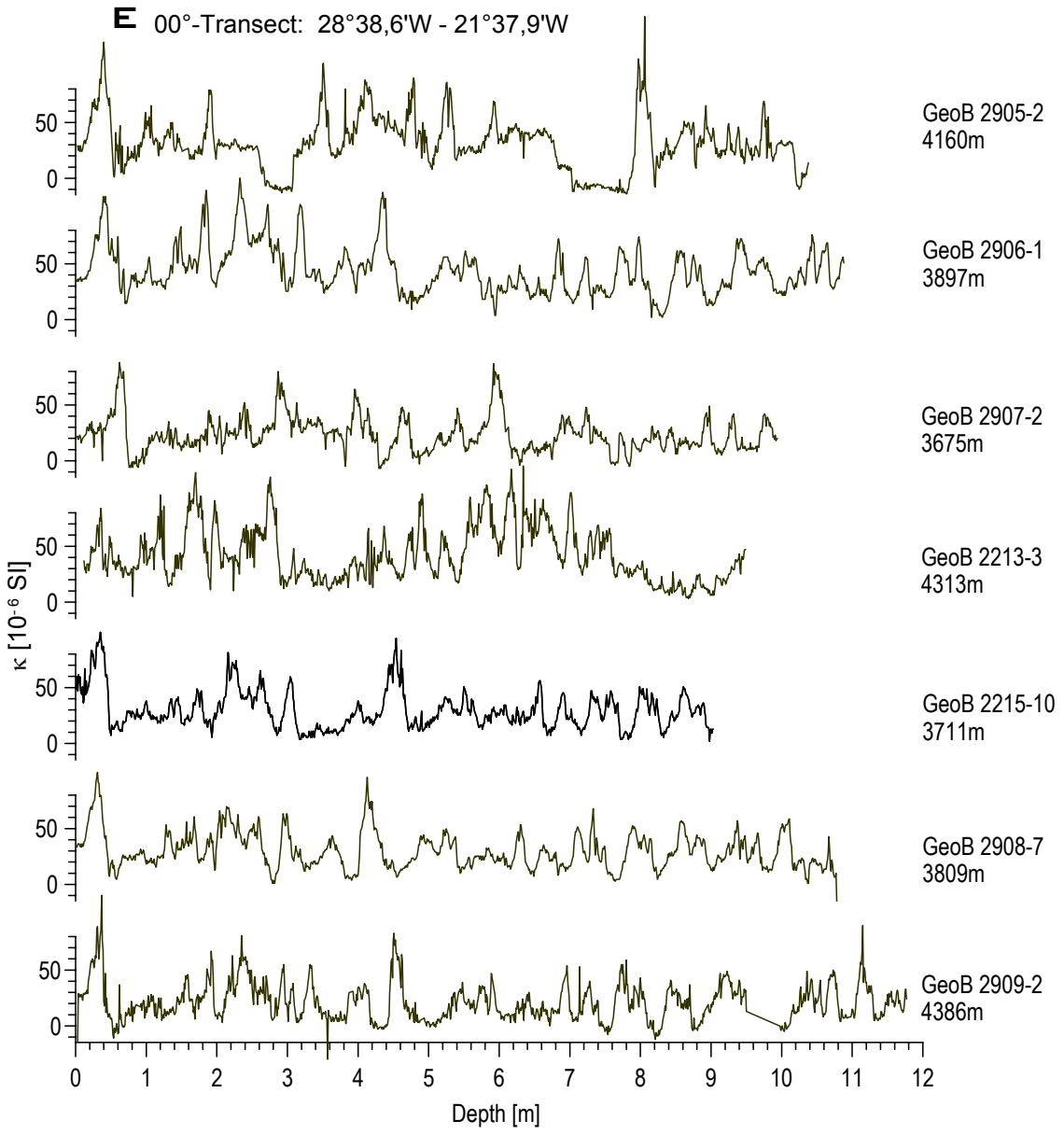

Fig.6. The cores of transect **E** exhibit much lower values in magnetic susceptibility. These decreases between the northern transects and that at 0° result primarily from higher carbonate dilution at the equatorial sites and more intense diagenesis.

Fig.5.(left). Magnetic susceptibility profiles of transects at °4 **(C)** and °2 N **(D)**. Again most of the sediment sequences are affected by turbidites and, as documented in great detail in the following manuscripts, by early diagenesis. Presumably due to shallow sampling sites GeoB 1503-1 and 1504-2 show a complete different signature in contrast to the other ones.

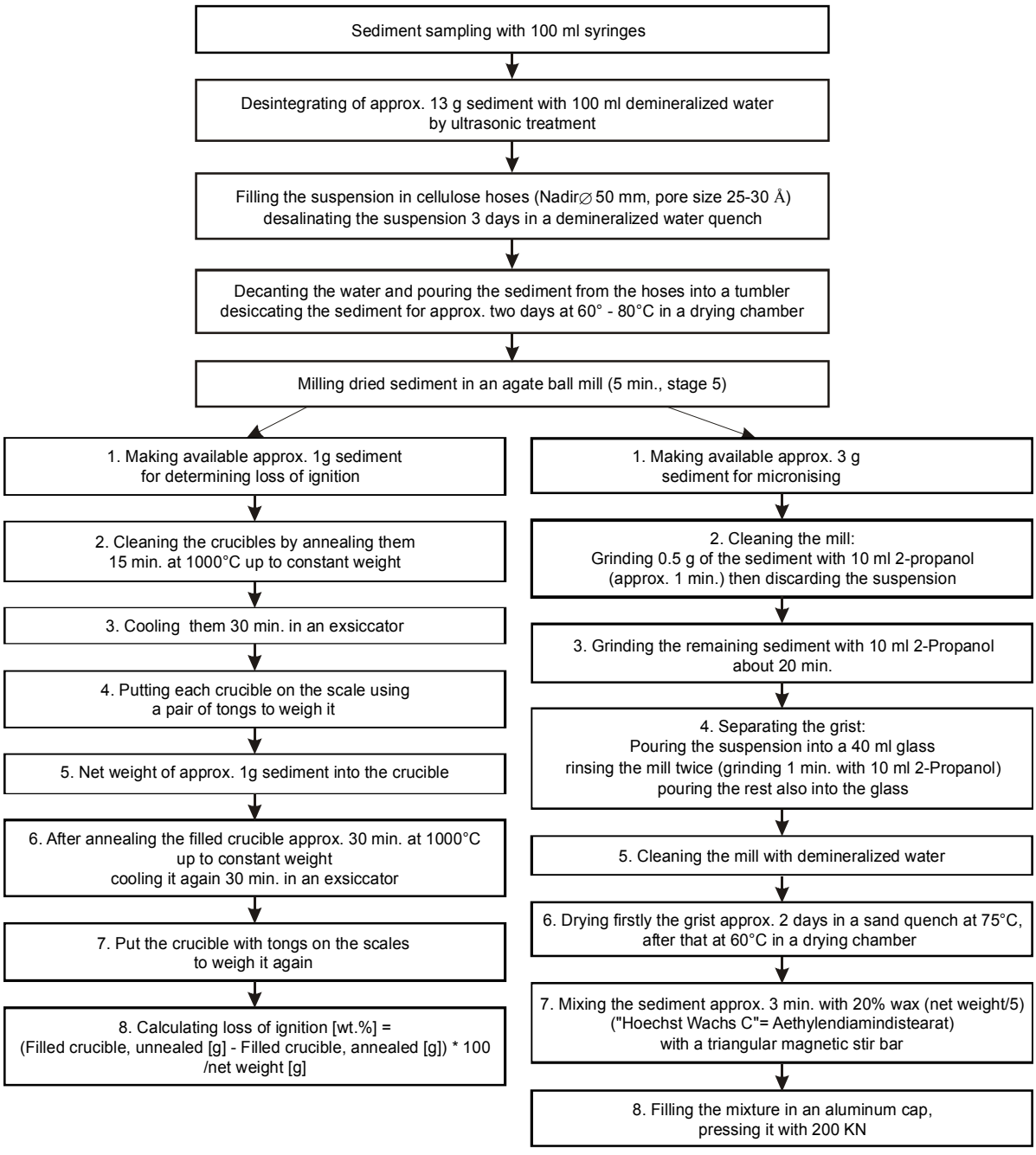

Fig.7. Workflow of the sample preparation for conventional XRF fluorescence spectroscopy. The first five steps comprise sampling and homogenization of the material. Then the flow is divided in two branches. To the left the required steps for determining the ignition loss, which corresponds to the volatile components of the sample, is described (e.g. water, CO_2, SO_2 and F). On the right side further treatment of the material to obtain powder with a grain-size < 2µm is displayed. Finally the powder is mixed with wax and then pressed into a tablet.

1.3 References

Berner RA (1981) A new classification of sedimentary environments. J Sed Petrol 51: 359-365

Bloemendal J, Lamb B, King J (1988) Paleoenvironmental implications of rock - magnetic properties of late Quaternary sediment cores from the eastern equatorial Atantic. Paleoceanography 3: 61 -87

Bloemendal J, King JW, Hall FR, Doh S-J (1992) Rock magnetism of late Neogene and Pleistocene deep-sea sediments: Relationship to sediment source, diagenetic processes, and sediment lithology. J Geophys Res 97: 4361-4375

Canfield DE, Berner RA (1987) Dissolution and pyritization of magnetite in anoxic marine sediments. Geochim Cosmochim Acta 51: 645-659

Chamley H (1989) Clay Sedimentology. Springer-Verlag New York. 623 p

Dapples EC (1962) Stages of diagenesis in the development of sandstones. Bull Geol Soc Am 73: 913-934

Colley S, Thomson J, Wilson TRS, Higgs NC (1984) Post-depositional migration of elements during diagenesis in brown clay and turbidite sequences in the North East Atlantic. Geochim Cosmochim Acta 48: 1223-1235

Farina M, Esquivel DMS, Lins de Barros, HGP (1990) Magnetic iron-sulphur crystals from a magnetotactic microorganism. Nature 343: 256-258

Frederichs T, Bleil U, Däumler K, von Dobeneck T, Schmidt A (1999) The magnetic view on the marine paleoenvironment: Parameters, techniques, and potentials of rock magnetic studies as a key to paleoclimatic and paleoceanographic changes. In: Fischer G, Wefer G (eds) Use of Proxies in Paleoceanography: Examples from the South Atlantic. Springer Berlin, pp 575-599

Froelich PN, Klinkhammer GP, Bender ML, Luedtke NA, Heath GR, Cullen D, Dauphin P, Hammond D, Hartman B, Maynard V (1979) Early oxidation of organic matter in pelagic sediments of the eastern equatorial Atlantic: Suboxic diagenesis. Geochim Cosmochim Acta 43: 1075-1090

Funk J (1997) Sedimentologische, organisch-geochemische und geophysikalische Untersuchungen am Kern 2908-7. Fachbereich Geowissenschaften, Universität Bremen (unpublished diploma thesis) 78 p

Higgs HC, Thomson J, Wilson TRS, Croudace IW (1994). Modification and complete removal of eastern Mediterranean sapropels by postdepositional oxidation. Geology 22: 423 - 426

Kasten S, Zabel M, Heuer V, Hensen C (2004) Processes and signals of nonsteady-state diagenesis in deep-sea sediments and their pore waters. In: Wefer G, Mulitza S and Ratmeyer V (eds) The South Atlantic in the Late Quaternary: Reconstruction of Material Budget and Current Systems. Springer-Verlag, pp 431-459

König I, Drodt M, Suess E, Trautwein AX (1997) Iron reduction through the tan - green color transition in deep-sea sediments. Geochim Cosmochim Acta 61: 1679-1683

Lyle M (1983) The brown-green color transition in marine sediments: A marker of the Fe(III)-Fe(II) redox boundary. Limnol Oceanogr 28: 1026-1033

Mann S, Sparks NHC, Frankel RB, Bazylinski DA, Jannasch HW (1990) Biomineralization of ferrimagnetic greigite (Fe_3S_4) and iron pyrite (FeS_2) in a magnetotactic bacterium. Nature 343: 258-261

Müller PJ, Hartmann M, Suess E (1988) The chemical environment of pelagic sediments. In: Halbach P, Friedrich G, von Stackelberg U (eds) The manganese nodule belt of the Pacific Ocean. Enke, Stuttgart, 254 p.

Passier HF, Dekkers MJ, de Lange GJ (1998) Sediment chemistry and magnetic properties in an anomalously reducing core from the eastern Mediterranean Sea. Chem Geol 152: 287-306

Robinson SG, Sahota JTS, Oldfield F (2000) Early diagenesis in North Atlantic abyssal plain sediments characterized by rock magnetic and geochemical indices. Mar Geol 163: 77-107

Sarnthein M, Tetzlaff G, Koopmann B, Wolter K, Pflaumann, U 1981. Glacial and interglacial wind regimes over the eastern subtropical Atlantic and North-West Africa. Nature 293: 193-196

Tarduno JA, Wilkison SL (1996) Non-steady state magnetic mineral reduction, chemical lock-in, and delayed remanence acquisition in pelagic sediments. Earth Planet Sci Lett 144: 315-326

Thomson J, Higgs NC, Wilson TRS, Croudace IW, de Lange GJ, van Santvoort, PJM (1995) Redistribution and geochemical behaviour of redox - sensitive elements around S 1, the most recent eastern Mediterranean sapropel. Geochim Cosmochim Acta 59: 3487-3501

van Santvoort PJM, de Lange GJ, Thomson J, Cussen H, Wilson TRS, Krom MD, Ströhle K (1996) Active post-depositional oxidation of the most recent sapropel (S1) in sediments of the eastern Mediterranean Sea. Geochim Cosmochim Acta 60: 4007-4024

Wilson TRS, Thomson J, Colley S, Hydes DJ, Higgs NC, Sorensen J (1985) Early organic diagenesis: The significance of progressive subsurface oxidation fronts in pelgic sediments. Geochim Cosmochim Acta 49: 811-822

1.4 Publications

This study includes four manuscripts:

· Two of them are published in the Book '*The South Atlantic in the Late Quaternary: Reconstruction of Material Budget and Current System'* a quasi final report, which delineates and summarizes the work of the special research collaboration 261.

· The third article has been published as a result of an international symposium on fundamental rock magnetism and environmental applications in a conference volume.

· As part of the interdisciplinary cooperation with the Geochemical Section of the Department of Geosciences, University of Bremen, Dipl.-Geol. Anja Reitz conducted high resolution geochemical and rockmagnetic measurements in the framework of her diploma-thesis, which I partly advised. The results are documented in the fourth paper.

J.A. Funk, T. von Dobeneck and A. Reitz (2004)
Integrated Rock Magnetic and Geochemical Quantification of Redoxomorphic Iron Mineral Diagenesis in Late Quaternary Sediments from the Equatorial Atlantic

In: G. Wefer, S. Mulitza and V. Ratmeyer (eds.)

The South Atlantic in the Late Quaternary: Reconstruction of Material Budget and Current Systems. Springer-Verlag Berlin Heidelberg, pp 237-260

This paper thoroughly describes the methods and parameters applied in this thesis. Particularly the interdisciplinary geochemical/magnetic approach is outlined here, mainly the half-core-logging techniques which display early diagenetic processes in high resolution records. Innovative proxy parameters are presented, which stand for magnetite depletion, precipitation and iron relocation. It is shown that these alterations of the pristine climate signal are paralleled by layers enriched in organic carbon. Deposited during times of enhanced primary productivity in the surface water these 'sapropelic layers' itself represent changes in climate and oceanic circulation. Two case studies are used to demonstrate how the degradation of the buried organic matter was accompanied by suboxic conditions and recurrence of reductive dissolution of magnetic minerals. By a statistical approach it is attempted to reconstruct the pristine signal.

J.A. Funk, T. von Dobeneck, T. Wagner and S. Kasten (2004)
Late Quaternary Sedimentation and Early Diagenesis in the Equatorial Atlantic Ocean: Patterns, Trends and Processes Deduced from Rock Magnetic and Geochemical Records

In: G. Wefer, S. Mulitza and V. Ratmeyer (eds.)

The South Atlantic in the Late Quaternary: Reconstruction of Material Budget and Current Systems. Springer-Verlag Berlin Heidelberg, pp 461-497

The article is also of multidisciplinary character with special emphasis on the post depositional alterations of the studied records. It has a wide geographical and temporal scope, covering the sedimentary history of the Late Quaternary and comprising data sets of 16 gravity cores retrieved in the equatorial Atlantic area of the Mid Atlantic Ridge. Their age models and the rock magnetic properties of the sediments are presented in order to give an overview of magnetite concentration, magnetic grain size and magnetic mineralogy. A systematic use of a combination with geochemical analyzes and color datasets enables a precise interpretation of diagenesis patterns, accumulation rates and sedimentation systems in a regional context. A synthesis of the results of a long period of research in this area is integrated.

T. von Dobeneck and J. Funk (2002)
Integrated Rock Magnetic and Geochemical Proxies for Iron Mineral Dissolution and Precipitation in Marine Sediments Based on Single Sample and New Split Core Scanning Techniques

In: Leonardo Sagnotti and Andrew P. Roberts (eds.)

Fundamental RockMagnetism and Environmental Application
Quaderni di Geofisica, No. 26, pp 183-185

This paper gives a short overview of the new rock magnetic and environmental applications. The geochemical/magnetic iron diagenesis proxies Fe/k_{nd} for magnetite dissolution, Ti/k_{nd} for magnetic mineral precipitation and Fe/Ti for iron relocation are introduced.

A. Reitz, C. Hensen, S. Kasten, J.A. Funk and G.J. deLange (in press)
A combined geochemical and rock-magnetic investigation of a redox horizon at the last glacial/ interglacial transition

Physics and Chemistry of the Earth

The main objective of this study is to investigate in detail a sediment section encompassing an active iron redox boundary. Conventional rock magnetic and geochemical methods were performed on a high-resolution scale in order to detect characteristic enrichments of redox-sensitive elements and the extend of magnetic mineral dissolution. A color change attributed to the iron redox boundary is observed in the vicinity of the last glacial/interglacial transition. Drastic changes in the depositional conditions during the last deglaciation were made responsible for a change in the redox environment of the sediment causing non-steady state diagenesis. Additionally, the development and the movement of the Fe^{2+}/Fe^{3+} - redox boundary with respect to climate change has been reconstructed.

Chapter 2

Integrated Rock Magnetic and Geochemical Quantification of Redoxomorphic Iron Mineral Diagenesis in Late Quaternary Sediments from the Equatorial Atlantic

J.A. Funk[1*], T. von Dobeneck[1,2] and A. Reitz[3]

[1]*Universität Bremen, Fachbereich Geowissenschaften, Postfach 33 04 40, D-28334 Bremen, Germany*
[2]*Paleomagnetic Laboratory 'Fort Hoofddijk', Faculty of Earth Sciences Utrecht University, Budapestlaan 17, 3584 CD Utrecht, The Netherlands*
[3]*Geochemistry Department, Faculty of Earth Sciences Utrecht University, P.O. Box 80 021, 3508 TA Utrecht, The Netherlands*

Abstract: Rock magnetic and geochemical data logged by fast, non-destructive X-ray fluorescence and susceptibility half core scanning techniques have been combined to create high-resolution records of redoxomorphic iron mineral diagenesis in suboxic marine sediments. The great potential of this approach and advantage to standard single sample methods is demonstrated on two Late Quaternary sequences from the central Equatorial Atlantic (GeoB 2908-7 and 4317-2). Reductive dissolution of ferric minerals, most prominently magnetite (Fe_3O_4) and hematite (Fe_2O_3), induced by organic carbon degradation is shown to represent a gradual, mineral- and grain-size selective process. Proportionality of Fe, Ti and magnetite concentrations in the unaltered sections lead us to define proxy parameters for magnetite depletion (Fe/κ_{nd}) below and precipitation (κ_{nd}/Ti) above the modern and numerous fossil redox boundaries, while iron relocation was detected on basis of the Fe/Ti ratio. By calibrating all three ratios internally, we reconstruct and quantify primary deposition and secondary change of both, magnetite and total Fe profiles. Fine-scaled C_{org} variations (0.1 to 0.6 %) and susceptibility losses (up to $200 \cdot 10^{-6}$ SI) show high signal resemblance and appear to be equivalent signatures of cyclic productivity pulses in the study area. Some minor suboxic events are still expressed in the rock magnetic proxy signal, but are not accompanied by residual C_{org} enrichments.

Introduction

Numerous paleoenvironmental studies on suboxic to anoxic sediments have combined rock magnetic and chemical data (e.g. Vigliotti et al. 1999) to identify mineral alterations due to *redoxomorphic diagenesis* (Dapples 1962), a "collective noun for processes of early diagenesis involving both reductive and oxidative stages" (Robinson et al. 2000). Redox reactions including dissolution, depletion, relocation and precipitation of iron occur in and around sapropels (Passier et al. 1998), turbiditic sequences (Robinson et al. 2000) and organically enriched sediments deposited under conditions of upwelling (Tarduno 1994), reduced bottom water circulation (Calvert and Pedersen 1993) or eutrophication (Snowball 1993). The cited studies were concerned with reconstructions of paleoproductivity and sediment accumulation, with alteration of primary minerals and diagenetic overprinting of paleo- and rock magnetic information (Dekkers et al. 1994), and with the establishment of cyclostratigraphic age models based on orbital rhythms (Langereis and Dekkers 1999; van Santvoort et al. 1997).

The geochemical settings for redoxomorphic diagenesis are alike in all mentioned situations: Bacterially mediated oxidation of embedded organic matter follows a declining energy yield sequence of terminal electron acceptors from interstitial

From WEFER G, MULITZA S, RATMEYER V (eds), 2004, *The South Atlantic in the Late Quaternary: Reconstruction of Material Budget and Current Systems.* Springer-Verlag Berlin Heidelberg, pp 237-260

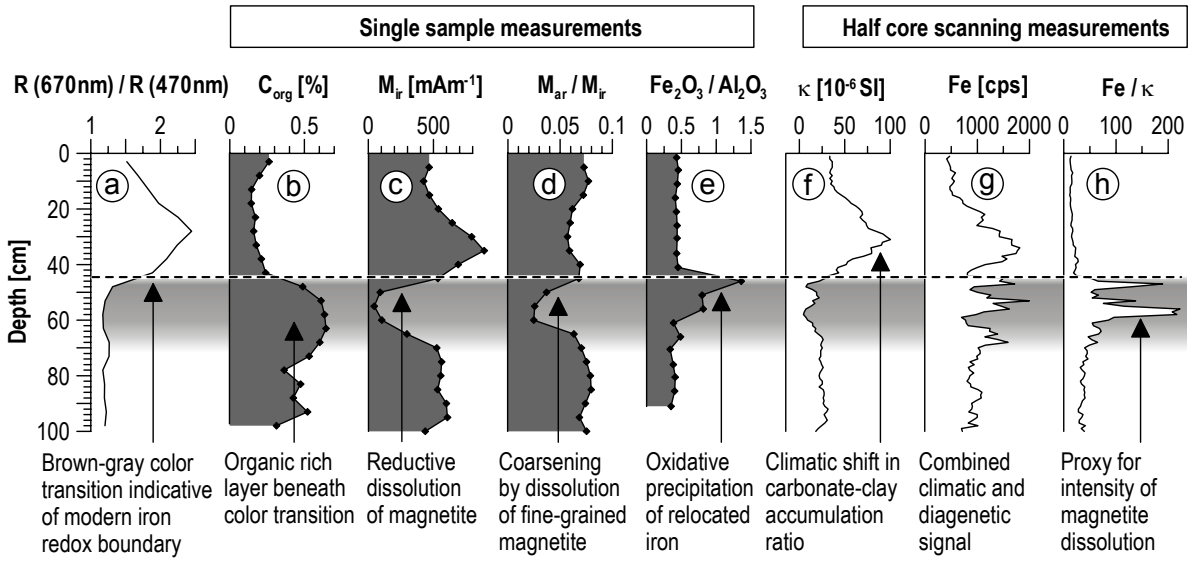

Fig. 1. Characteristic signatures of redoxomorphic iron mineral diagenesis at the active iron redox boundary (dotted line) exemplified by equatorial Atlantic gravity core GeoB 2908-7. Gray curve fillings represent single sample, white fillings half core scanning measurements. The horizontal band symbolizes the magnetite dissolution layer. Curves represent **(a)** ratio of red and blue reflectance, **(b)** organic carbon content, **(c)** isothermal remanent magnetization, **(d)** magnetogranulometric ratio, **(e)** iron/aluminum ratio, **(f)** magnetic susceptibility, **(g)** iron content, **(h)** iron/susceptibility ratio.

oxygen and nitrate to Mn (IV) oxides, Fe (III) oxides, and sulfate (Froelich et al. 1979). At the stage of iron reduction this degradation leads to gradual dissolution of magnetic primary ferric iron minerals such as magnetite, maghemite and hematite. This process is illustrated (Fig. 1) by exemplary rock magnetic and geochemical data of an active iron redox boundary located at about 45 cm depth (Fig. 1a) in an Equatorial Atlantic sediment core. Characteristic features of organically enriched layers (Fig. 1b) are local minima in magnetic mineral concentration (Fig. 1c) and a relative decrease of the finer vs. coarser magnetite fractions (Fig. 1d) and of ferrimagnetic vs. antiferromagnetic oxides, which is due to grain size and mineral selectivity of reductive mineral dissolution. The resulting ferrous iron anoxically precipitates in situ as paramagnetic phase or diffuses upwards to the active iron redox boundary to form authigenic, generally paramagnetic Fe^{3+} oxihydroxides as well as biogenic magnetite (Smirnov and Tarduno 2000). Relocation of iron (Fig. 1e) is shown by the element ratio of (mobile) iron and (stable) aluminum (Thomson et al. 1999).

The most easily measurable and universal, hence widely used magnetic parameter susceptibility κ (Fig. 1f) cumulates all iron mineral concentrations with pronounced emphasis on ferrimagnetic species. Two sharp signal minima of susceptibility deviating from the general trend of other climate proxy signals, e.g. $\delta^{18}O$, are indicative, but not specific of diagenesis effects. This is unfortunate as core scanning techniques generate high resolution susceptibility logs at rates of about 100 data points per hour.

At half that speed runs a new logging device capable of measuring iron concentrations, the X-ray fluorescence (XRF) core scanner (Jansen et al. 1998). This fully automatic instrument developed and built at the Netherlands Institute for Sea Research (NIOZ, Texel) is also available at the Department of Geosciences, University of Bremen. For most of the exemplary sediment section Fe counts (Fig. 1g) mimic respective susceptibility signals as both parameters largely delineate terrigenous content. However, as XRF data are largely unbiased by mineralogy, they do not follow susceptibility variations due to alterations converting strongly magnetic into weakly magnetic iron species. The Fe/κ ratio of both logs (Fig. 1h) therefore highlights exactly those intervals, where such shifts

occur. The double spikes correspond primarily to the two susceptibility minima of Fig. 1f, but partly also to a Fe precipitation layer at the Fe^{2+}/Fe^{3+} redox zone (Fig. 1g). Both are not resolved in the single sample measurements of Figs. 1b-d, which are followed by the broader underlying peak in Fig. 1h. We are not aware of any preceding examples where magnetic parameters were explicitly normalized by Fe and Ti content to define quantitative proxies for magnetic mineral diagenesis. However a good step in this direction was taken by Rosenbaum et al. (1996) by utilizing crossplots of concentrational magnetic parameters against iron and titanium content to detect diagenetic magnetite and hematite loss in limnic sediments .

By combining both scanning techniques in the above depicted way, diagenetically affected sediment sections can be detected at a hitherto unprecedented speed and precision - provided that the primary composition of the terrigenous sediment fraction remains fairly constant. It is the aim of this contribution to investigate implications and prospects of this new technique and to discuss its results in the context of established element and rock magnetic analytics.

Materials

Quaternary sediment sequences of two gravity cores recovered from marginal positions of the Equatorial Atlantic Divergence Zone (Fig. 2) provide suitable conditions to demonstrate the full potential of the new methods described here. Both show organic carbon enrichments in glacial periods and related reductive iron mineral diagenesis of various intensities and frequencies.

Gravity core GeoB 2908-7 was recovered during R/V Meteor cruise M 29/3 from 3809 m water depth in the western Equatorial Atlantic (00°06.4'N, 03°19.6'W) near the Central Equatorial Fracture Zone, gravity core GeoB 4317-2 during cruise M 38/1 (Fischer et al. 1998) from 3507 m water depth on the eastern slope of the Mid-Atlantic Ridge (04°21.3'N, 30°36.2'W). These sediments span the last 360 000 years and 500 000 years, respectively. The foraminiferal/nannofossil oozes feature continuous glacial/interglacial cycles manifested in oxygen isotopes, carbonate content and organic carbon content. The sampling sites are located within the trajectory of the boreal winter NE trade wind, represented by the Passat and Harmattan

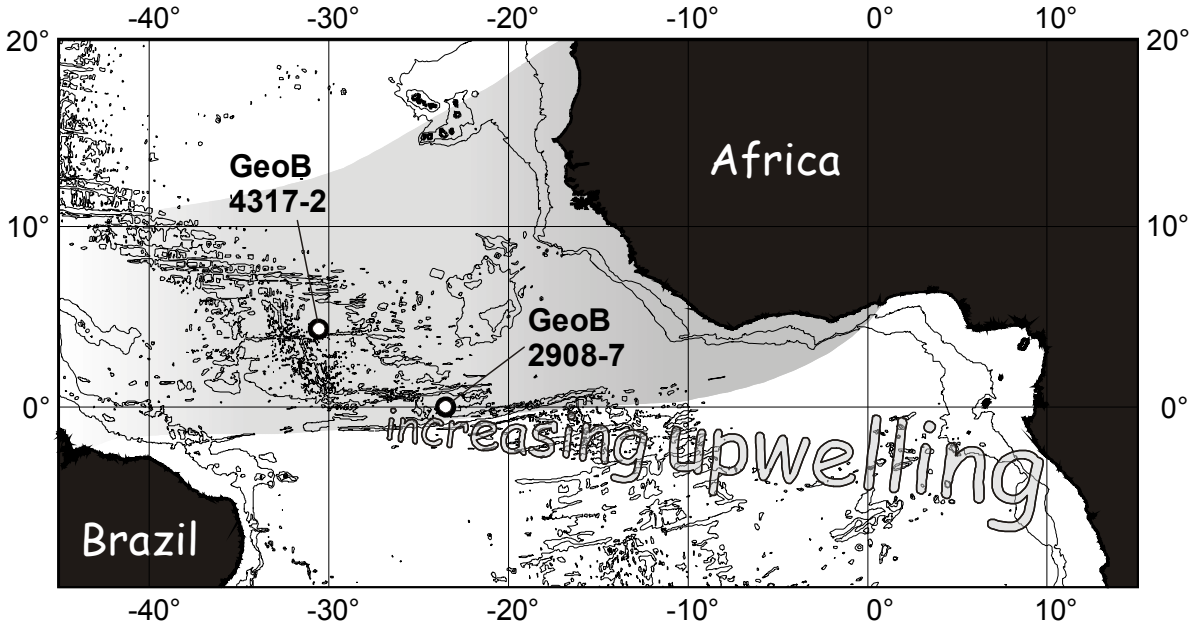

Fig. 2. Study area with sites of gravity cores GeoB 4317-2 and 2908-7. Saharan dust fall area is marked in gray. Eastwards increasing upwelling at the Equatorial Divergence enhances productivity and organic carbon accumulation.

wind systems. They receive huge amounts of terrigenous material from the Saharan dust plume (Ruddiman et al. 1989), which is the dominant source of detrital iron and magnetic minerals in the Equatorial Atlantic (Bloemendal et al. 1992). Rainout within the Intertropical Convergence Zone is the major particle removal process from the atmosphere. The surface currents in this region are equally controlled by trade winds, generating the Equatorial Divergence upwelling system, an enhanced productivity region.

Methods

Single Sample Rock Magnetic Measurements

The work halves of both cores were sampled onboard at 5 cm intervals for paleo- and rock magnetic measurements (oriented 6.2 cm^3 cube samples) and later resampled at the same positions for powder XRF element analyses.

After paleomagnetic analysis, the cube samples were investigated by standard remanence-based measurements carried out with the automated *2G* SQUID rock magnetometer of the Marine Geophysics Division at the Department of Geosciences, University of Bremen. Anhysteretic remanent magnetization (M_{ar}), a grain-size selective parameter primarily quantifying submicron magnetite (single/pseudo-single domain size) was imparted in an alternating field decaying from 250 mT with a superimposed constant field of 0.04 mT. Isothermal remanent magnetization (M_{ir}), acquired in a pulsed field of 250 mT, equally quantifies magnetite, but with considerably less influence of particle size. The M_{ar}/M_{ir} ratio (Maher 1988) is therefore a well-established magnetite grain-size index. Saturation isothermal remanent magnetization (M_{sir}) acquired in a pulsed field of 2.5 T was subsequently overprinted by a back field of – 0.3 T to evaluate the relation of low coercive (magnetite) to high coercive (hematite, goethite) mineral concentrations, the so-called S-ratio (Bloemendal et al. 1992) defined as

$$S_{-0.3T} = 0.5 \cdot (1 + M_{-0.3T} / M_{sir})$$

Kruiver and Passier recently demonstrated [2001] the presence of considerable internal variability and overlap within the coercivity distributions of both magnetite and hematite, which may modulate this parameter independent of actual relative mineral concentrations. The above given standard interpretation of $S_{-0.3\ T}$ should therefore be treated with caution when dealing with drastically changing grain sizes or mineral phases of various (lithogenic, authigenic, biogenic) origin.

The viscous loss of the initial M_{sir} in 24 hours was termed M_{vr}. 'Magnetic viscosity' is due to metastable single domain magnetite particles near the superparamagnetic (SP) threshold grain-size of approximately 20 nm (Butler and Banerjee 1975). Similarly fine SP hematite particles may act in the same sense (Banerjee 1971). The ratio M_{vr}/M_{sir} therefore quantifies the relative contribution of ferri- and antiferromagnetic particles with grain sizes near the SP/SSD threshold. Its general tendency compares to the more customary, but less sensitive frequency-dependent susceptibility $\kappa_{fd\%}$, which is commonly used to quantify the ultra-fine magnetite fraction in environmental materials (Dearing et al. 1996). Because of instrumental limitations of the used *Bartington* Susceptometer, the $\kappa_{fd\%}$, data measured on the weakly magnetic material investigated here were regarded as being to noisy to support detailed interpretation and are therfore not shown. Nevertheless, all measured $\kappa_{fd\%}$, data sets are, within their error limits, in full agreement with the M_{vr}/M_{sir} ratio used here.

Single sample susceptibility (κ) data of all samples are also not shown, as they coincide very well with scanning susceptibility data available at much higher resolution. They were, however, used to determine the carbonate free dry mass susceptibility χ_{cfdm}. This parameter is derived from single sample volume susceptibility measurements by mathematically eliminating the effects of porosity, pore water and carbonate dilution. It refers exclusively to fluctuations of magnetic mineral linked to diagenesis or terrigenous sedimentation.

For hysteresis measurements miniature samples < 50 mg have been prepared using a technique described by von Dobeneck, (1996). Measurements were carried out with a *PMC* M2900 alternating gradient force magnetometer. By processing with the HYSTEAR program (von Dobeneck 1996), we derived basic hysteresis parameters such

as the specific saturation magnetization σ_s and remanent magnetization σ_{rs}, the magnetogranulometric M_{rs}/M_s ratio by Day et al. (1977), the coercive field B_c, and the median field B_{rh} of the remanent (symmetric) hysteresis component. The equally hysteresis-based susceptibility parameter χ_{nf} quantifies contributions of paramagnetic and diamagnetic sediment matrix constituents, while χ_{tot}, the slope of the induced (antisymmetric) hysteresis component at zero field, cumulates all induced magnetizations. The mass specific ferrimagnetic susceptibility χ_{fer} is their difference:

$$\chi_{fer} = \chi_{tot} - \chi_{nf}$$

Single Sample Element Analyses

The organic carbon content was determined with a *LECO* CS-300 infrared analyzer after removal of carbonate by 6 % HCl. Analytical accuracy was checked using a standard every 10 to15 sample.

Element analyses of the first meter of core GeoB 2908-7 were performed at 1 cm resolution by Inductively Coupled Plasma Atomic Emission Spectroscopy (ICP-AES). After total digestion of 50 mg freeze-dried sediment in a mixture of 3 ml HNO_3 (65% s.p.), 2 ml HF (48% s.p.) and 2 ml HCl (30% s.p.) at 200°C and evaporating the solution, using a microwave device, the residual was homogenized with a solution of 0.5 ml HNO_3 (65% s.p.) and 4.5 ml MilliQ-water, also in the microwave. For each rank, one blank and a reference standard (MAG-1, USGS; Gladney and Roelandts 1988) have been treated like the samples. The resulting solutions were analyzed with a *Perkin-Elmer* optima 3300 RL ICP-AES system. The relative standard deviation is less than 3%.

Pressed powder tablets of selected sediment layers from both studied cores were also analyzed for absolute concentrations of major and minor elements using a wavelength dispersive *Philips* PW 1400 X-ray fluorescence spectrometer. Prior to analysis, the samples were disintegrated by ultrasonic treatment, dialyzed and washed to remove pore water, ball-milled and pressed.

These two very precise element analytics are far too laborious to be generally applied for high resolution studies of full sediment cores or core collections. They were only applied in specific sections and replaced by the much faster XRF scanning for the remaining core lengths. The comparison of absolute single sample and relatice scanning methods provides a basis for calibration and error estimate for the latter.

In this study mainly the terrigenous elements Al, Fe and Ti are of interest. To detect relocations of redox sensitive elements, dilution effects resulting from changes in biogenous accumulation must be compensated, which is commonly done by normalizing their concentrations to Al or Ti. According to Thomson et al. (1999), this procedure implies the following inherent assumptions:

Al and Ti are conservative elements which do not suffer appreciable diagenesis (Thomson et al. 1998). Carbonate and opal have insignificant contents of redox sensitive elements. Each terrigenous element under study is assumed to be deposited at a constant ratio relative to Al and Ti (same source material). Aluminum resides naturally in alumosilicates associated with the silt and clay fraction of the sediment. Thus, it is considered as a surrogate of fine-grained material (Mudroch and Azcue 1995). During continental weathering Al, Ti, Fe, and Mn are relatively immobile and are therefore considered as refractory elements (Canfield 1997).

Scanning Susceptibility Measurements

The magnetic volume susceptibility κ was determined with a custom-made, automated split-core susceptibility scanner employing a *Bartington* MS2 susceptometer with a high resolution MS2F (Ø15 mm) spot sensor (Fig. 3.a). Its lateral sensitivity is approximated by a Gaussian distribution with a half width of 12 mm. Vertically, a layer of 10 mm contributes over 90 % to the signal (Nowaczyk and Antonow 1997; Lecoanet et al. 1999). Measurements were taken at 1 cm spacing on archive halves in the sensitive mode. Instrument drift was controlled after each step by a zero measurements in air. The raw data were specified in SI units using an empirically derived calibration factor of 18.1. With a digital precision of 0.1 scale units, the numerical resolution is therefore in the order of $\pm 1 \cdot 10^{-6}$ SI.

Strictly speaking, magnetic susceptibility is not

directly proportional to ferri- or paramagnetic mineral content, because many matrix minerals (e.g. calcite, opal) and pore water have a weakly negative diamagnetic background susceptibility shifting κ to lower, sometimes negative values. This effect can create numerical artefacts in ratios using κ as denominator. An effective counter-strategy used here is to simply subtract a flat value κ_{dia} for diamagnetism from κ yielding a 'non-diamagnetic' susceptibility κ_{nd}:

$$\kappa_{\mathrm{nd}} = \kappa - \overline{\kappa}_{\mathrm{dia}} \approx \kappa + 15 \cdot 10^{-6}$$

This value is a minimum estimate based on typical values for pure calcite, opal and water (Thompson and Oldfield 1986). A more specific value for κ_{dia} could well be determined on the basis of known porosities and diamagnetic mineral contents. In that case, reliable susceptibility estimates for all matrix components (calcite, opal, silicates) would be required, but are typically not at hand for non-stoechiometric mineral phases. Circumventing these problems, the proposed flat value for κ_{dia} can simply be justified by the fairly uniform background diamagnetism inherent to every atom, which is even present in the case of a para- or ferrimagnetic component.

Scanning XRF Measurements

Relative element contents of potassium (K), calcium (Ca), titanium (Ti), manganese (Mn), iron (Fe), copper (Cu) and strontium (Sr) were determined at a depth resolution of 1 cm using a *NIOZ* XRF core scanner (Fig. 3.b). This computer controlled logging system has been developed for fast, non-destructive major element analysis on split sediment cores. The output data represent relative element concentrations, which are given in counts per second [cps]. The core halves are fixed by a pneumatic sample holder and passed at preset positions along the source and detection unit by a stepping motor. The sensor averages over an area of 1 cm^2. The response depth ranges from tenths to hundreds of a µm for the above mentioned element range. The instrument and its applications are described by Jansen et al. (1998) and Röhl and Abrams (2000). Absolute detection limits depend on measurement time, surface and lithology and are therefore not easily expressed. The limitations of this instrument are clearly demonstrated by comparative diagrams of single sample and scanning data in the following chapter.

Results

Combined Geochemical and Rock Magnetic Stratigraphy of Core GeoB 4317-2

The organic carbon content of core GeoB 4317-2 varies rhythmically between 0.08 and 0.5 wt.% with a mean of 0.20 wt.% (Fig. 4a). The changes observed are attributed to a glacial-interglacial cyclicity of productivity (Lyle 1988) with enhanced C_{org} deposition during cold periods, particularly marine oxygen isotope stages (MIS) 6, 10 and 12. According to the definition by Kidd et al. (1978), discrete layers thicker than 1 cm containing 0.5 to 2.0 wt.% of organic carbon are denoted as *sapropelic*, with over 2.0 wt.% as *sapropels*. With presently almost oligotrophic conditions and less than *sapropelic* C_{org} contents in glacial sections, the sediments were nevertheless zonally affected by suboxic diagenesis. The following data clearly demonstrate that sequences with a relatively high organic carbon content correlate with zones of marked magnetite dissolution (gray shaded horizons in Fig. 4). The magnetogranulometric ratio M_{ar}/M_{ir} (grain-size proxy of ferrimagnetic minerals, Fig. 4b) is sensitive both to variations in the primary terrigenous input and to iron oxide dissolution. Fine grained magnetite is more susceptible to dissolution than coarser grained magnetite because of its higher surface-to-volume ratio, resulting in a shift to coarser grain-size distributions (Karlin and Levi 1983). Most parts of the M_{ar}/M_{ir} signal of core GeoB 4317-2 show a cyclic change of magnetite grain-size related to climatic variations of wind intensity and/or to productivity related effects of a mild reductive diagenesis. Magnetite dissolution layers (DL) I and more clearly II and III deviate from this pattern featuring an abrupt coarsening at or slightly below the C_{org} maxima and a peak of relative fining due to reprecipitation directly above. The lower pervasiveness of magnetite reduction in DL I as compared to DL II and III may result from

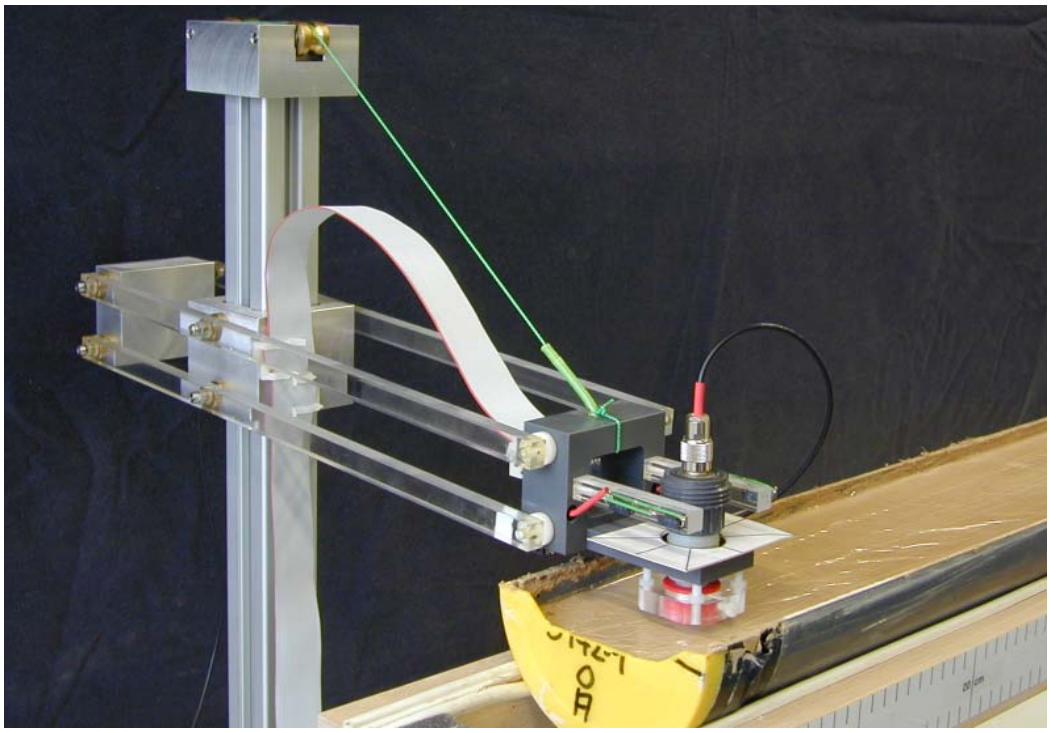

Fig. 3. a) Automated magnetic susceptibility half core logger with a self-leveling Bartington MS2F spot sensor mounted on optically controlled lever.

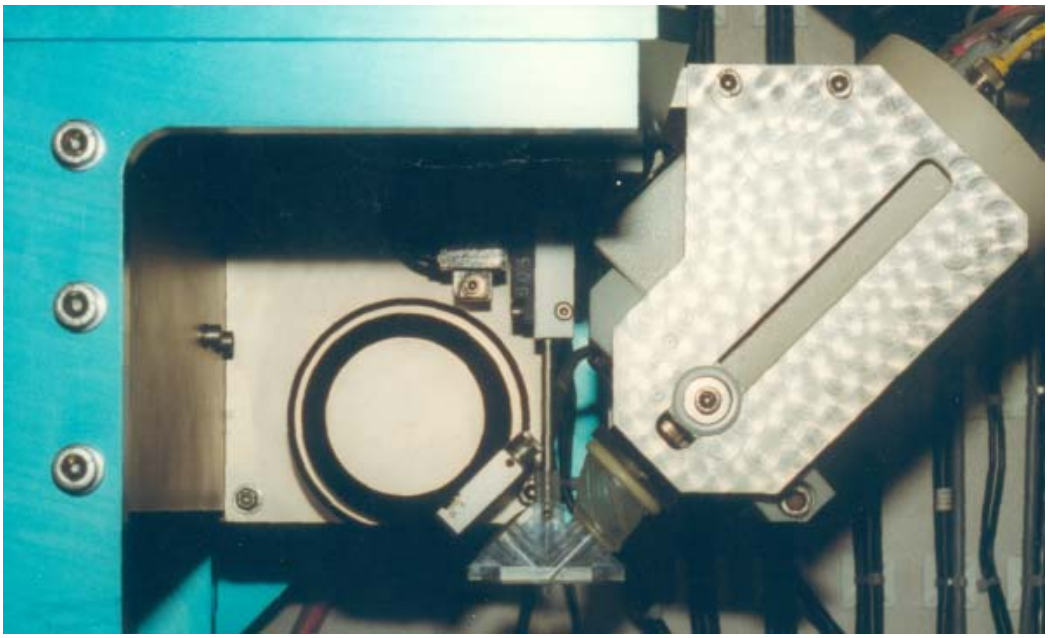

Fig. 3. b) Automated X-ray fluorescence half core scanner for non-destructive element analysis with X-ray source (left), prism attached to core surface (center, core not shown) and X-ray detector (right).

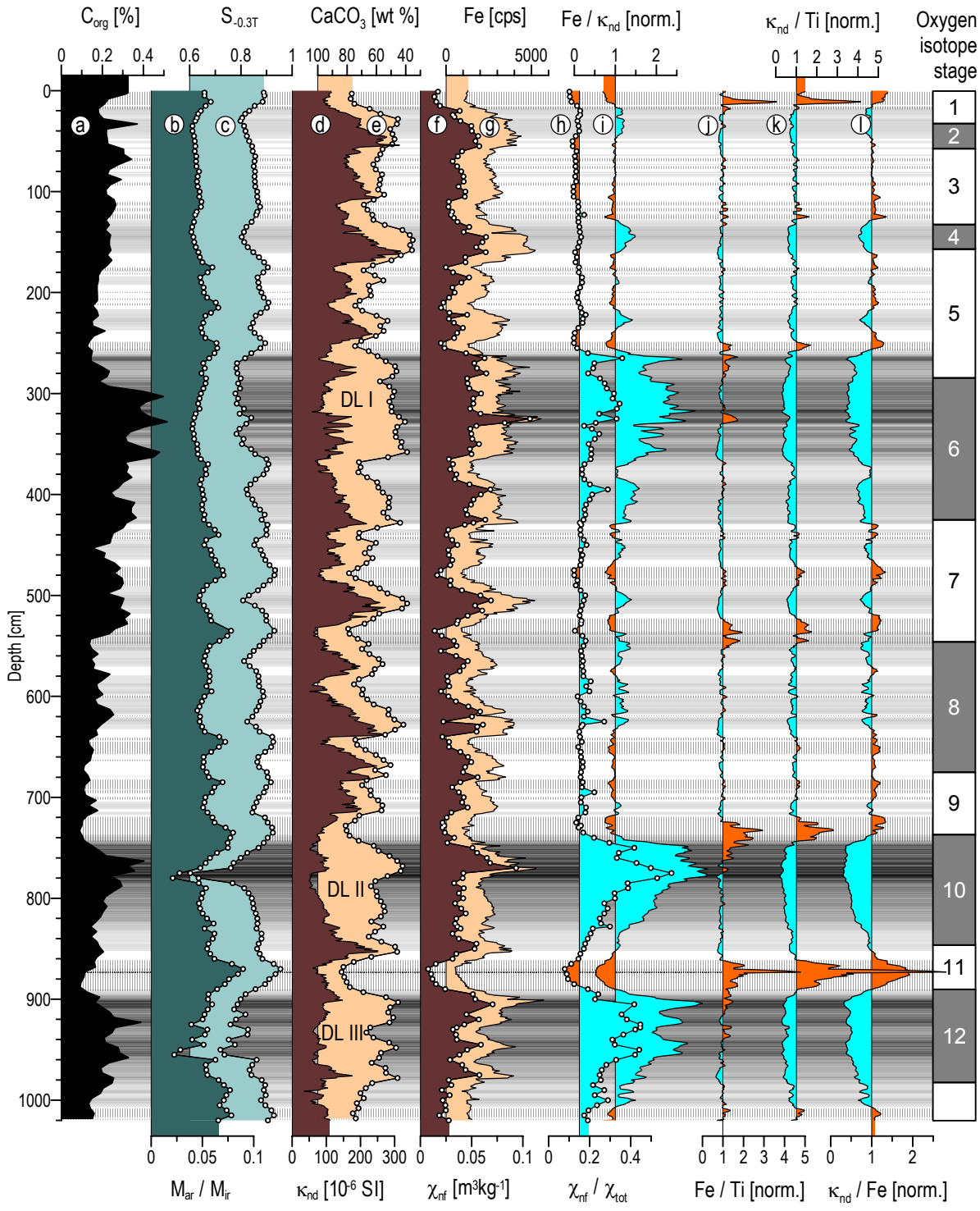

Fig.4. Geochemical and rock magnetic profiles of core GeoB 4317-2. Labels DL I to III indicate major magnetite dissolution layers. Background shading indicates degree of magnetite dissolution based on Fe/κ_{nd}. Magnetic mineral precipitation zones based on κ_{nd}/Ti are shown as hatched areas.

the shorter duration of suboxic conditions, ie. from the respective burial history. Mild forms of reduction affect primarily ultra-fine (SP) magnetic ferric minerals. They are therefore less apparent in remanence-based parameter records such as M_{ar}/M_{ir}, but still prominent in parameters derived from induced magnetizations such as χ_{nf}/χ_{tot} (Fig. 4h)

The $S_{-0.3T}$ index (Fig. 4c) mirrors the ratio of high- to low-coercive components, in general hematite and magnetite (Bloemendal et al. 1992). This parameter shows distinct minima, relative hematite enrichments, in the dissolution layers, suggesting that reductive diagenesis has a lesser effect on hematite than on magnetite. This observation will be further substantiated and discussed at the end of this chapter.

Pronounced $CaCO_3$ variations ranging from 35 to 84 wt.% reflect mainly cycles of carbonate dissolution due to glacial emplacement of corrosive Circumpolar Deep Water (de Menocal et al. 1993; Bickert and Wefer 1996). In absence of significant opal contents the non-carbonate sediment fraction (Fig. 4e) is largely representative of the terrigenous content (Schmieder et al. 2000). In most parts it matches the magnetic susceptibility record κ in great detail. However, both signal clearly diverge in the three major dissolution layers I, II and III, where susceptibility (Fig. 4d) is far too low for glacial conditions (Bloemendal 1988). As reductive diagenesis involves transformation of magnetic into non-magnetic iron phases, the correlation of rock magnetic logs to climatic cycles is strongly compromised in these intervals. In interglacial layers, carbonate maxima resulting from much better preservation conditions correspond reasonably well to susceptibility lows.

The non-ferrimagnetic susceptibility (χ_{nf}, Fig. 4f) is the slope of the linear outer branch of a saturation hysteresis loop (von Dobeneck 1996). This parameter quantifies contributions of paramagnetic phases plus a small, nearly constant offset due to diamagnetic matrix minerals. Relative Fe counts measured with the XRF scanner (Fig. 4g) and χ_{nf} closely mimic each other throughout the sediment sequence implying that most iron is located in paramagnetic mineral phases like iron-bearing silicates. The much higher level of conformity of non-$CaCO_3$ with total Fe records compared to magnetic susceptibility underlines this statement.

The ratio of non-ferrimagnetic to total susceptibility (χ_{nf}/χ_{tot}, Fig. 4h) delineates unequivocally where magnetite dissolution takes place. The prevailing stable baseline value (~ 0.15) represents an average 15 % contribution of paramagnetism to total susceptibility, a characteristic source signature. This parameter value doubles or even triples at the peaks of reductive dissolution implying that about two thirds of the primary magnetite have vanished. The ratio Fe/κ_{nd} (Fig. 4i), based exclusively on fast logging measurements, follows the χ_{nf}/χ_{tot} trends in most every aspect, but provides much higher spatial resolution and detail at a fraction of measurement time. Both parameters image magnetite depletion layers as distinctive, internally subdivided sawtooth patterns with upwards increasing dissolution levels. For the three major dissolution layers, the diagenetic features stretch vertically over about 100 cm. The slightly elevated Fe/κ_{nd} signals at numerous other mildly reductive layers are much narrower and also more symmetric features.

For reasons elaborated in the methods section, redox sensitive elements as Fe are often normalized to the stable terrigenous element Al (Karlin 1990a; Karlin 1990b). As this light element is not within the range of the XRF scanner (K to Sr), we use here the immobile terrigenous element Ti as normalizer assuming that the sedimentary iron and titanium minerals are identical or have a common origin. From a fairly constant background level the Fe/Ti ratio (Fig. 4j) shows distinct multiple enrichment peaks immediately above the lower two dissolution layers, while the effect above dissolution layer I is smaller. A sharp subsurface peak at 11 cm depth, a broader peak at 540 cm and many less developed peaks pinpoint additional faint iron precipitation horizons associated with underlying layers of partial magnetite dissolution.

An alternative and related, but magnetic mineral selective Fe precipitation proxy is κ_{nd}/Ti (Fig. 4k), also derived by combining susceptibility and XRF logs. Other than the Fe/Ti signal, κ_{nd}/Ti has no stable baseline as it also registers magnetite depletion (inversely to Fe/κ_{nd}). The iron residing in nonmagnetic minerals is either not bioavailable, immobile or ferrous, while the ferric iron in all

magnetic minerals is generally bioavailable (Lovley et al. 1987). Subtle distinctions of the lower slopes of the Fe/Ti and κ_{nd}/Ti peaks, particularly at the upper boundary of magnetite dissolution layer II, probably result from cancellation effects of superimposing magnetite depletion and subsequent precipitation.

Magnetic mineral precipitation cannot be seen in susceptibilities, only the M_{ar}/M_{ir} and $S_{-0.3T}$ signals indicate enrichment by a very fine, probably biogenic (Karlin et al. 1987; Robinson et al. 2000; Tarduno et al. 1998) magnetite phase. Obviously, this secondary magnetite has been precipitated after reductive dissolution of primary magnetite during partial burn-down of the initially broader C_{org} enrichment layer.

The κ_{nd}/Fe ratio (Fig. 4.l) indicates magnetic mineral depletion as well as enrichment effects and is therefore a bivalent proxy. However, as magnetic and total iron enrichment often go along, this parameter may not identify precipitation correctly. Defining a baseline value for standardization is also less evident.

Combined Geochemical and Rock Magnetic Stratigraphy of Core GeoB 2908-7

Core GeoB 2908-7, recovered about 450 km southeast of core GeoB 4317-2, has on average 35 % higher C_{org} contents with a mean of 0.27 wt.% and variations between 0.1 and 0.66 wt.% (Fig. 5a). The C_{org} signal carries a typical equatorial Atlantic climate signature, modulated by orbitally forced changes in trade wind zonality (Verardo and McIntyre 1994). Productivity is more pronounced at this site due to stronger upwelling and higher productivity towards the Equatorial Divergence Zone. More frequent productivity pulses cause higher sedimentation rates and greatly increase the number of organically enriched layers and of resulting magnetite dissolution and precipitation horizons. While in core GeoB 4317-2 dissolution zones are mainly found at major terminations, core GeoB 2908-7 carries consecutive diagenetic features also at stadials (Fig. 5).

The M_{ar}/M_{ir} ratio of core GeoB 2908-7 (Fig. 5b) also shows much stronger overprint of the primary signal. Ten layers of intense dissolution appear as deep, notchlike grain-size shifts (abrupt magnetite coarsening) in the record. In combination with climatically unexpected susceptibility minima (Fig. 5d), these peaks indicate massive loss of fine-grained magnetite, whereas high-coercive iron mineral phases ($S_{-0.3T}$, Fig. 5c) are less affected. A synopsis of C_{org}, dissolution and precipitation proxies suggests that also many minor M_{ar}/M_{ir} and $S_{-0.3T}$ shifts may be related to partial magnetite dissolution in organically enriched horizons. It is not totally clear from these data, however, to what extent these signatures still carry traits of grain-size and mineral variations of primary detrital iron oxides.

The wide range of susceptibilities κ_{nd} from 0.9 to $100 \cdot 10^{-6}$ SI documents two superimposing influences: The eolian iron input from the African continent is systematically lower at this more southern site (Ruddiman et al. 1989) and frequently overprinted by reductive dissolution. The large scale variations in $CaCO_3$ content from 51 to 90 wt.% mainly reflect intensified carbonate dissolution due to glacial advances of Circumpolar Deep Water (Bickert and Wefer 1996). This cyclical dilution of the terrigenous (non-$CaCO_3$) phase (Fig. 5e), is inversely correlated to magnetic susceptibility.

Over most of the sediment column this initial accumulation pattern is also conserved in the very similar non-ferrimagnetic susceptibility (c_{nf}, Fig. 5f) and bulk iron (Fe Fig. 5g) records. Distinct narrow discrepancies from 40 to 55 cm, at 440 cm and at 590 cm, all can be attributed to precipitation of non-magnetic iron phases. This interpretation is clearly supported by enhanced Fe/κ_{nd} ratios (Fig. 5i), indicating that this parameter does not only identify dissolution of ferrimagnetics (decreasing denominator κ_{nd}), but also precipitation of paramagnetics (increasing numerator Fe).

Fine-scaled variability is observed in the ratios of ferrimagnetic, non-ferrimagnetic and total Fe (Fig. 5h,i,l) and respective relations to Ti (Fig. 5j,k). In spite of lower signal levels, particularly regarding Ti counts, and therefore poorer signal-to-noise ratios, complex suites of alternating fine-scale depletion and enrichment layers are recognized. Some precipitations situated within dissolution zones are purely paramagnetic (e.g., at 445 and 820 cm) and do not appear in the κ_{nd}/Ti ratio.

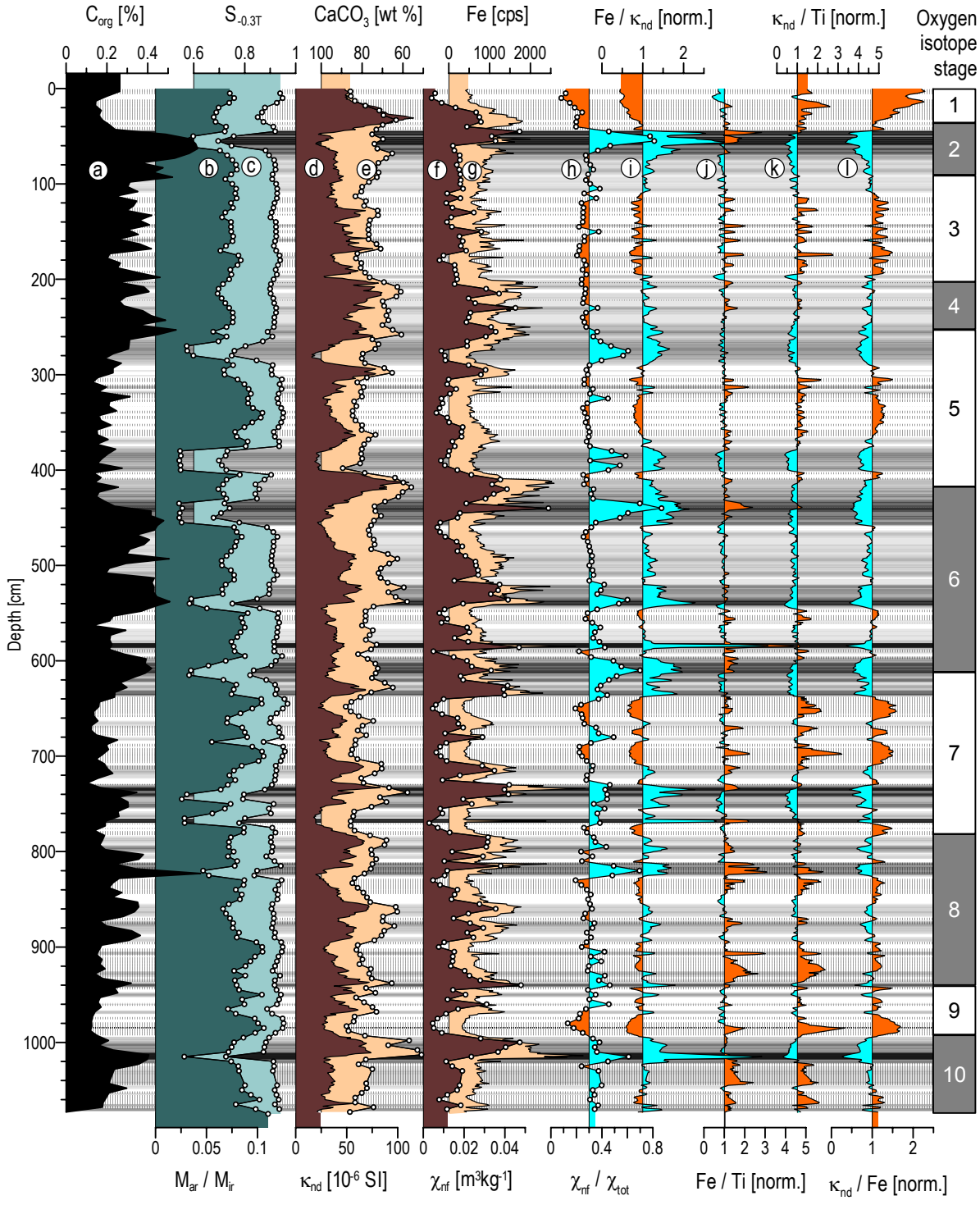

Fig.5. Geochemical and rock magnetic profiles of core GeoB 2908-7. Background shading indicates magnetite dissolution stage based on Fe/κ_{nd}. Magnetic mineral precipitation zones based on κ_{nd}/Ti are shown as hatched areas.

Detailed Analysis of the Active Fe Redox Boundary in Core GeoB 2908-7

For a better definition of redoxomorphic processes and proxy parameters, additional and more detailed rock magnetic and geochemical analyses of the subsurface sediments encompassing the present-day iron redox boundary are presented in Figure. 6. The same section already shown in the introductory Figure 1 and as top of the core GeoB 2908-7 logs in Figure 5 is now presented with an extended parameter spectrum to illustrate and discuss alternative methods. The 28 selected rock magnetic and geochemical data sets are displayed in a three-part compilation of concentration (Fig. 6.I), dissolution (Fig. 6.II) and precipitation (Fig. 6.III) signatures. A comparison of data sets from low (5 cm spacing, circles) and high resolution (1 cm spacing, dots) single sample measurements with core logging data (no symbols) shows assets and drawbacks of the traditional versus scanning methods. High-resolution magnetic hysteresis (dark gray) and ICP-AES element measurements (hatched) covering the top 100 cm of core GeoB 2908-7 in 1 cm steps allow to verify and investigate some fine-scaled structures (horizontal lines) visible in the combined XRF/ susceptibility scanning data, to calibrate XRF logging data and to determine their noise floor.

The organic carbon enrichment at 44-78 cm (Fig. 6.I a) triggers reductive dissolution of magnetite (Fig. 6.I b) and, to a minor extent, hematite (Fig. 6.I c) affecting visibly the total susceptibility signal (Fig. 6.I d), but not its paramagnetic component (Fig. 6.I e). The latter log however resembles the total Fe content (Fig. 6.I f,g) and shows three conspicuous peaks within the reductive layer. These are neither found in the Ti (Fig. 6.I h,i) nor in the magnetic iron mineral (Fig. 6.I b,c) records and must therefore be regarded as non magnetic Fe precipitation. In contrast, the broad iron enrichment peak from 18 to 42 cm is shared by Ti and κ logs and represents a primary relative maximum of terrigenous accumulation. Comparing Fe and Ti data sets (Fig. 6.I f-i), determined both by scanning and single sample methods, it is apparent that in case of Fe (Fig. 6.I f,g) even the fine-scaled features largely coincide, while for the rarer element Ti (Fig. 6.I h,i), the noise floor of the scanning XRF measurement obviously disturbs the signal.

The next series of plots (Fig. 6II) groups relational, i.e. concentration independent active iron redox boundary over a width of about 20 cm (coarse residue fraction). The coercive field (Fig. 6.II c) shows a superposition of two effects: a low in the reduction zone (loss of magnetically hard SD/PSD particles), but also a noticeable increase in coercivity between 35 to 45 cm. This gradient delineates the irreversible loss of ultra-fine grained (< 30 nm), magnetically very soft SP magnetite. As SP particles have considerably higher specific susceptibilities than all other magnetite grain-size fractions (Heider et al. 1996), their depletion is equally reflected in a sharp decline of χ_{cfdm} (Fig. 6.II f). Losses are at maximum in C_{org}-enriched layers, where reactive carbon and magnetite nanoparticles coexist in intimate contact enabling or facilitating redox reactions between both solid phases.

As earlier mentioned, the $S_{-0.3\ T}$ parameter (Fig. 6.II d) mirrors the reductive layer as a relative enrichment of hematite compared to magnetite. It is not sure, though, whether this actually implies a higher dissolution resistance of hematite. From a geochemical viewpoint, the hematite reduction is energetically favorable to magnetite reduction and has a much higher reaction rate constant (Canfield et al. 1992; Haese 2000). This argument regards only isolated grains but not inclusions in silicate minerals that are protected against reductive dissolution (Walden and White 1997). But a purely rock magnetic argument may be more decisive: coarse and fine hematite have similar remanence carrying capacities (both are SD particles), while coarse magnetite (MD) particles hold much less remanence than fine (SD/PSD). Consequently, the S-Ratio relates a grain-size independent hematite content to a measure of magnetite content, which is heavily biased towards small (sub-micron) particles. Any diagenetic process reducing the sub-micron fractions of both minerals proportionally would therefore effectively shift the $S_{-0.3\ T}$ parameter to smaller values. This grain-size effect introduced by the SD remanence and coercivity of residual coarse hematite equally explains the otherwise surprising increase of the remanent coercive field B_{rh} (Fig. 6.II e) over the magnetite depletion

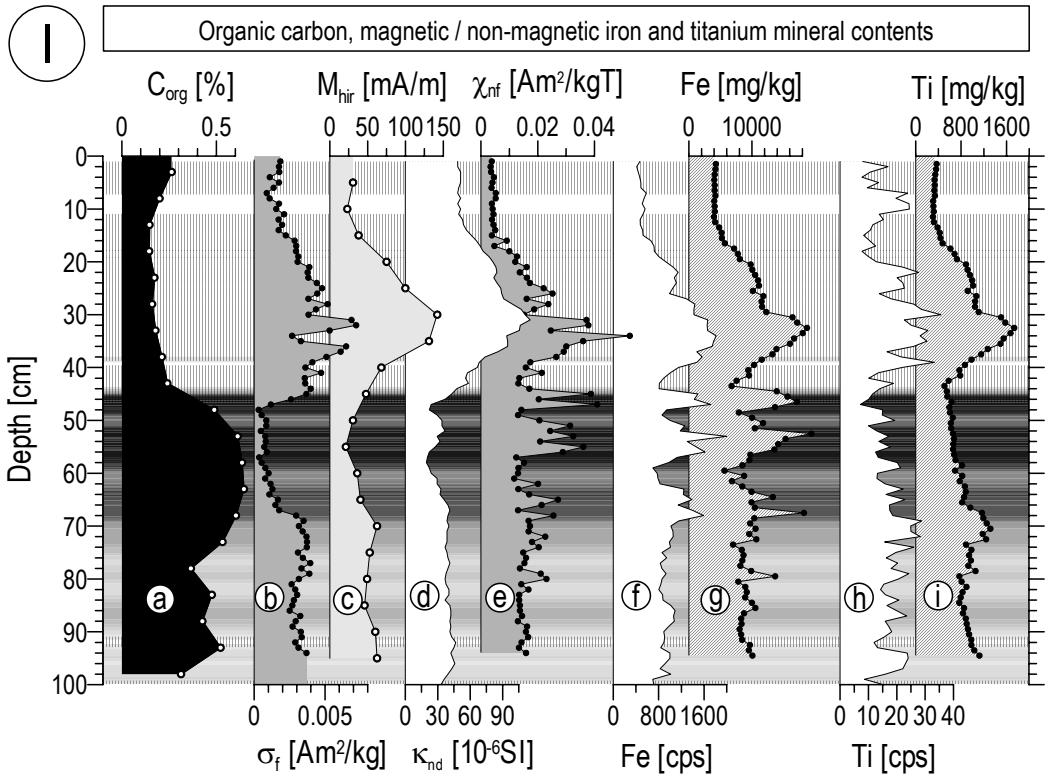

Fig.6.I. Magnetomineral and element concentration profiles (core GeoB 2908-7, 0-100 cm) encompassing the active Fe redox boundary. The shown parameters quantify **a)** organic carbon, **b)** magnetite, **c)** hematite, **d)** ferri- and paramagnetism, **e)** paramagnetic iron, **f, g)** total iron and **h, i)** titanium. The latter element data were acquired by XRF scanning (f, h) and single sample ICP-AES (g, i) measurements, respectively. Background shading indicates the degree of magnetite dissolution based on Fe/κ_{nd}. Magnetic mineral precipitation zones according to κ_{nd}/Ti are shown as hatched areas. Plot symbols and fillings refer to sampling density and method (see legend Fig. 6.III).

layer.

As shown in Figure 5 with less spatial resolution, the two magnetite dissolution proxies χ_{nf}/χ_{tot} (Fig. 6.II g) and Fe/κ_{nd} (Fig. 6.II h) clearly delimit the diagenetically affected zone by multiple overlapping peaks protruding from a stable plateau level. The Fe/χ_{fer} ratio (Fig. 6.II i), combining high resolution XRF and hysteresis measurements, delineates this even more impressively, because the denominator measures strictly ferrimagnetic iron and can therefore approach near zero values boosting the ratio to high numbers. In case of the χ_{nf}/χ_{tot} and Fe/κ_{nd} ratios, the denominators have positive lower limits in paramagnetic susceptibility. It could, however, be argued that peaks in all three ratios may not result from decreasing denominators, but rather from an increase of the numerator χ_{nf} or Fe, i.e., non-magnetic iron precipitation. Since the primary accumulation of Fe and Ti is highly proportional (Fig. 6III a,d) and Ti is minimally affected by diagenetic mobilization (Brown et al.,2000), the latter element should be an unambiguous normalizer for susceptibility. Two alternatives to Fe/κ_{nf} and Fe/χ_{fer} are therefore the Ti-based ratios Ti/κ_{nd} (Fig. 6II j) and Ti/χ_{fer} (Fig. 6II k). These AGFM and ICP-AES derived data convincingly document the high degree of coincidence between Fe- and Ti-related magnetic mineral dissolution records and dispel doubts on major Fe precipitation effects in the present case. The scanner-based equivalents (Fig. 6II h,j) generally agree, but the poor signal to noise level of the Ti measurement seriously reduces the interpretability of the Ti/κ_{nf} ratio leaving Fe/κ_{nf} without alternative.

The third series of plots (Fig. 6 III) deals with

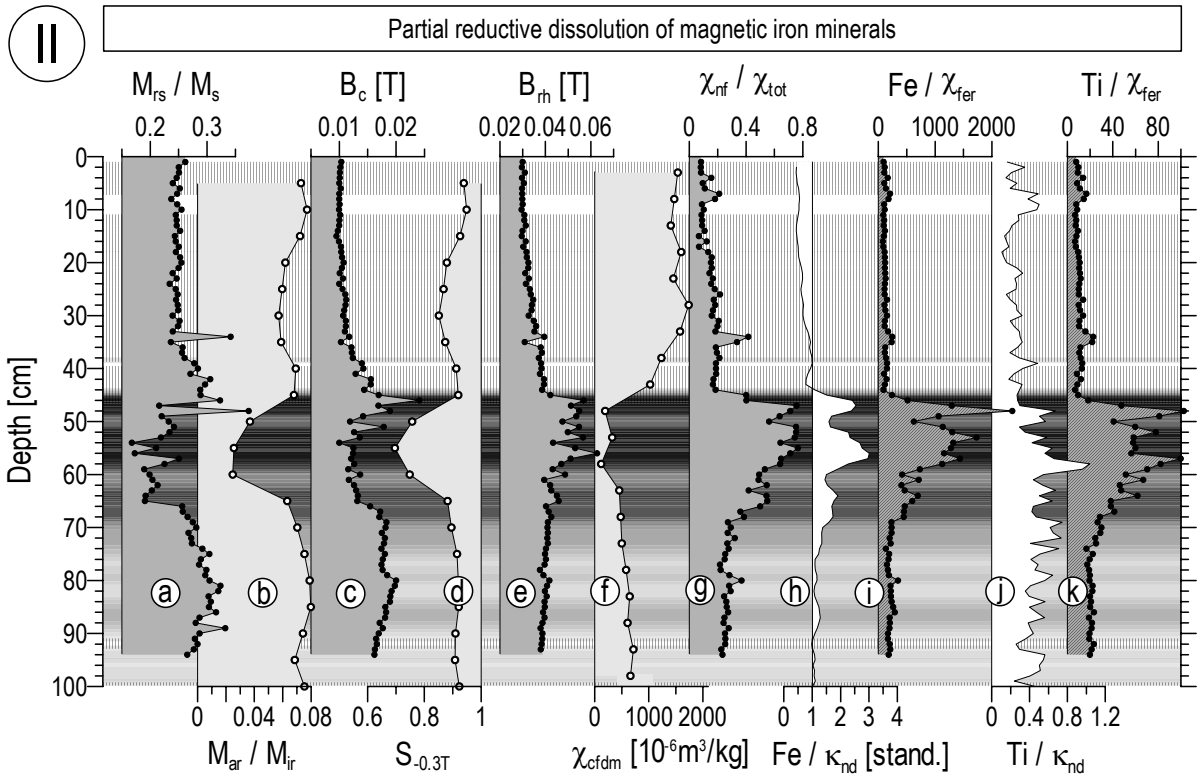

Fig.6.II. Integrated rock magnetic and geochemical profiles (core GeoB 2908-7, 0-100 cm) indicating reductive iron diagenesis below the active Fe redox boundary. The shown parameters measure **a)** magnetite grain-size (domain state) after Day et al. (1977), **b)** relative contribution of fine grained magnetite, **c)** coercive field, **d)** S-ratio (values below 1 denote increasing influence of high-coercive magnetic iron oxides, primarily hematite), **e)** hysteresis derived remanence coercive field, **f)** carbonate-free dry mass susceptibility, **g)** paramagnetic contribution to susceptibility. Newly proposed magnetite dissolution proxies relating **h, i)** Fe content or **j, k)** Ti content to nondiamagnetic or ferrimagnetic susceptibility. The ratios are based on XRF and susceptibility scanning measurements (h, j), and on single sample ICP-AES and hysteresis data (i, k); normalization is explained in chapter 5.2. Background shading indicates the magnetite dissolution stage based on Fe/k_{nd}. Magnetic mineral precipitation zones according to k_{nd}/Ti are shown as hatched areas. Plot symbols and fillings refer to sampling density and method (see legend Fig. 6.III).

Fe relocation and precipitation effects and starts out by comparing the inert terrigenous normalizers Ti and Al. As in other marine records (van Santvoort et al. 1996) the Al-normalized Ti profile (Fig. 6 III a) remains almost constant and distinctly different from the Fe/Ti (Fig. 6 III b,c) and Fe/Al (Fig. 6 III d) ratios. It is therefore clear that the sharply defined maxima in logs III b-d at and below the Fe redox front can only result from diagenetic iron enrichment (König et al. 1997) which more than doubles the primary detrital Fe content. Interestingly, complementary minima (sources) visible in the Fe_{exess} record (Fig. 6 III e), defined as

$$Fe_{excess} = Fe_{tot} - (Al_{tot}\ [Fe/Al_{average}),$$

where Fe_{tot} (Al_{tot}) refers to the measured element content per sample, are much shallower and broader than the maxima (sinks) implying that the mobilized and precipitated iron was drawn from an iron depletion zone largely exceeding the directly underlying magnetic mineral dissolution zone. This can also be seen by extra-polating the very stable primary Fe/Al ratio (Fig. 6 III d) of the oxygenated

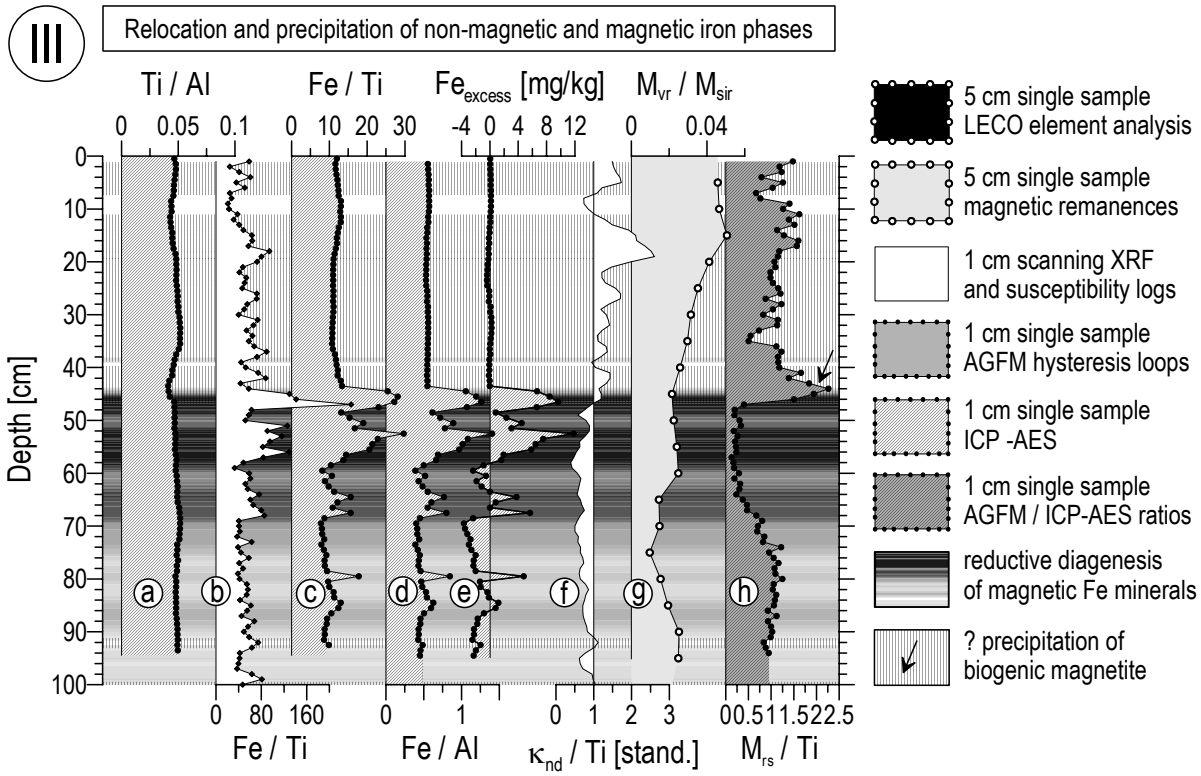

Fig.6.III. Integrated rock magnetic and geochemical profiles (core GeoB 2908-7, 0-100 cm) indicating iron relocation and precipitation in and above the active Fe reduction zone. The shown parameters delineate **a)** equivalence of Ti and Al as normalizers of terrigenous input, iron enrichment detected by element ratios of **b)** Fe/Ti (XRF scanner)**, c)** Fe/Ti (ICP-AES) and **d)** Fe/Al (ICP-AES), **e)** Fe excess based on Fe/Al ratio of 0 – 40 cm. The newly proposed proxies quantify authigenic enrichment by **f)** ferrimagnetic Fe minerals (scanner data), **g)** ultra-fine (SP) magnetite particles (single sample remanence data), **h)** fine (SD) magnetic Fe mineral particles (hysteresis and ICP-AES data), most likely bacterial magnetosomes. Background shading indicates the degree of magnetite dissolution based on Fe/κ_{nd}. Magnetic mineral precipitation zones according to κ_{nd}/Ti are shown as hatched areas. Plot symbols and fillings refer to sampling density and method (see legend).

top layer down-wards.

Three individual precipitation layers, each approximately 5 cm wide, can be discerned. They are located below, within and above the organically enriched and magnetically depleted zone and separated by magnetic mineral dissolution maxima. From geochemical considerations, two of these enrichments have to be regarded as relict peaks from former redox boundaries during prolonged non-steady state conditions. The theoretical question (Burdige 1993), whether the upper (upward shift of the Fe redox boundary due to Holocene sedimentation) or the middle (downward shift of the Fe redox boundary to due to enhanced Holocene bottom water oxygenation) peak represents the active Fe precipitation zone is clearly answered by the sediment's color (Fig.1a): The brown-green color transition (Lyle 1983) is located precisely at 45 cm depth.

In comparison to Fe/Al (Fig. 6 III d) and Fe/Ti (Fig. 6 III b,c) the κ_{nd}/Ti ratio (Fig. 6 III f) remains at a fairly stable low level over the precipitation zones implying that the iron relocated here primarily resides in nonmagnetic phases. The Ti-based scan-

ner data are again too noisy to allow an interpretation of minor features. However, it is obvious that there is a marked upward increase in κ_{nd}/Ti from the Fe redox boundary (46 cm) culminating at a depth of 20 cm and sharply decaying above. Although no pore water data are available for this core, this interval is very likely to represent the nitrate zone, where magnetite biomineralization by anaerobic, nitrate respirating dissimilatory iron-reducing microorganisms (Lovley et al. 1987) and magnetotactic bacteria (Bazylinski et al. 1988; Blakemore 1975; Petermann and Bleil 1993) widely occurs. The shape of the κ_{nd}/Ti profile is paralleled by the M_{vr}/M_{sir} ratio (Fig. 6 III g) sensing ultra-fine, magnetically viscous magnetite particles (SP/SD transition; grain-sizes around 20 nm); (Worm and Jackson 1999). This magnetite fraction carries a two- to threefold higher susceptibility than all coarser fractions (Heider et al. 1996) and is therefore over-represented in susceptibility-based parameters. Its presence throughout the nitrate zone indicates a bacterially mediated reduction of amorphous ferric iron yielding superparamagnetic magnetite as metabolic byproduct and electron acceptor. As noted above, the minute size of these SP particles makes them a first victim of even mild reductive dissolution (Frederichs et al. 1999) and explains for their depletion from deeper sediment layers.

The M_{rs}/Ti ratio (Fig. 6 III h) focuses mainly on relative enrichments of slightly larger, magnetically stable magnetite particles (stable SD; grain-sizes 30-100 nm) and excludes SP particles. Its profile clearly marks the magnetite dissolution zone (46-70 cm), topped by a narrow, but clearly defined peak (40-46 cm, black arrow) just above the Fe redox boundary. This is probably an enrichment of fossil magnetosomes as described by Tarduno and Wilkison (1996). The producers, magnetotactic bacteria, are nitrate reducers and assimilate and oxidize ferrous iron available near the Fe redox boundary. Although potentially significant for paleo- and rock magnetic data (Tarduno et al. 1998), biogenic magnetite precipitation appears to play a negligible role in terms of absolute iron concentrations here as it is completely absent in the Fe/Al record (Fig. 6 III d).

Discussion and Conclusions

Efficiency, Data Quality and Calibration of Scanning Techniques

These studies demonstrate that combining rock magnetic and geochemical methods is very effective both in detecting redoxomorphic diagenesis of magnetic and nonmagnetic iron minerals and in distinguishing between variations in primary input and secondary overprint. At the present, traditional single sample methods still offer a greater variety, accuracy and selectivity of procedures and proxy parameters. The great advantage of the newly proposed proxies based on scanning techniques is therefore the efficiency of data acquisition. With the now available non-destructive XRF core scanner combined with well established high-resolution spot measurements of magnetic susceptibility, the data basis can be established in a small fraction of the time required for conventional single sample hysteresis and element analyses.

Sample preparation and data acquisition rates for the two alternative methods employed here are compiled in Table 1. Scanning methods are about 20 to 50 times faster than single sample techniques. Diagenetic layers are often fine-scaled and typically require centimeter spacing records for ample resolution. Only the scanning techniques permit to study long and multiple sediment cores at such high-resolutions in affordable time.

The price to pay for the enormous gain in speed is a loss in sensitivity. The necessary technical compromises accepted by transforming XRF spectrometry into a surface scanning technique clearly impair the quantification of minor elements such as Ti and Mn (Fig.6 I f-i). The theoretical, but not necessarily influential error sources of XRF analyses are manifold: grain-size, surface and matrix effects, instability of source and detector, sample roughness, inhomogeneity and porosity, count statistics, not to forget the imponderables of an automated algorithm transforming X-ray emission spectra into relative element concentrations. These effects make it in some instances questionable to transform XRF counts into absolute concentrations. As a detailed error assessment is complicated and beyond the scope of this paper, we simply argue on

Analytic method	Sample preparation procedures	Preparation time	Measurement time
XRF element analysis, powder measurement	Sampling, drying, grinding, weighting, pressing	60 min per sample	50 min per sample
ICP – AES element analysis	Sampling, freeze drying, homogenizing, digestion	35 min per sample	5 min per sample
Magnetic remanence measurements	Sampling	5 min per sample	10-60 min per sample
Magnetic hysteresis measurement	Sampling, drying, weighting, impregnating	20 min per sample	10-20 min per sample
XRF scanning element analysis	Cleaning of split core surface	5 min per 1 m core section	2 min per data point
Susceptibility scanning measurement	Cleaning of split core surface	5 min per 1 m core section	1 min per data point

Tab. 1. Comparison of single sample and scanning analytical methods

basis of repeatability and consistence with calibrated, precise single sample measurements.

In Figure 7 the XRF scanner data of Fe and Ti [wet bulk sample, counts per second] of core GeoB 4317-2 are correlated with calibrated conventional XRF measurements [wt.%] of single samples obtained from identical core depths. The linear regression lines and equations, the 95% confidence ranges and Pearson's correlation coefficients altogether indicate that for Fe contents of 1-5 wt.%, XRF counts can be reliably calibrated (Fig. 7a). In case of the lower Ti contents of 0.1-0.5 wt.%, the scatter and zero-offset of scanning XRF analyses is considerably larger, yet there is sufficient correlation to interpret at least first order variations quantitatively (Fig. 7b).

For the scanning susceptibility measurements the potential error sources are fewer and less problematic. Unevenness and inhomogeneity of the core surface may cause minor signal deviations as do fluctuating sample and sensor temperatures. Typically, measurements can be repeated within some 5–10% and systematically reproduced by single sample data. The lateral shape (but not the vertical extension!) of the sediment volumes contributing respectively to XRF and susceptibility scanner measurements are quite similar in area. Therefore, the error resulting from combining these parameters in a single ratio remains small.

Normalization of Proposed Diagenesis Proxies

The ratios Fe/κ_{nd}, κ_{nd}/Fe, κ_{nd}/Ti and Fe/Ti do not quantify the progression of iron mineral diagenesis by their absolute value since they also depend on local magnetic mineral source characteristics. Site specific references for the terrigenous input can usually be inferred from the stable signal platforms observed in sediment sections with low C_{org} contents (see Figs. 4 and 5). These baseline levels are used here to normalize the continuous records. This approach implies that the initial proportion of accumulated magnetic and nonmagnetic Fe and Ti minerals did not extensively vary through time. In the equatorial Atlantic as in other open ocean settings with a single predominant terrigenous sediment source this assumption is probably acceptable. It may not be fulfilled, however, if contributions from geologically differing sources strongly alternate within the record.

By normalizing these ratios, positive deviations from unity quantify the grade of magnetic mineral

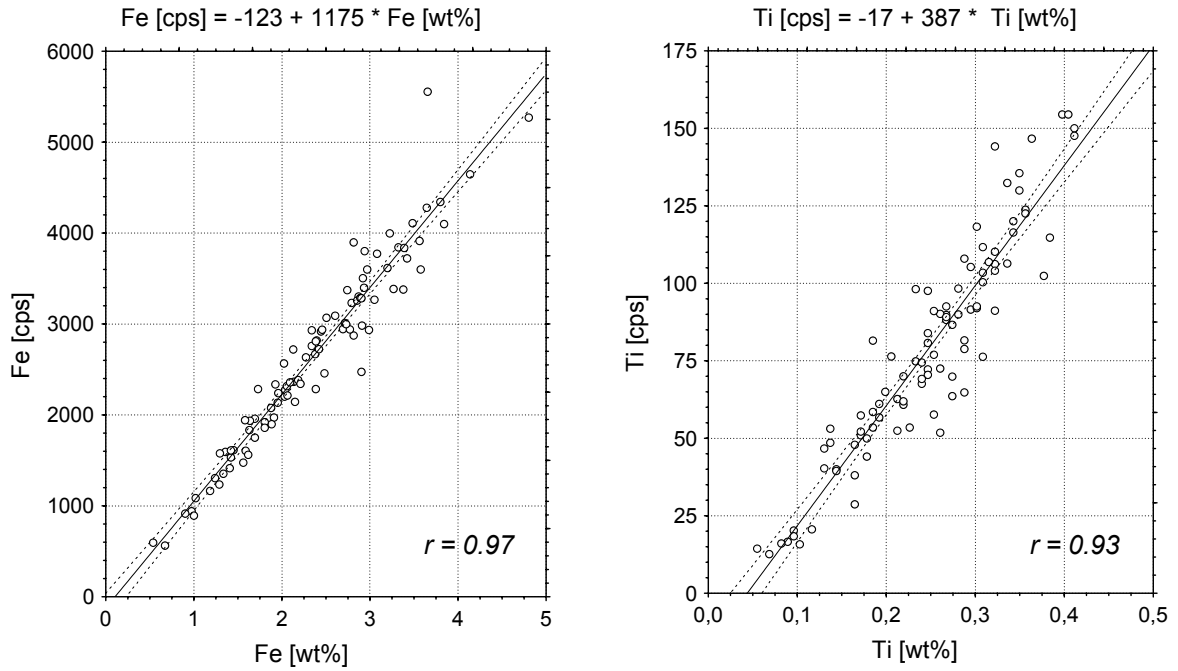

Fig.7. Calibration of relative (a) Fe and (b) Ti XRF scanner data [cps] of core GeoB 4317-2 by conventional single sample XRF analyses [wt.% oxide]. Shown here are Pearson's correlation coefficients r, linear regression equations, regression lines and their 95% confidence ranges.

dissolution and authigenesis as well as iron depletion and enrichment, respectively. In the following the proxy parameters shall be symbolized as

$$\left[\mathrm{Fe}/\kappa_{\mathrm{nd}}\right]_{\mathrm{n}} = \frac{\mathrm{Fe}/\kappa_{\mathrm{nd}}}{\left(\mathrm{Fe}/\kappa_{\mathrm{nd}}\right)_{\mathrm{base}}};$$

$$\left[\kappa_{\mathrm{nd}}/\mathrm{Fe}\right]_{\mathrm{n}} = \frac{\kappa_{\mathrm{nd}}/\mathrm{Fe}}{\left(\kappa_{\mathrm{nd}}/\mathrm{Fe}\right)_{\mathrm{base}}};$$

$$\left[\kappa_{\mathrm{nd}}/\mathrm{Ti}\right]_{\mathrm{n}} = \frac{\kappa_{\mathrm{nd}}/\mathrm{Ti}}{\left(\kappa_{\mathrm{nd}}/\mathrm{Ti}\right)_{\mathrm{base}}};$$

$$\left[\mathrm{Fe}/\mathrm{Ti}\right]_{\mathrm{n}} = \frac{\mathrm{Fe}/\mathrm{Ti}}{\left(\mathrm{Fe}/\mathrm{Ti}\right)_{\mathrm{base}}};$$

It is of no relevance, whether the XRF element data are inserted as raw or calibrated values. The problem of discontinuities in the Fe/κ record due to zero or negative values of k is resolved by using the strictly positive non-diamagnetic susceptibility κ_{nd}. Sections with very low Ti contents can result in unrealistic, noise related positive peaks in Ti-based ratios. This problem should be avoidable in the future by normalizing with Al. This element will be measurable with the next generation of XRF core scanners.

Quantification of Depletion and Enrichment Processes

Prior to further considerations, it shall be recalled that the terms 'depletion' and 'enrichment' have fundamentally different meanings, when being applied to magnetic minerals or iron content: to deplete or enhance a layer magnetically, it suffices to dissolve, alter or precipitate magnetic minerals in

situ; iron relocation is not required. Ferrimagnetism itself has no balanced budget, as it is easily exchanged into or from the (paramagnetic) total Fe reservoir. However, depletion and enrichment of paramagnetic iron in marine sediments is always balanced and involves dissolution and relocation by diffusive transport in the pore water soluble ferrous form. The ferrimagnetic mineral content, (titano-) magnetite or maghemite with a susceptibility equivalent of 10-100 ppm, is typically several orders of magnitude smaller than the nonmagnetic iron mineral content. Consequently, the magnetic fraction is very subordinate in the total iron budget, but largely dominates the rock magnetic properties.

The integration of concentration dependent rock magnetic and geochemical parameters permits to quantitatively reconstruct diagenetic changes in magnetic and nonmagnetic iron budgets as will be demonstrated for core GeoB 4317-2.

With suitable threshold values for the ratios $[Fe/\kappa_{nd}]_n$ and $[\kappa_{nd}/Ti]_n$, the sediment column can be subdivided into magnetically pristine ($[Fe/\kappa_{nd}]_n \approx 1$, $[\kappa_{nd}/Ti]_n \approx 1$), enriched ($[\kappa_{nd}/Ti]_n > 1$), weakly ($2 > [Fe/\kappa_{nd}]_n > 1$) and strongly ($[Fe/\kappa_{nd}]_n > 2$) depleted sections. In Figure 4, 5 and 9 this classification has already been implicitly introduced: background patterns are shaded (magnetically depleted) and hatched (magnetically enriched) to correlate and clarify the specific signatures of diagenesis in all parameter records. In Figure 8 the same categories were used as grouping variables in crossplots of concentrational rock magnetic and geochemical parameters of core GeoB 4317-2. The samples assumed as pristine (black dots) show an almost perfect mutual proportionality of susceptibility, Fe and Ti contents. In all three cases the respective regression lines (dashed; Fig. 8a-c) approximately pass through the origin.

The regression equations have been used to define the primary (predicted) susceptibility and Fe content of all modified samples on basis of their Ti contents. The measured (Fig. 9c,e, thick lines) and the Ti-derived (Fig. 9c,e, thin lines) parameters were subtracted to quantify the diagenesis related excess (orange) and deficiency (cyan) of κ_{nf} and Fe in scaled, absolute values (Fig. 9b,d, loss/gain). Together, Figures 8 and 9 describe and link the rock magnetic and geochemical perspective and put it into a joint stratigraphic framework. The range and correlation of magnetic and nonmagnetic Fe loss and gain is visualized in crossplot Figure 8d.

From the data point distribution of the magnetically depleted and enhanced samples (Fig. 8) some fundamental characteristics and trends of redoxomorphic iron diagenesis in the central Equatorial Atlantic can be derived:

(1) Loss of susceptibility, i.e. dissolution of magnetite, by reductive diagenesis is limited to C_{org} and Fe rich layers deposited during glacials and their terminations and amounts up to $200 \cdot 10^{-6}$ SI (75% of the initial k). Enhancement of susceptibility, probably by bacterial biomineralization, takes place around C_{org} and Fe poor carbonate maxima overlying the magnetically depleted zones. It reaches up to $50 \cdot 10^{-6}$ SI and may almost double the Ti-derived pristine value. Susceptibility losses greatly exceed the gains.

(2) The Ti-derived pristine susceptibility signal (Fig. 9c, cyan) shows only a weak positive correlation with C_{org} (Fig. 9a) while the budget curve of diagenetic loss and gain (Fig. 9b) is almost an inverse mirror image of C_{org}. Assuming a proportionality of mineralized C_{org} and magnetite dissolution, this would imply that some magnetic depletion peaks during cold oxygen (sub)stages 2, 4, 5.4, 7.4 and 8 are no longer present in the C_{org} record. Very likely, these 'minor' C_{org} maxima were eliminated by a downward progressing oxidation front. As the susceptibility loss is permanent, it may - in analogy to barium - represent a more authentic archive of past C_{org} accumulation than C_{org} content itself, at least under the favorable conditions encountered in the equatorial Atlantic.

(3) With total Fe contents ranging between 1 to 5 wt.% (Fig. 9e, thick black line) the average depletions accounting for less than 0.5 wt.% can be considered as moderate. Susceptibility is greatly reduced in all iron-depleted zones. The iron enrichments (Fig. 9 e, orange) may enhance pristine contents by up to 3 wt.%. Total iron precipitation correlates positively with susceptibility and hence magnetic iron precipitation (Fig. 8d triangles). Yet, the highest Fe enrichments are found around paleo-oxidation fronts, where susceptibility is at loss (Fig. 8 d diamonds and Fig.9 b,d).

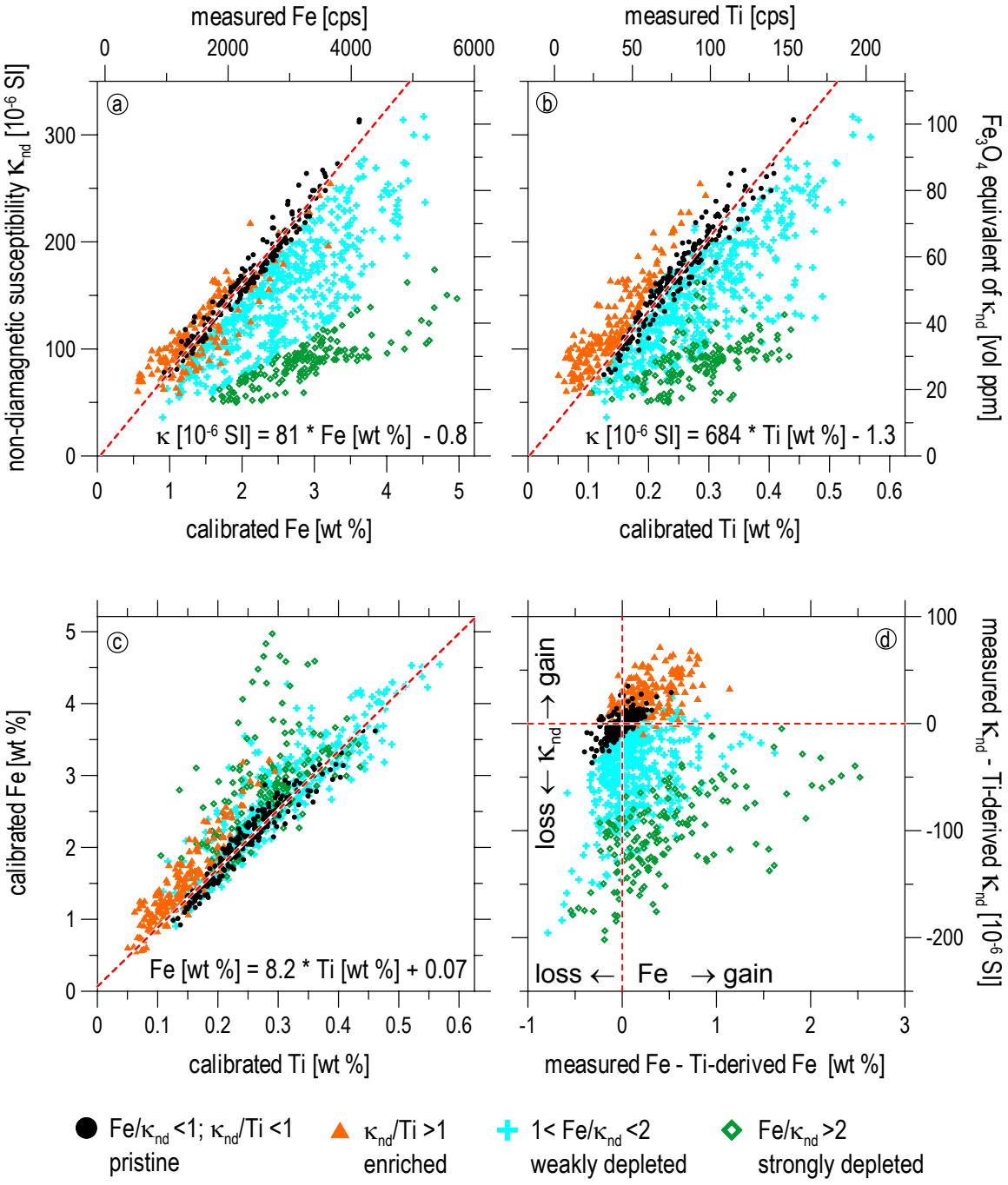

Fig.8. Crossplots of non-diamagnetic susceptibility, Fe and Ti contents of core GeoB 4317-2 quantifying diagenetic loss and gain of magnetic and total Fe. The newly introduced proxies κ_{nd}/Ti and Fe/κ_{nd} are used as criteria to categorize magnetically pristine (black dots), enriched (orange triangles) and weakly (cyan crosses) to strongly (green diamonds) depleted sections (see legend). Diagenetically unaffected sediments show high mutual proportionality of susceptibility, Fe and Ti contents. Their linear regression lines (dashed red lines) pass very near the origin **a-c)**. The regression equations can be used to derive pre-diagenetic κ_{nd} and Fe values for altered sediments on basis of the unaffected Ti contents. In **d),** the differences between measured and Ti-derived pristine susceptibilities as well as Fe contents are cross-plotted. The data scatter over the four quadrants visualizes range and linkage of magnetic and non-magnetic Fe loss and gain in the course of redoxomorphic diagenesis.

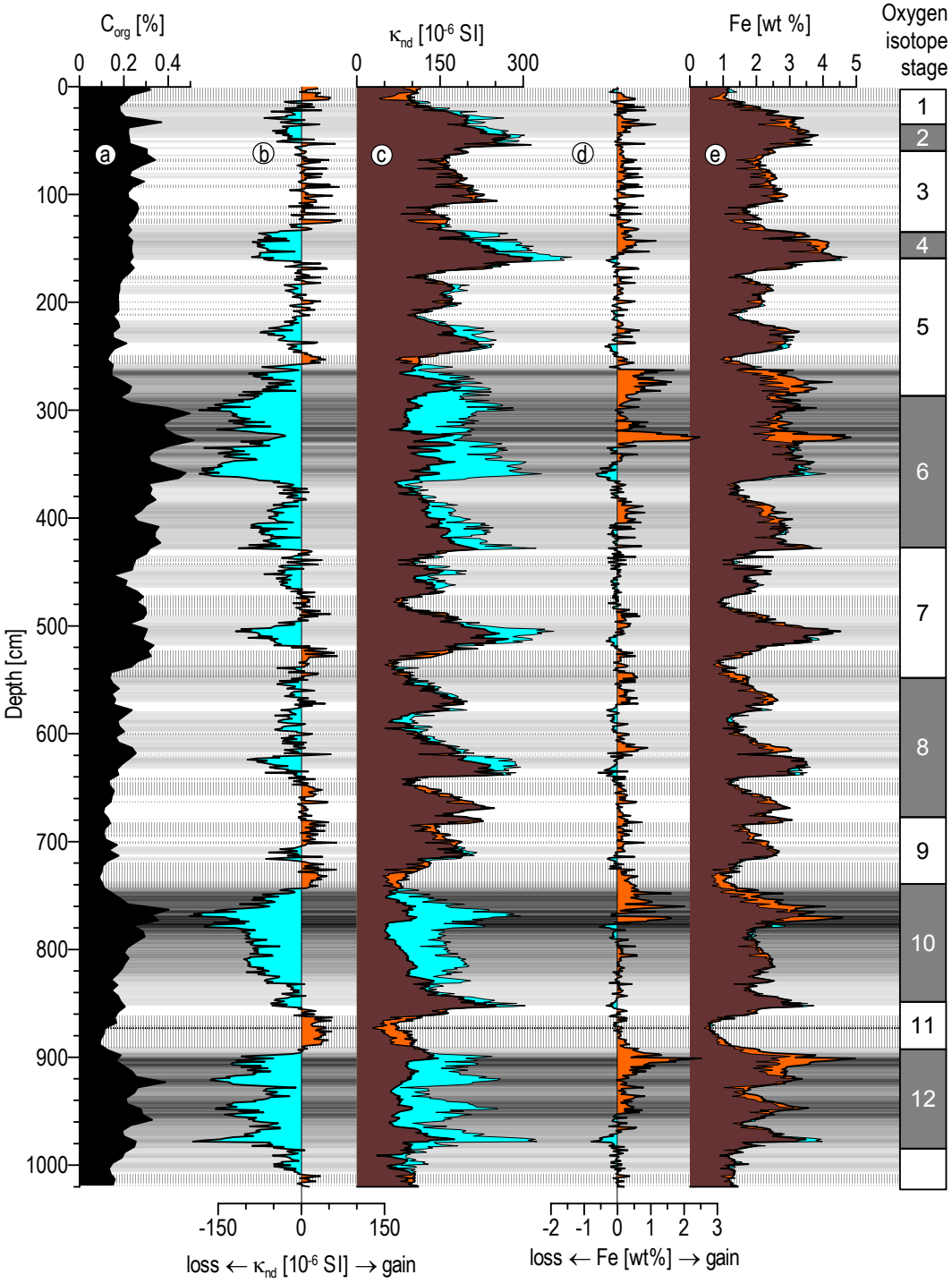

Fig.9. Stratigraphic compilation of C_{org} content **a)** with measured (thick lines) and Ti-derived pristine (thin lines) susceptibility **c)** and Fe **e)** records of core GeoB 4317-2. The calculated loss (cyan) and gain (orange) of magnetic **b)** and non-magnetic **d)** iron is scaled accordingly to curves (c) and (e). Note the reverse patterns of (a) and (b) and the much higher relative losses of magnetic minerals compared to total iron. Background shading indicates the degree of magnetite dissolution based on Fe/κ_{nd}. Magnetic mineral precipitation zones according to κ_{nd}/Ti are shown as hatched areas.

Acknowledgements

We thank officers and crews of RV *Meteor* for their efficient support during cruises M 29/3 and M 38/1. Arguments and constructive criticism raised by U. Bleil and the two peer reviewers, M. Dekkers and S. Banerjee, have greatly improved this manuscript and are gratefully acknowledged. T. Wagner provided C_{org} data of core GeoB 4317-2. U. Röhl made the XRF scanner measurements possible and was very helpful. This study was funded by the Deutsche Forschungsgemeinschaft (Sonderforschungsbereich 261 at Bremen University, contribution No. 385). J.A. Funk was supported by the Deutsche Forschungsgemeinschaft in the framework of Graduiertenkolleg 221. T. von Dobeneck is a visiting research fellow at Utrecht University supported by the Netherlands Research Center for Integrated Solid Earth Science (ISES). Data are available under www.pangaea.de/Projects/SFB261.

References

Banerjee SK (1971) Decay of marine magnetic anomalies by ferrous ion diffusion. Nature: Physical Science 229: 181–183

Bazylinski DA, Frankel RB, Jannasch HW (1988) Anaerobic magnetite production by a marine, magnetotactic bacterium. Nature 334: 518–519

Bickert T and Wefer G (1996) Late Quaternary deep water circulation in the South Atlantic: Reconstruction from carbonate dissolution and benthic stable isotopes. In: Wefer G, Berger WH, Siedler G, Webb DJ (eds) The South Atlantic: Present and Past Circulation. Springer, Berlin, pp 599-620

Blakemore RP (1975) Magnetotactic bacteria. Science 190: 377-379

Bloemendal J, Lamb B, King J (1988) Paleoenvironmental implications of rock - magnetic properties of Late Quaternary sediment cores from the eastern Equatorial Atantic. Paleoceanography 3: 61-87

Bloemendal J, King JW, Hall FR, Doh S-J (1992) Rock magnetism of late Neogene and Pleistocene deep-sea sediments: Relationship to sediment source, diagenetic processes, and sediment lithology. J Geophys Res 97: 4361-4375

Brown ET, Le Callonnec L, German CR (2000) Geochemical cycling of redox-sensitive metals in sediments from Lake Malawi: A diagnostic paleotracer for episodic changes in mixing depth. Geochim Cosmochim Acta 64: 3515-3523

Burdige DJ (1993) The biochemistry of manganese and iron reduction in marine sediments. Earth Sci Rev 35: 249-284

Butler RF and Banerjee SK (1975) Theoretical single-domain grain size range in magnetite and titanomagnetite. J Geophys Res 80: 4049–4058

Calvert SE and Pedersen TF (1993) Geochemistry of recent oxic and anoxic marine sediments: Implications for the geological record. Mar Geol 113: 67-88

Canfield DE, Raiswell R, Bottrell S (1992) The reactivity of sedimentary iron minerals toward sulfide. Amer J of Sci 292: 659-683

Canfield DE (1997) The geochemistry of river particles from the continental USA: Major elements. Geochim Cosmochim Acta 61: 3349 - 3365

Dapples EC (1962) Stages of diagenesis in the development of sandstones. Bull Geol Soc Am 73: 913-934

Day R, Fuller M, Schmidt VA (1977) Hysteresis properties of titanomagnetites: Grain-size and compositional dependence. Phys Earth Planet Inter 13: 260-267

Dearing JA, Dann RJL, Hay K, Lees JA, Loveland PJ, Maher BA, O'Grady K (1996) Frequency dependent susceptibility measurements of environmental materials. Geophys J Int 124: 228-240

Dekkers MJ, Langereis CG, Vriend SP, van Santvoort PJM, de Lange GJ (1994) Fuzzy c-means cluster analysis of early diagenetic effects on natural remanent magnetisation acquisition in a 1.1 Myr piston core from the Central Mediterranean. Phys Earth Planet Inter 85: 155-171

deMenocal PB, Ruddiman WF, Pokras EM (1993) Influences of high- and low- latitude processes on African terrestrial climate: Pleistocene eolian records from equatorial Atlantic ocean drilling program Site 663. Paleoceanography 8: 209-242

Fischer G and cruise participants (1998) Report and preliminary results of *Meteor* cruise M38/1. Ber Fachber Geowiss Univ Bremen 94, pp 1-178

Frederichs T, Bleil U, Däumler K, von Dobeneck T, Schmidt A (1999) The magnetic view on the marine paleoenvironment: Parameters, techniques, and potentials of rock magnetic studies as a key to paleoclimatic and paleoceanographic changes. In: Fischer G and Wefer G (eds) Use of Proxies in Paleoceanography: Examples from the South Atlantic, Springer, Berlin, pp 575-599

Froelich PN, Klinkhammer GP, Bender ML, Luedtke NA, Heath GR, Cullen D, Dauphin P, Hammond D, Hartman B, Maynard V (1979) Early oxidation of

organic matter in pelagic sediments of the eastern equatorial Atlantic: Suboxic diagenesis. Geochim Cosmochim Acta 43: 1075-1090

Gladney ES and Roelandts I (1988) 1987 compilation of elemental concentration data for USGS BHVO-1, MAG-1, QLO-1, RGM-1, SCO-1, SDC-1, SGR-1 and STM-1. Geostandards Newsletters 12: 253-362

Haese, RR (2000) The reactivity of iron. In: Schulz HD and Zabel M (eds), Marine Geochemistry. Springer, Berlin, pp 233-262

Heider F, Zitzelsberger A, Fabian F (1996) Magnetic susceptibility and remanent coercive force in grown magnetite crystals from 0.1 μm to 6 mm. Phys Earth Planet Inter 93: 239-256

Jansen JHF, Van der Gaast SJ, Koster AJ (1998) CORTEX, a shipboard XRF-scanner for element analyses in split sediment cores. Mar Geol 151: 143-153

Karlin R (1990a) Magnetic mineral diagenesis in suboxic sediments at Bettis Site W-N, NE Pacific Ocean. J Geophys Res 95: 4421-4436

Karlin R (1990b) Magnetite diagenesis in marine sediments from the Oregon continental margin. J Geophys Res 95: 4405-4419

Karlin R and Levi S (1983) Diagenesis of magnetic minerals in recent haemipelagic sediments. Nature 303: 327-330

Karlin R, Lyle M, Heath GR (1987) Authigenic magnetic formation in suboxic marine sediments. Nature 326: 490-493

Kidd RB, Cita MB, Ryan WBF (1978) Stratigraphy of eastern Mediterranean sapropel sequences recovered during DSDP Leg 42A and their paleoenvironmental significance. In: Hsü KJ and Montadert L et al. (eds), Initial Reports of the Deep Sea Drilling Project 42A, U.S. Government Printing Office, Washington: pp 421-443

Kruiver PP and Passier HF (2001) Coercivity analysis of magnetic phases in sapropel S1 related to variations in redox conditions, including an investigation of the S ratio. Geochemistry Geophysics Geosystems 14 December: 1-21

König I, Drodt M, Suess E, Trautwein AX (1997) Iron reduction through the tan - green color transition in deep-sea sediments. Geochim Cosmochim Acta 61: 1679-1683

Langereis CG and Dekkers MJ (1999) Magnetic cyclostratigraphy: High resolution dating in and beyond the Quaternary and analysis of periodic changes in diagenesis and sedimentary magnetism. In: Maher B and Thompson R (eds) Quaternary Climates, Environments and Magnetism. Cambridge University Press, pp 352-382

Lecoanet H, Lévêque F, Segura S (1999) Magnetic susceptibility in environmental applications: Comparison of field probes. Phys Earth Planet Inter 115: 191-204

Lovley DR, Stolz JF, Nord GL Jr, and Phillips EJP (1987) Anaerobic production of magnetite by a dissimilatory iron-reducing microorganism. Nature 330: 252–254

Lyle M (1983) The brown-green color transition in marine sediments: A marker of the Fe(III)-Fe(II) redox boundary. Limnol Oceanogr 28: 1026-1033

Lyle M (1988) Climatically forced organic carbon burial in equatorial Atlantic and Pacific Oceans. Nature 335: 529-532

Maher BA (1988) Magnetic properties of some synthetic submicron magnetites. Geophys J 94: 83–96

Mudroch A and Azcue JM (1995) Manual of aquatic sediment sampling. Lewis Publishers, Boca Raton, 219 p

Nowaczyk NR and Antonow M (1997) High-resolution magnetostratigraphy of four sediment cores from the Greenland Sea I. Identification of the Mono Lake excursion, Laschamp and Biwa I / Jamaica geomagnetic polarity events. Geophys J Int 131: 310-324

Passier HF, Dekkers MJ, de Lange GJ (1998) Sediment chemistry and magnetic properties in an anomalously reducing core from the eastern Mediterranean Sea. Chem Geol 152: 287-306

Petermann H and Bleil U (1993) Detection of live magnetotactic bacteria in South Atlantic deep-sea sediments. Earth Planet Sci Lett 117: 223-228

Robinson SG, Sahota JTS, Oldfield F (2000) Early diagenesis in North Atlantic abyssal plain sediments characterized by rock magnetic and geochemical indices. Mar Geol 163: 77-107

Röhl U and Abrams LJ (2000) High-resolution downhole and nondestructive core measurements from Sites 999 and 1001 in the Caribbean Sea: Application to the Late Paleocene thermal maximum. In: Leckie RM, Sigurdsson H, Acton GD, Draper G (eds) Proc ODP Sci Results 165. College Station, TX, pp 191-203

Rosenbaum JG, Reynolds RL, Adam DP, Drexler J, Sarna-Wojcicki AM, Whitney GC, (1996) Record of middle Pleistocene climate change from Buck Lake, Cascade Range, southern Oregon - evidence from sediment magnetism, trace-element geochemistry, and pollen. Bull Geol Soc Am 108: 1328-1341

Ruddiman WF and Janecek TR (1989) Pliocene-Pleistocene biogenic and terrigenous fluxes at equatorial Atlantic Sites 662, 663, and 664. In: Ruddiman W and Sarnthein M (eds) Proc ODP Sci Results 108. College Station, TX, pp 211-240

Schmieder F, von Dobeneck T, Bleil U (2000) The Mid-Pleistocene climate transition as documented in the

deep South Atlantic Ocean: Initiation, interim state and terminal event. Earth Planet Sci Lett 179: 539-549

Smirnov AV and Tarduno JA (2000) Low-temperature magnetic properties of pelagic sediments (Ocean Drilling Program Site 805C): Tracers of maghemitization and magnetic mineral reduction. J Geophys Res 105: 16,457-16,471

Snowball IF (1993) Geochemical control of magnetite dissolution in subarctic lake sediments and the implications for environmental magnetism. J Quater Sci 8: 339-346

Tarduno JA (1994) Temporal trends of magnetic dissolution in the pelagic realm: Gauging paleoproductivity? Earth Planet Sci Lett 123: 39-48

Tarduno JA, Tian W, Wilkison S (1998) Biogeochemical remanent magnetization in pelagic sediments of the western equatorial Pacific Ocean. Geophys Res Lett 25: 3987-3990

Tarduno JA and Wilkison SL (1996) Non-steady state magnetic mineral reduction, chemical lock-in, and delayed remanence acquisition in pelagic sediments. Earth Planet Sci Lett 144: 315-326

Thompson R and Oldfield F (1986) Environmental Magnetism. Allen & Unwin, London, UK, 227 pp

Thomson J, Jarvis I, Green DRH, Green D (1998) Oxidation fronts in Madeira abyssal plain turbidites: Persistence of early diagenetic trace-element enrichments during burial, Site 950. In: Weaver PPE, Schmincke H-U, Firth JV, Duffield W (eds) Proc ODP Sci Results 157. College Station, TX, pp 559-571

Thomson J, Mercone D, de Lange GJ, van Santvoort PJM (1999) Review of recent advances in the interpretation of eastern Mediterranean sapropel S1 from geochemical evidence. Mar Geol 153: 77-89

van Santvoort PJM, de Lange GJ, Langereis CG, Dekkers MJ, Paterne M (1997) Geochemical and paleomagnetic evidence for the occurence of 'missing' sapropels in eastern Mediterranean sediments. Paleoceanography 12: 773-786

van Santvoort PJM, de Lange GJ, Thomson J, Cussen H, Wilson TRS, Krom MD, Ströhle K (1996) Active post-depositional oxidation of the most recent sapropel (S1) in sediments of the eastern Mediterranean Sea. Geochim Cosmochim Acta 60: 4007-4024

Verardo DJ and McIntyre A (1994) Production and destruction: Control of biogenous sedimentation in the tropical Atlantic 0-300,000 years B.P. Paleoceanography 9: 63-86

Vigliotti L, Capotondi L, Torii M (1999) Magnetic properties of sediments deposited in suboxic - anoxic environments: Relationships with biological and geochemical proxies. In: Tarling DH and Turner P (eds), Paleomagnetism and Diagenesis in Sediments. Geol Soc Spec Publ London, 151: pp 71-83

von Dobeneck T (1996) A sytematic analysis of natural magnetic mineral assemblages based on modelling hysteresis loops with coercivity-related hyberbolic basis functions. Geophys J Int 124: 675-694

Walden J and White K (1997) Investigation of the controls on dune colour in the Namib Sand Sea using mineral magnetic analyses. Earth Planet Sci Lett 152: 187-201

Worm H-U and Jackson M (1999) The superparamagnetism of Yucca Mountain Tuff. J Geophys Res B: Solid Earth 104: 25,415-25,425

Chapter 3

Late Quaternary Sedimentation and Early Diagenesis in the Equatorial Atlantic Ocean: Patterns, Trends and Processes Deduced from Rock Magnetic and Geochemical Records

J.A. Funk[1*], T. von Dobeneck[1,2], T. Wagner[3] and S. Kasten[1]

[1]*Universität Bremen, Fachbereich Geowissenschaften, Postfach 33 04 40, D-28334 Bremen, Germany*
[2]*Paleomagnetic Laboratory 'Fort Hoofddijk', Faculty of Earth Sciences Utrecht University, Budapestlaan 17, 3584 CD Utrecht, The Netherlands*
[3]*Woods Hole Oceanographic Institution, Marine Chemistry and Geochemistry Dept., Fye Laboratory (MS#4), 360 Woods Hole Rd, Woods Hole, MA 02543-1543, USA*
[*] *corresponding author (e-mail): funk@uni-bremen.de*

Abstract: This is an interdisciplinary and synoptic study of Equatorial Atlantic sediment formation in the Late Quaternary aimed at untangling the interlaced signatures of terrigenous and biogenous deposition and early diagenesis. It is based on a stratigraphic network of 16 gravity core records arranged along one meridional and three zonal transects (4°N, 0° and 4°S) crossing the Amazon and Sahara plumes as well as the Equatorial Divergence high productivity region. All newly introduced sediment sequences are collectively dated by their coherent $CaCO_3$ content profiles and two available $\delta^{18}O$ age models. To infer proxy records indicative of individual fluxes and processes, we analyze environmental magnetic parameters describing magnetite concentration, magnetic grain sizes and magnetic mineralogy along with $CaCO_3$, C_{org}, Fe, Mn, Ba and color data. Diagenetically affected layers are identified by a newly introduced Fe/κ index. Reach and climatic variability of the major regional sedimentation systems is delimited from lithological patterns and glacial/interglacial accumulation rate averages. The most prominent regional trends are the N-S decrease in terrigenous accumulation and the Equatorial Divergence high in glacial C_{org} accumulation, which decays much faster south- than northwards. Glacial enrichments in C_{org} and proportional depletions in $CaCO_3$ content appear to reflect sedimentary carbonate diagenesis more than lysoclinal oscillations and dominate temporal lithology changes. Suboxic iron mineral reduction is low at Ceará Rise and Sierra Leone Rise, but more intense on both flanks of the Mid-Atlantic ridge, where it occurs within organic rich layers deposited during oxygen isotope stages 6, 10 and 12, in particular at the terminations. To the equator, these zones reflect a full precessional rhythm with individual diagenesis peaks merging into broader magnetite-depleted zones. Rock magnetic and geochemical data show, that the depths of the Fe^{3+}/Fe^{2+} redox boundary in the Equatorial Atlantic are not indicative of average productivity and were frequently shifted in the past. They are now located just above the topmost preserved productivity pulse. At 4°N, this organically enriched layer coincides with glacial stage 6, at 0° with glacial stage 2. Subsequent oxic and suboxic degradation of organic material entails stratigraphically coincident carbonate and magnetite losses opening new analytical perspectives.

Introduction

The Equatorial Atlantic is an interesting and well established research area for the general discussion of marine sedimentation, land-ocean linkage and early diagenesis through Quaternary climates. Its model character results from pronounced west-east asymmetries with regard to transport pathways and flux rates of terrigenous matter, which has both lithogenic (e.g. Ratmeyer et al. 1999a,b) and organic (e.g. Wagner 2000, Dupont et al. 2000) components.

From WEFER G, MULITZA S, RATMEYER V (eds), 2004, *The South Atlantic in the Late Quaternary: Reconstruction of Material Budget and Current Systems.* Springer-Verlag Berlin Heidelberg, pp 461-497

In its western part, terrigenous sedimentation is dominated by the massive discharge of the Amazon river (Showers and Angle 1986, Bleil and von Dobeneck, this volume). Under modern interglacial conditions, much of the suspended load is deposited on the shelf or carried away by the northwestward North Brazil Current (NBC). The sea-level fall in glacial periods causes erosion of the inner continental shelf and channels the discharge directly into the Amazon Canyon (Milliman et al. 1975; Damuth 1977), intensifying mass-flow events on the slopes of the Amazon Fan (Maslin and Mikkelsen 1997). Terrigenous particle fluxes reach the Ceará Rise either by surface transport via a retroflection of the NBC into the North Equatorial Countercurrent (Johns et al. 1990) or by intensified nepheloid transport via the southeastward directed North Atlantic Deep Water (NADW) flow (Kumar and Embley 1977; François and Bacon 1991).

In its eastern part, supply and distribution of terrigenous matter is controlled by eolian dust transport from African source areas. Passat and Harmattan wind systems carry large amounts of dust to the deep-sea in response to glacial-interglacial variations in African aridity (deMenocal et al. 1993; Ruddiman 1997; Sarnthein et al. 1981; Tiedemann et al. 1989). Main glacial source areas for dust reaching the central and eastern Equatorial Atlantic were localized in the semi-desert Sahel Zone surrounding Lake Chad (Ruddiman and Janecek 1989; Bonifay and Giresse 1992). Various paleoclimatic studies have demonstrated that fluctuations in African aridity closely corresponded to changes in high latitude ice volume and North Atlantic sea surface temperatures (Sarnthein et al. 1982; Street-Perrott and Perrott 1990; Tiedemann et al. 1994; see review in Zabel and Wagner, this volume). DeMenocal et al. (1993) proposed that African terrestrial climate responded most sensitively to high latitude sea surface temperatures and an intensification of the trade winds at low latitudes during peak glacial conditions while precessional forcing in the tropics was lowest. Both mechanisms are considered to promote stronger African aridity and enhanced dust transport in glacial periods.

Apart from the aspect of land-ocean linkage, the equatorial sector of the Atlantic Ocean plays a key role for the interhemispheric transfer of deep and surface water masses and the complex interchange of African and South American continental climate, which effectively forces the movement of the surface waters of the low latitude current system (e.g Pickard and Emery 1990; Wefer et al. 1996). It is through this wide gap between tropical Africa and South America that young, oxygen-rich NADW flows south into the South Atlantic and further to the Indian and Pacific Ocean, thus conveying oxygen to most major deep ocean basins (Broecker and Denton 1989). Above and below the NADW, Antarctic Intermediate Water (AAIW) and corrosive Antarctic Bottom Water (AABW) flow northwards through the equatorial region into the North Atlantic causing distinct gradients in deep ocean chemistry especially in the western Equatorial Atlantic (Curry 1996; Lutjeharms 1996; Rhein et al. 1996).

The interaction of atmospheric and oceanic circulation patterns controls organic and carbonate carbon production and preservation in the modern Equatorial Atlantic. These boundary conditions recurrently changed in response to orbitally forced Quaternary glacial-interglacial cycles (deMenocal et al. 1993; Duplessy et al. 1996; Raymo et al. 1997; Sarnthein et al.,1994; Verardo and McIntyre 1994) leaving characteristic features in the sedimentological, geochemical and micropaleontological deep sea record of all low latitude oceans. The coupling of high latitude forced dust supply and productivity-driven organic sedimentation nourishes the assumption that a combination of mechanisms similar to those observed in the modern Arabian Sea and off NW-Africa had control on organic carbon accumulation below the Equatorial Divergence. The persistently high supply of clay-sized lithogenic dust (up to 85% of the bulk lithogenic matter at ODP Site 663 in the central Equatorial Atlantic according to Rath et al. (1999)) probably accelerated the interaction with newly formed labile organic matter.

Climate-related changes in oceanic circulation and productivity led to the cyclic formation of organic-rich layers (ORLs) in marine sediments and can usually be associated with orbital rhythms (Lyle 1988; Rossignol-Strick et al. 1982). ORLs are not only found in high-productivity regions and stagnant basins, but also in presently oligotrophic open oceans. Mesozoic to Quaternary Equatorial Atlantic

sediment sections typically include horizons of darker color, which are relatively enriched in organic carbon (Wagner 2002). The Pleistocene to modern layers were formed during glaciations by enhanced organic carbon fluxes from more productive surface waters. The higher productivity of the glacial tropical Atlantic Ocean is attributed to increased oceanic and coastal upwelling as well as to a generally stronger mixing in response to stronger temperature gradients, winds, and currents (Müller et al. 1983). The accumulation of organic carbon was additionally favored by a slow-down of bottom water exchange with better preservation conditions for freshly deposited organic matter (Verardo and McIntyre 1994).

In interglacial periods, the formation of Antarctic bottom waters was reduced (Oppo and Fairbanks 1987) and more young, oxygen-rich NADW moved southwards to the equatorial Atlantic region (Boyle and Keigwin 1985) thereby enhancing organic carbon remineralization in the water column, and, by downward diffusion, also in the underlying suboxic glacial sediments (Kasten et al. 2001). Effects and signatures of such downward propagating oxidation fronts have also been observed at the tops of organic-rich turbidites (Wilson et al. 1985; Wilson et al. 1986) and were shown to significantly alter sapropel units in the eastern Mediterranean (Higgs et al. 1994; van Santvoort et al. 1996; Passier and Dekkers 2002).

Magnetic and geochemical sediment properties react sensitively and irreversibly to temporarily reducing conditions. In the absence of energetically more favorable electron acceptors, detrital magnetite is progressively reduced and subsequently transformed into authigenic iron sulfides (Karlin and Levi 1983; Karlin and Levi 1985; Canfield and Berner 1987; Karlin 1990). Organic-rich turbidite deposits (Robinson et al. 2000), paleooxidation fronts (Sahota et al. 1995), sapropels (Passier et al. 1998; van Santvoort et al. 1997), and pelagic sediment sequences (Tarduno 1994) have been characterized via the processes of reductive magnetite diagenesis. In a methodical companion paper, Funk et al. (this volume) describe a novel non-destructive method to detect the level of diagenetic magnetite depletion and enhancement by combining rock magnetic analytics with X-ray fluorescence spectrometry. Suboxic carbon diagenesis, however, not only alters $Mn^{(IV)}$ and $Fe^{(III)}$ minerals. In an earlier process, aerobic degradation of organic matter liberates CO_2 which in turn dissolves calcium carbonate (Martin and Sayles 1996; Schulte and Bard, submitted).

This two-part synthesis addresses the physical mixing and chemical interaction of terrigenous and biogenous sediment fluxes in a temporal and regional context and investigates the distribution of ORLs from a paleoceanographic perspective. For this interdisciplinary interpretation geophysical and geochemical proxy records of Late Quaternary sediment sequences arranged in three zonal core profiles have been combined. The study region links the Ceará Rise in the west, the Sierra Leone Rise in the east, the Equatorial Divergence Zone in the center and the boundary regions to the oligotrophic subtropical gyre in the south.

In the first, sedimentologically oriented part, we take a synoptic view at glacial-interglacial patterns and trends of primary accumulation and secondary alteration of carbon, carbonate and ferric iron minerals. By exploiting the analogy of magnetite and calcite dissolution in the course of early diagenesis, we provide new insights into general and regional formation processes of Equatorial Atlantic sediment records.

In the second, geochemically oriented part, some specific signatures of early organic carbon and iron mineral diagenesis are identified with additional parameters and discussed in detail. We investigate the brown/green subsurface color transition and its varying depth position. A partial oxidation of the organic carbon profiles is detected by magnetic and geochemical proxy records. There is also clear evidence for magnetic mineral dissolution below and neoformation above modern and fossil iron redox boundaries.

Materials

This study combines data of 16 selected gravity cores retrieved in the Equatorial Atlantic on six RV *Meteor* cruises (M6/6, M9/4, M16/1, M16/2, M23/3, M29/3, M38/1) between February 1988 and April 1997, and one hydraulic piston core of ODP Site 663 recovered on Leg 108 (Fig. 1, Tab. 1). The

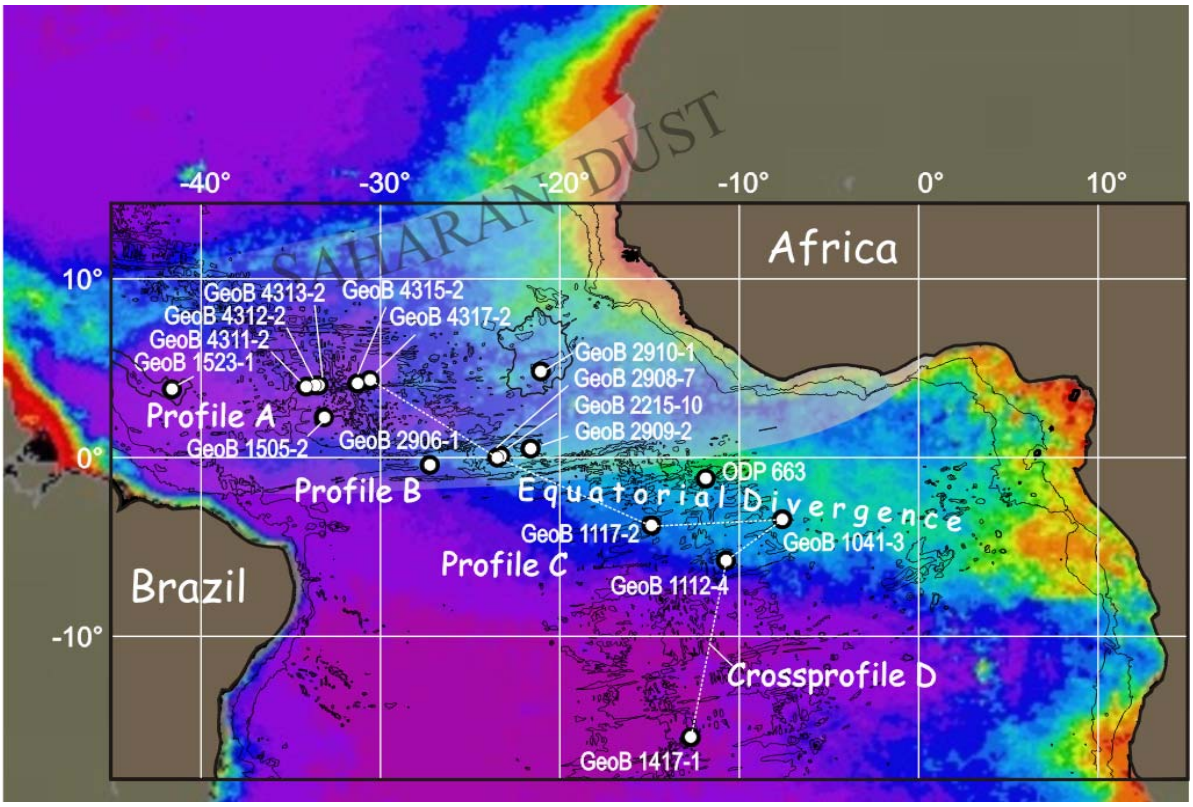

Fig. 1. The sampling sites of cores investigated (white dots) form three zonal transects at 4°N (profile A), 0° (profile B) and 4°S (profile C) and a NW-SE oriented cross transect (profile D, dotted line). The colored graph depicts primary productivity as visualization of the phytoplankton pigment concentration, with increasing values from lilac to red hues (http://seawifs.gsfc.nasa.gov, data collected over the time period November 1978 – June 1986). Saharan dust fall is indicated with a light gray shaded area.

core sites form three zonal transects at 4°N (profile A), 0° (profile B) and 4°S (profile C) and a NW-SE oriented 'quasi-meridional' cross transect (profile D) from 4°N to 15°S. From a total of 23 cores newly investigated for this study, nine were found to be of sufficient quality and interest to be presented here in combination with seven previously published cores.

Profile A (GeoB 1523-1, 1505-2, 4311-2, 4312-2, 4313-2, 4315-2, 4317-2, 2910-1) stretches from the Ceará Rise over the western and eastern flanks of the Mid-Atlantic Ridge to the Sierra Leone Rise. This zone is presently oligotrophic ('blue ocean') and receives high fluvial and eolian input from the Amazon River and the Sahara.

Profile B (GeoB 2906-1, 2908-7, 2215-10, 2909-2, ODP 663) follows the western and central parts of the Equatorial Divergence Zone, a mesotrophic (‘green ocean’) open oceanic upwelling belt. In its western part, this transect is concordant with the boreal winter Intertropical Convergence Zone (ITCZ) and the Southern margin of the Saharan winter dust plume (Wagner 2000).

Profile C (GeoB 1117-2, 1112-4, 1041-3) is south of this line, but it equally transects southern and central parts of the Equatorial Divergence Zone.

Profile D (GeoB 4317-2, 2908-7, 1117-2, 1041-3, 1112-4) cuts from the center of the Saharan dust plume across the Equatorial Divergence Zone into the oligotrophic subtropical South Atlantic. It was assembled from representative cores of profiles A-C and extended by an additional RV *Meteor* gravity core from 15°S (GeoB 1417-1).

Profiles A and D form the basis for a statistical analysis of zonal and meridional trends in Equatorial Atlantic sedimentation and diagenesis. All cores of

Core/ Site	Latitude	Longitude	Core Recovery [m]	Water Depth [m]	Location	Research Cruise, Reference
Profile A						
GeoB 1523-1	3°49,9'N	41°37,3'W	6,65	3292	Ceará Rise	M16/2, [1]
GeoB 1505-2	2°16,0'N	33°00,9'W	8,50	3706	Western flank MAR	M16/2, [1]
GeoB 4311-2	3°59,6'N	34°08,1'W	9,11	4005	Western flank MAR	M38/1, [2]
GeoB 4312-2	4°02,8'N	33°35,6'W	6,01	3438	Western flank MAR	M38/1, [2]
GeoB 4313-2	4°02,8'N	33°26,3'W	8,98	3178	Western flank MAR	M38/1, [2]
GeoB 4315-2	4°10,0'N	31°17,0'W	9,38	3199	Eastern flank MAR	M38/1, [2]
GeoB 4317-2	4°21,3'N	30°36,2'W	12,04	3507	Eastern flank MAR	M38/1, [2]
GeoB 2910-1	4°50,7'N	21°03,2'W	13,91	2703	Sierra Leone Rise	M29/3
Profile B						
GeoB 2906-1	0°24,8'S	27°15,3'W	10,91	3897	Western flank MAR	M29/3
GeoB 2908-7	0°06,4'N	23°19,6'W	10,94	3809	Equatorial MAR	M29/3
GeoB 2215-10	0°00,4'S	23°29,7'W	9,04	3711	Equatorial MAR	M23/3, [3]
GeoB 2909-2	0°29,9'N	21°37,9'W	11,80	4386	Equatorial MAR	M29/3
ODP 663	1°11,9'S	11°52,7'W	153,5	3706	Eastern flank MAR	Leg 108, [4]
Profile C						
GeoB 1117-2	3°48.9'S	14°53.8'W	15,30	3984	Brazil Basin MAR	M9/4, [5]
GeoB 1112-4	5°46,7'S	10°45,0'W	6,91	3125	Guinea Basin MAR	M9/4, [5]
GeoB 1041-3	3°28.5'S	7°36.0'W	11,53	4033	Guinea Basin MAR	M6/6, [6]
Cross Profile D						
GeoB 4317-2	4°21,3'N	30°36,2'W	12,04	3507	Eastern flank MAR	M38/1, [2]
GeoB 2908-7	0°06,4'N	23°19,6'W	10,94	3809	Equatorial MAR	M29/3
GeoB 1117-2	3°48.9'S	14°53.8'W	15,30	3984	Brazil Basin MAR	M9/4, [5]
GeoB 1041-3	3°28.5'S	7°36.0'W	11,53	4033	Guinea Basin MAR	M6/6, [6]
GeoB 1112-4	5°46,7'S	10°45,0'W	6,91	3125	Guinea Basin MAR	M9/4, [5]
GeoB 1417-1	15°32,2'S	12°42,4'W	5,63	2845	MAR	M16/1, [7]

Tab. 1. List of gravity cores, sampling sites, recovered lengths, depth soundings, locations and cruises. Indices correspond to cruise reports by (1) Schulz et al. (1991), (2) Fischer et al. (1998), (3) Wefer et al. (1994), (4) deMenocal et al. (1993), (5) Wefer et al. (1989), (6) Wefer et al. (1988), (7) (Wefer et al. (1991).

profiles A and B were newly investigated for this study, with the exception of cores GeoB 1523-1 (Rühlemann et al. 1996), 1505-2 (Zabel et al. 1999), 2910-1 (Haese et al. 1998) and ODP 663 (deMenocal et al. 1993). For core GeoB 4317-2 dry bulk densities were provided by P.J. Müller (unpublished, Universität Bremen). For the profiles C and D we refer to literature cvdata published by Bickert (1992) and Thießen (1993) (GeoB 1117-2 and 1041-3) and Meinecke (1992) (GeoB 1112-4 and 1417-1). Core data and age models are available in the PANGAEA database (www.pangaea.de).

The cores were collected at water depths ranging between 4400 m and 2700 m (Tab. 1). Their records reach 300 to 500 kyr back, covering the full Late Quaternary. A specific chapter is devoted to the chronostratigraphy. The calcareous biogenic

sediments consist mainly of foraminiferal and nannofossil oozes (Fischer et al. 1998), have only minor contents of opal (< 5 %) (Gingele and Dahmke 1994, deMenocal et al. 1993) and considerably differing portions of clastic and clayey material (total range 5-70 %). This broad lithological variability is reflected in vivid sediment color changes illustrated for two cores in Fig. 15.

Methods

Rock Magnetic Analyses

Magnetic volume susceptibility κ was measured on split-core archive halves with a *Bartington* MS2 susceptibility meter with MS2F-type spot sensor at 1 cm intervals. Magnetic volume susceptibility consists of ferri- (κ_{fer}), para- (κ_{para}) and diamagnetic (κ_{dia}) contributions. Under oxic marine conditions $\kappa \approx \kappa_{fer}$ is a linear measure of minerals of the (titano) magnetite and -maghemite series. The diamagnetic susceptibility κ_{dia} is a negative, almost constant background signal which was subtracted from κ using an average value of $-15 \cdot 10^{-6}$ for carbonate, quartz and water according to Schmieder et al. (2000). The resulting parameter is termed non-diamagnetic magnetic susceptibility (κ_{nd}) and is proportional to ferri- and paramagnetic mineral contents.

The combined magnetic/geochemical ratio Fe/κ_{nd} has been identified as a quantitative proxy parameter for reductive magnetite diagenesis (Funk et al., this volume) suitable for most open ocean settings. While for pristine sediments this ratio is typically at a constant, source-dependent value, the diagenetic depletion of ferric minerals leads to a marked decrease of susceptibility and increase of Fe/κ_{nd}. Using κ instead of κ_{nd} in this ratio can lead to singularities in the case of nearly diamagnetic sediments ($\kappa \approx 0$).

By neglecting the influence of paramagnetic and antiferromagnetic components on susceptibility, the magnetite accumula-tion rate AR_{mag} can be estimated from the magnetic volume susceptibility κ_{nd} by using the equation of Schmieder et al. (2000):

$$AR_{\mathrm{mag}} = \frac{\kappa_{\mathrm{nd}} \cdot SR \cdot \rho_{\mathrm{mag}}}{\kappa_{\mathrm{mag}}}$$

with sedimentation rate SR, a magnetite volume susceptibility κ_{mag} of 3.1 and density ρ_{mag} of 5200 kg/m^3. Accumulation rates are based on linearly interpolated ages and therefore tend to create artificial variability at tie points.

Cores GeoB 4317-2 and GeoB 2908-7 were subsampled at 5 cm intervals for hysteresis measurements using a preparation technique described by von Dobeneck (1996). Hysteresis and backfield measurements to maximum fields of 300 mT were carried out on a *Princeton Measurement Corporation* M2900 alternating gradient force magnetometer. The program 'HYSTEAR' by von Dobeneck (1996) was used for data processing. It provides the ratio of non-ferrimagnetic susceptibility to total susceptibility χ_{nf}/χ_{tot}, a measure of the relative contribution of paramagnetic and diamagnetic sediment constituents to total susceptibility. This hysteresis-based ratio is similar to the above described diagenesis proxy parameter Fe/κ_{nd} (Funk et al., this volume).

For rock magnetic remanence measurements cubic 6.2 cm^3 single samples were collected from split-core sections at 5 cm intervals. An anhysteretic remanent magnetization M_{ar} was imparted by superimposing a DC field of 0.04 mT over a decaying AC demagnetizing field of 250 mT. M_{ar} particularly quantifies magnetite of single-domain (SD; 0.03<d<0.1 µm; Dunlop,1973) and pseudo-single-domain (PSD; 0.1 µm<d<1-10 µm; Parry,1965) size. An isothermal remanent magnetization M_{ir} was generated in a direct field of 250 mT, which primarily quantifies the total concentration of magnetite. The M_{ar}/M_{ir} ratio is therefore a proxy parameter of magnetite grain-size (Maher 1988). Both M_{ar} and M_{ir} were measured with a *2G Enter-prises* horizontal pass-through SQUID magneto-meter.

Saturation isothermal remanent magnetization M_{sir} was acquired in an applied DC field of 2.5 T using a *2G Enterprises* pulse magnetizer. The incremental increase of magnetization from 300 mT to 2.5 T is referred to as M_{hir} and quantifies high coercive magnetic minerals, here essentially

hematite. Subsequent to acquisition and measurement of M_{sir}, a back field magnetization M_{bf} at – 300 mT was created to calculate the $S_{-0.3T}$ ratio (Bloemendal et al. 1992) defined as

$$S_{-0.3T} = 0.5 \cdot \left(1 - M_{bf(-0.3T)} / M_{sir}\right)$$
$$\cong M_{ir(0.3T)} / M_{sir} = M_{ir(0.3T)} / \left(M_{ir(0.3T)} + M_{hir}\right)$$

This ratio varies between 0 and 1. A value of 1 represents pure magnetite, lower numbers denote increasingly larger magnetic influence of hematite. The conversion of $S_{-0.3T}$ into relative magnetite and hematite contents involves a highly non-linear and grain-size dependent transfer function.

The rock magnetic data of cores GeoB 1523-1, 1505-2 and 2909-2 were earlier measured using differing field settings and instruments for M_{ar} (0.05 mT direct field, 100 mT and 300 mT alternating fields) and S_{ir} (880 mT, 1000 mT)). Wherever possible, these literature data were converted to recent measurement conditions by using average recalibration factors derived from remanence acquisition curves. This procedure clearly improves the comparability of recent and earlier records, but should not be expected to yield totally consistent data.

X-ray Fluorescence Spectroscopy

Ca, Mn and Fe were determined by X-ray Fluorescence Spectroscopy (XRF) at a depth resolution of 1 cm on surfaces of archive core halves using a non-destructive XRF core logging system especially developed for marine sediments. The general method and its applications are described by Jansen et al. (1998) and Röhl and Abrams (2000). Resulting element data are relative concentrations given in counts per second [cps], but can be calibrated (Funk et al. this volume). Absolute concentrations of aluminum and barium of selected sediment layers were analyzed at 5 cm intervals using a wavelength dispersive *Philips* PW 1400 XRF spectrometer. Prior to analysis, the samples were disintegrated by ultrasonic treatment, dialyzed and washed to remove pore water, ball-milled and pressed.

$CaCO_3$ and TOC Analyses

Analyses of total carbon (TC) and total organic carbon (TOC) of bulk sediments in 5 cm intervals were carried out with a *LECO*-CS 300 infrared analyzer. 100 mg of freeze-dried and homogenized sediment were analyzed with respect to TC. Analytical accuracy was checked using a standard every 10 to 15 samples. For determination of TOC the same amount of sediment was acidified with 6% HCl and measured in the same way. Calcium carbonate content was calculated in weight percentage of the bulk sample by:

$$CaCO_3 \text{ wt.\%} = (\text{TC wt.\%} - \text{TOC wt.\%}) \cdot 8.33$$

Color Reflectance Spectroscopy

Color reflectance of split core surfaces was measured (Fischer et al. 1998) with a handheld *Minolta CM – 2002* spectrophotometer at 5 cm intervals and 31 wavelengths within the visible spectrum from 400 to 700 nm. Iron (oxyhydr)oxides like hematite and goethite are highly reflective around 670 nm. $CaCO_3$ as the major matrix component in the sediments is characterized by a high reflectivity in the range of 470 nm. According to Mix et al. (1992) a 670/470 nm ratio of >1.5 characterizes the oxidized zone in sediments.

Chronostratigraphy

The chronostratigraphies of the newly investigated cores of this study are based on the independently established age models of two reference cores, each representing one of the two profiles A and B (Fig. 1). These two cores were selected owing to their nearly continuous and undisturbed stratigraphic records; they also serve here for further detailed investigations. The age model of core GeoB 4317-2 (Profile A, Fig. 2g,h) was established by correlating its variations in $CaCO_3$ content to that of the $\delta^{18}O$ dated (deMenocal et al. 1993) core ODP 663 (Fig. 3f,g). In the same way, core GeoB 2908-7 (Profile B, Fig.3b,c) was correlated to the $\delta^{18}O$ dated (Bickert,1992) core GeoB 1117-2 (Profile C, Fig.3h,i). According to these age mo-dels, core GeoB 4317-2 spans the last 500 kyr and core GeoB 2908-7 the last 360 kyr.

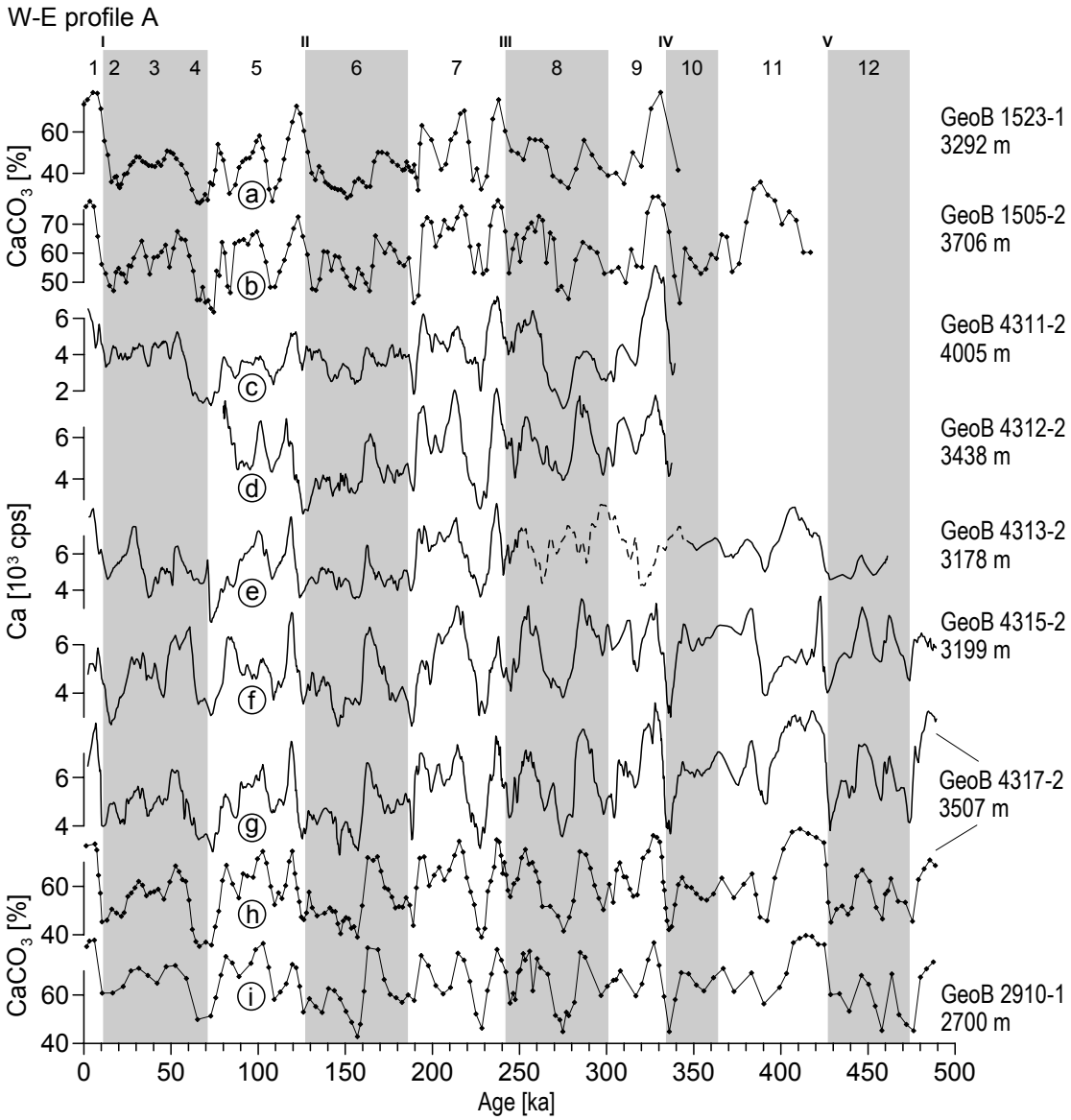

Fig. 2. Variations in $CaCO_3$ (diamonds) and Ca (plain lines) content of cores along profile A (4°N). The prevailing uniform signal pattern in the study area was used to correlate all records (for details and references see text). The $\delta^{18}O$ age model of ODP core 663 (**Fig.3f,g**) was first inherited to core GeoB 4317-2 and subsequently to all others. Ca **g**) and $CaCO_3$ **h**) records are clearly equivalent.

The remaining cores of each transect were primarily dated by correlation of calcium (Ca) records determined with a XRF core scanner in 1 cm intervals. In foraminiferal/nannofossil oozes, Ca profiles are representative of $CaCO_3$ content and allow likewise age modeling by graphic correlation, as demonstrated for cores GeoB 4317-2 (Fig. 2g,h) and GeoB 2908-7 (Fig. 3b,c). The initial Ca signal was smoothed by a three-point moving average.

By paralleling the sediment sequences it became obvious that the uppermost section of core GeoB 4312-2 was lost, possibly during coring (Fig. 2d). A strongly disturbed and diagenetically affected layer in core GeoB 4313-2 (Fig. 2e, dotted line) interrupts the otherwise characteristic pattern over 246 cm. Since no age control was available within this layer, the depth-age relation was assumed linear between top and bottom of this section.

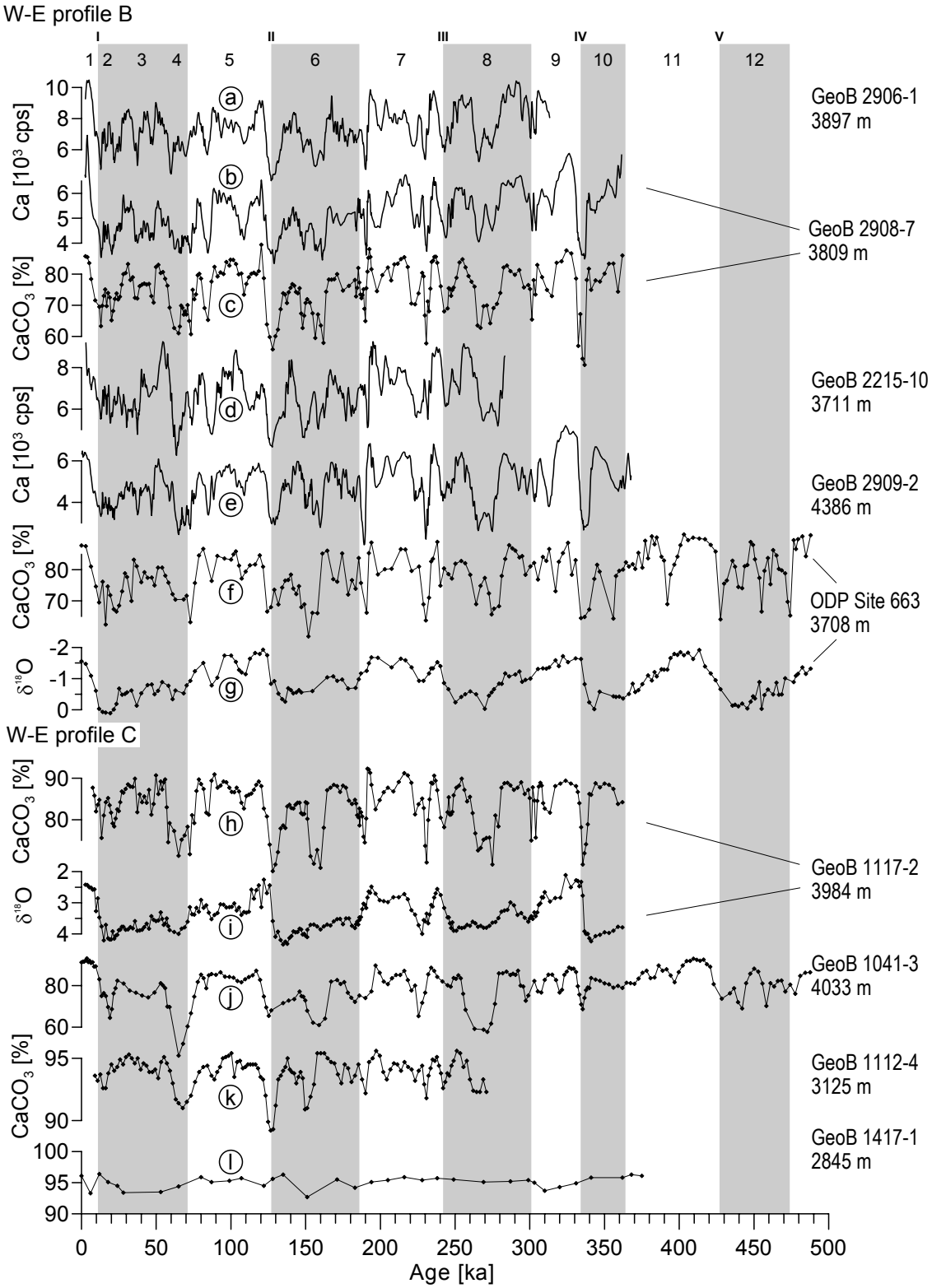

Fig. 3. Same procedure as for profile A has been applied for profile B. Here, core GeoB 2908-7 act as a 'master core' dated by correlation with GeoB 1117-2. Likewise presented are the variations in Ca **b**) and $CaCO_3$ **c**) content. The remaining cores of profile C and D were dated by former investigators (please see text).

The variations in $CaCO_3$ and Ca contents were compared with earlier dated carbonate records from the Equatorial Atlantic (GeoB 1523-1, 1505-2, 2910-1, 1041-3, 1112-4 and 1417-1, see Figs. 2, 3). The close match of the signal patterns down to finest details is striking. The good comparability of individual signal features within a large set of records made a convincing case for a minor readjustment of the earlier age model of core GeoB 2910-1 (Zabel et al. 1999), which resulted in an appre-ciable smoothing of the sedimentation rate in MIS 9. The now existing carbonate based stratigraphic network of the Late Quaternary Equatorial Atlantic Ocean forms a solid fundament for future work.

While the obvious similarities of the shown $CaCO_3$ signals are primordial for chronostratigraphic purposes, their equally obvious dissimilarities form a promising basis to analyze signal formation mechanisms in a regional and temporal framework. The potential and most likely contributing factors are:

1. Variations in primary productivity due to changing nutrient supply to the photic zone. The glacial weakening of the northwesterly North African summer monsoons strengthens the southwesterly trade winds (Kutzbach 1981) causing a rise of the Equatorial Atlantic thermo- and nutricline in the east and a synchronous fall in the west, together with more vigorous mixing and upwelling (Müller et al. 1983).

2. Variations in terrigenous dilution of carbonate by enhanced glacial dust flux from the Sahara and Sahel Zone. This material is eroded under conditions of greater aridity and carried by stronger glacial NE trade winds into the eastern Equatorial Atlantic (Sarnthein et al. 1982; deMenocal et al. 1993).

3. Variations in terrigenous dilution of carbonate by an enhanced discharge of Amazon detritus into the western Equatorial Atlantic during glacial sea level falls and low stands. At high stands, Amazonian sediments are mainly deposited on the continental shelf (Damuth 1977; François et al. 1990; Bleil and von Dobeneck, this volume).

4. Variations in carbonate preservation in the water column due to weaker overturning of glacial NADW resulting in a vertical expansion of AABW entailing a rise of the calcite lysocline by several hundred meters (Gardner and Burkle 1975; Boyle and Keigwin 1982; Raymo et al. 1990; Bickert and Wefer 1996). Curry and Lohmann (1986, 1990) demonstrated, that Quaternary carbonates deposited at the Sierra Leone Rise above 3750 m are generally well preserved, while Rühlemann et al. (1996) associate fractionation of foraminifera at 3300 m depth during extreme glacial stages with influence of southern-source deep water.

5. Variations in carbonate preservation due to carbonate dissolution by metabolic acids released in the course of aerobic OM decomposition in near-surface sediment layers (Martin and Sayles 1996; Pfeifer et al. 2002; Hensen et al., this volume). This process is particularly active in times of enhanced ocean fertility with enhanced $C_{org}/CaCO_3$ rain ratios. According to Martin and Sayles (1996), the modern sedimentary calcite dissolution rate at the presently oligotrophic and supralysoclinal Ceará Rise amounts to as much as 40-60% of the initially deposited $CaCO_3$, although this estimate should be handled with care (see review on carbonate dissolution in the South Atlantic by Henrich et al., this volume).

Patterns, Trends and Formation Processes of Sedimentary Records

Organic Carbon and Carbonate Records

We approach the multi-factorial problem of sedimentary signal formation in the Equatorial Atlantic by investigating and comparing the patterns and trends of various lithostratigraphic parameters, starting out with the relation of carbonate and organic carbon content.

A compilation of organic carbon and calcium carbonate contents along the meridional cross profile D exhibits very pronounced temporal patterns, regional trends and asymmetries (Fig. 4). Both parameters show pronounced climate cyclicity with large contrasts in organic carbon burial at a glacial/interglacial and substage rhythm.

Glacial C_{org} maxima vary widely between 0.25% and 2%, while interglacial C_{org} minima remain at the same low level of about 0.125% throughout the entire Equatorial Atlantic. This

uniformity of recent sedimentary TOC levels contrasts with large modern productivity gradients along profile D indicated by Coastal Zone Color Scanner (CZCS) images (compare to November 1978 – June 1986 chlorophyll pigment concentration in Figure 1). Wagner and Dupont (1999) already observed, that modern, enhanced marine organic carbon fluxes are largely remineralized and therefore not recorded in surface sediments. This situation appears to be a general feature of interglacial conditions. Apparently, only in glacial periods regional productivity pulses have been preserved in the sedimentary archive.

The northernmost core GeoB 4317-2 (4°N, Fig. 4a) is scarcely influenced by the Equatorial Divergence and presently under oligotrophic conditions. On the basis of preserved TOC, there is no evidence for enhanced glacial productivity after termination II. The youngest organic-rich layer (ORL) dates back to MIS 6 reaching the highest observed concentrations of about 0.5% TOC. Similar saw-tooth shaped TOC patterns precede in glacial stages 10 and 12, while MIS 8 compares to the low values encountered in MIS 2 and 4. It will be argued below, that these 'missing ORLs' (in analogy to the term 'missing sapropels' by van Santvoort 1997) may rather be due to a lack of organic carbon preservation than to a lack of deposition. In greater vicinity of the Equatorial Divergence as in core GeoB 2908-7, glacial TOC contents are increasingly higher (Fig. 4b) and fully developed in every glacial stage. A well-defined glacial/interglacial pattern (Lyle 1988) with steeply increasing values is even more evident in cores GeoB 1117-2 and 1041-3 (Bickert 1992) where individual precessional ORLs merge to broader bands covering entire glacial periods, however, with still clearly separated subpeaks.

In core GeoB 1041-3 these carbon enrichments reach TOC concentrations of *sapropelic layers* according to the definition by Kidd et al. (1978), since they are '*discrete, greater than 1 cm in thickness, set in open marine pelagic sediments and containing between 0.5% and 2.0% organic carbon by weight'*. Our data are consistent with findings of Verardo and McIntyre (1994) who describe a fourfold increase in TOC contents during MIS 2 from the margins to the center of the Equatorial Divergence upwelling. The two southernmost records GeoB 1112-4 and 1417-1 (Fig. 4e,f) show constantly high carbonate contents and accordingly low TOC and terrigenous contents. As shown by the enlarged carbonate record of GeoB 1112-4 in Fig. 3k, a faint climate signature at largely reduced amplitude remains.

It is a general feature of all investigated cores, that C_{org} and $CaCO_3$ records are in a broad sense clearly antisymmetric and anticorrelated. This negative correlation is at maximum at the Equatorial Divergence (r = -0.72), still relatively high in the adjacent northern regions (r = -0.46 to -0.36) and goes down to r = -0.17 in the oligotrophic subtropical gyre (Fig. 5a). This negative correlation is even more pronounced, if sediment sections next to terminations are excluded which obviously have been carbon-depleted by burn-down due to a downward progressing postglacial oxidation front (note irregularity in record asymmetry in particular around Termination II).

The inverse pattern of preserved $CaCO_3$ and TOC clearly prohibits the concept of assessing paleoproductivity from carbonate accumulation, which is generally based on the observation, that organic carbon and carbonate fluxes are globally well-correlated in deep-moored sediment traps (Brummer and Van Eijden 1992; Milliman 1993) throughout different oceanic productivity regimes (van Kreveld et al. 1996). Since fluctuations of deep water stratification are not sufficient for explaining the observed effects over the broad range of included core depths, we interpret the observed anticorrelation of $CaCO_3$ and TOC along the lines of Archer and Maier-Reimer (1994) and Martin and Sayles (1996) as an effect of enhanced glacial $C_{org}/CaCO_3$ rain rates entailing calcite dissolution by metabolic CO_2 release in the course of aerobic organic carbon degradation (Wilson and Thomson 1998; Schneider et al. 2000):

$$(CH_2O)_{106}(NH_3)_{16}(H_3PO_4) + 138\ O_2 + 124\ CaCO_3 \rightarrow$$
$$230\ HCO_3^- + 16\ NO_3^- + HPO_4^{2-} + 124\ Ca_2+ + 16\ H_2O$$

While from the stoichiometry of the Redfield ratio, the molar loss relationship of organic carbon and carbonate should not exceed 106:124 (= 1:1.17), ratios above 1:4 were observed in the oxic zones

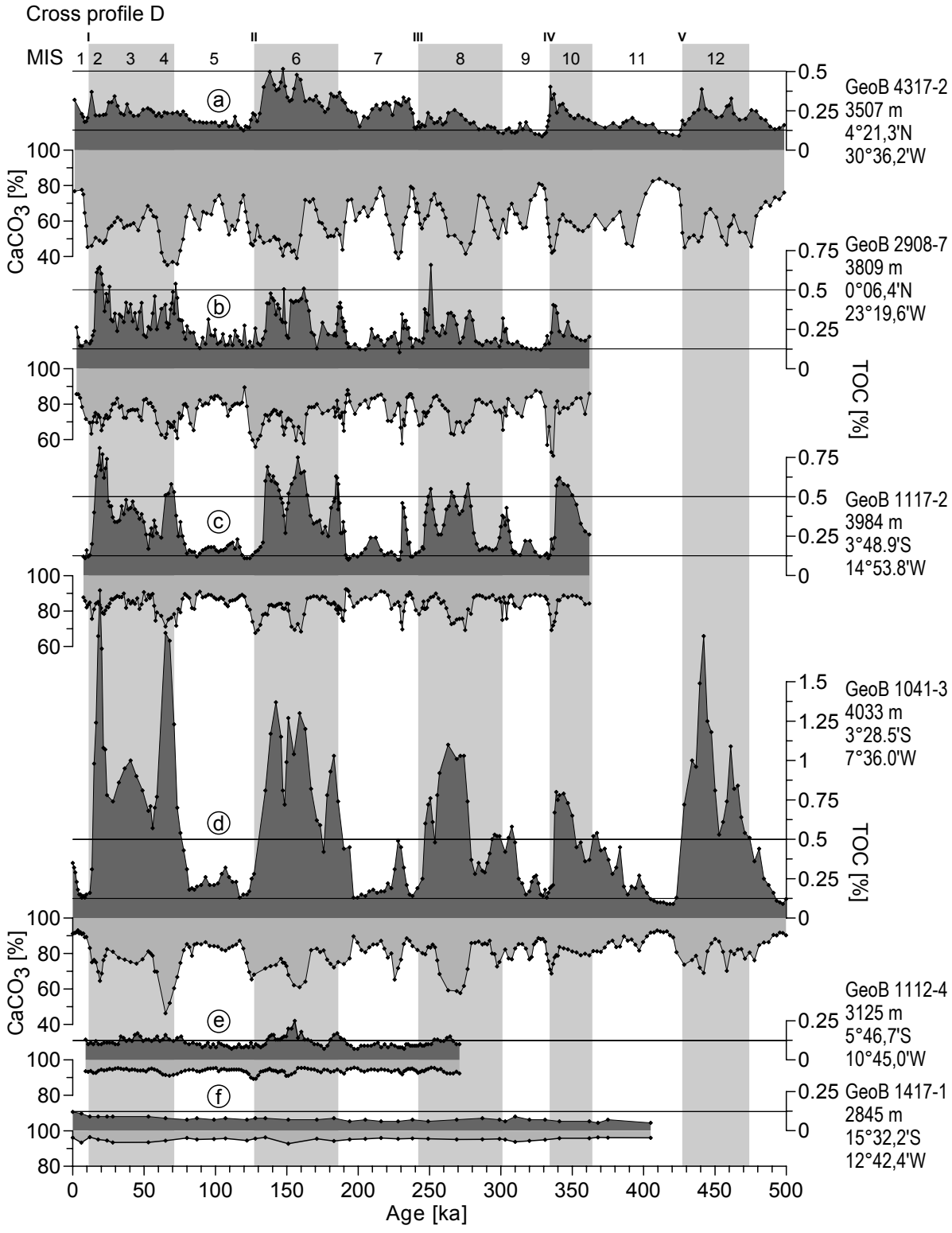

Fig. 4. Anticorrelated records of $CaCO_3$ (dark gray shaded) and C_{org} (light gray shaded) of the meridional cross profile D. Please note offset around terminations probably due to carbon depletion by burn-down in a downward progressing postglacial oxidation front.

of homogenous turbiditic units (Wilson and Thomson 1998). A plausible explanation for progressing carbonate dissolution in spite of relatively low residual TOC contents is bioturbation. Benthic macrofauna constantly mixes organic material from the sediment-water interface down into the shallow oxic zone over just a few cm depth, where it is metabolized and thereby triggers calcite dissolution. In the present-day Western Equatorial Atlantic, benthic R_{Corg} /R_{CaCO3} rain rate ratios are on the order of 1:1 (0.8 to 1.6) (Martin and Sayles 1996) contrasting drastically with average AR_{Corg}/ AR_{CaCO3} ratios documented in our data with numbers between 1:100 and 1:1000 (Fig. 5b). The more than 99% of organic carbon remineralized at around the sediment/water interface are partly available for $CaCO_3$ dissolution by the above depicted bioturbation/-irrigation mechanisms. For the Western Equatorial Atlantic, Martin and Sayles (1996) present model-based estimates of the carbonate dissolution efficiency by aerobic organic carbon degradation. Losses are estimated to reach between 24% and 73% of initial $CaCO_3$ content depending on conditions and assumptions.

The tilt of the connection lines between interglacial and glacial averages of $CaCO_3$ and TOC accumulation rates (Fig. 5b) is positive (productivity signal) or neutral only in strictly oligotrophic southern regions, while it is negative (dissolution signal) around and north of the Equatorial Divergence. Zonal averages of the AR_{Corg}/AR_{CaCO3} ratio of the central core GeoB 1041-3 show the highest contrast between glacial (1:125) and interglacial (1:400) conditions. Productivity estimates based on one or the other record would therefore come to very different and certainly contradictory conclusions.

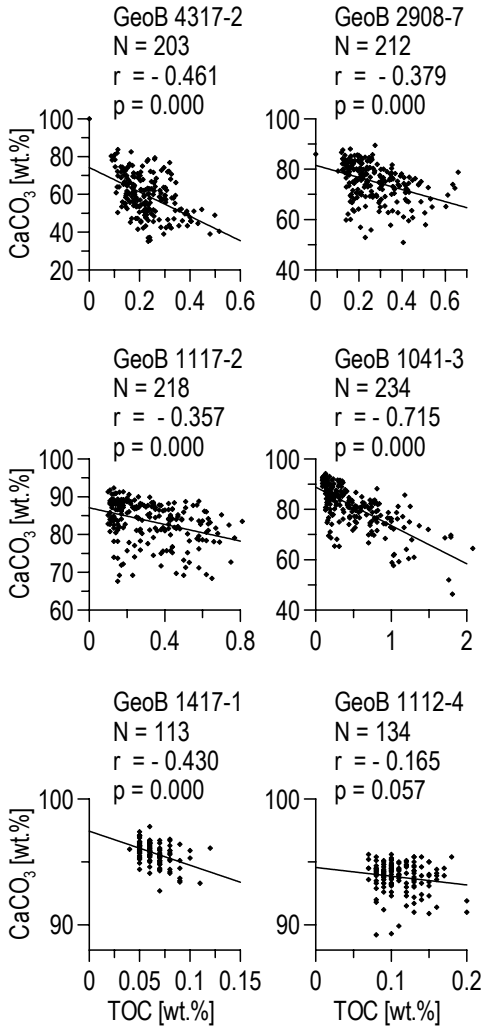

Fig. 5a. Crossplots of C_{org} and $CaCO_3$ contents of sediment sequences along cross profile D. The various negative Pearson's correlation coefficients at individual core sites probably reflect regional productivity-related calcite dissolution intensities.

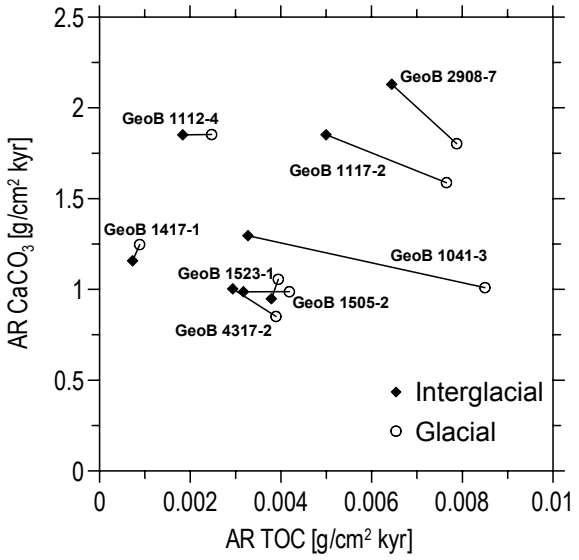

Fig.5b. Relation between interglacial (diamonds) and glacial (circles) averages of $CaCO_3$ and TOC accumulation rates.

Non-Carbonate, Iron and Magnetic Susceptibility Records

Variations in non-carbonate content (100%-$CaCO_3$%), iron content, and non-diamagnetic susceptibility (κ_{nd}, essentially a measure of ferri- and paramagnetic mineral content) of W-E profiles A and B are presented in Figs. 6a,b and 7 along with a newly introduced proxy parameter Fe/κ_{nd} indicating the extent of diagenetic magnetite dissolution (Funk et al., this volume). Near-baseline values of this very sensitive proxy parameter mark essentially pristine sections of the susceptibility signal, which can be interpreted in terms of mixed biogenic and lithogenic fluxes. Fe/κ_{nd} values exceeding 1 denote diagenetically overprinted rock magnetic signals.

Along transect A at 4°N mean values of κ_{nd} range from 133 to 183·10^{-6} SI, whereas the cores of transect B at 0° latitude exhibit much lower means between 36 and 59·10^{-6} SI. These decreases in magnetic susceptibility and, almost to the same extent, in iron content between the two transects at 4°N and 0° result primarily from two-fold higher carbonate dilution at the equatorial sites and more

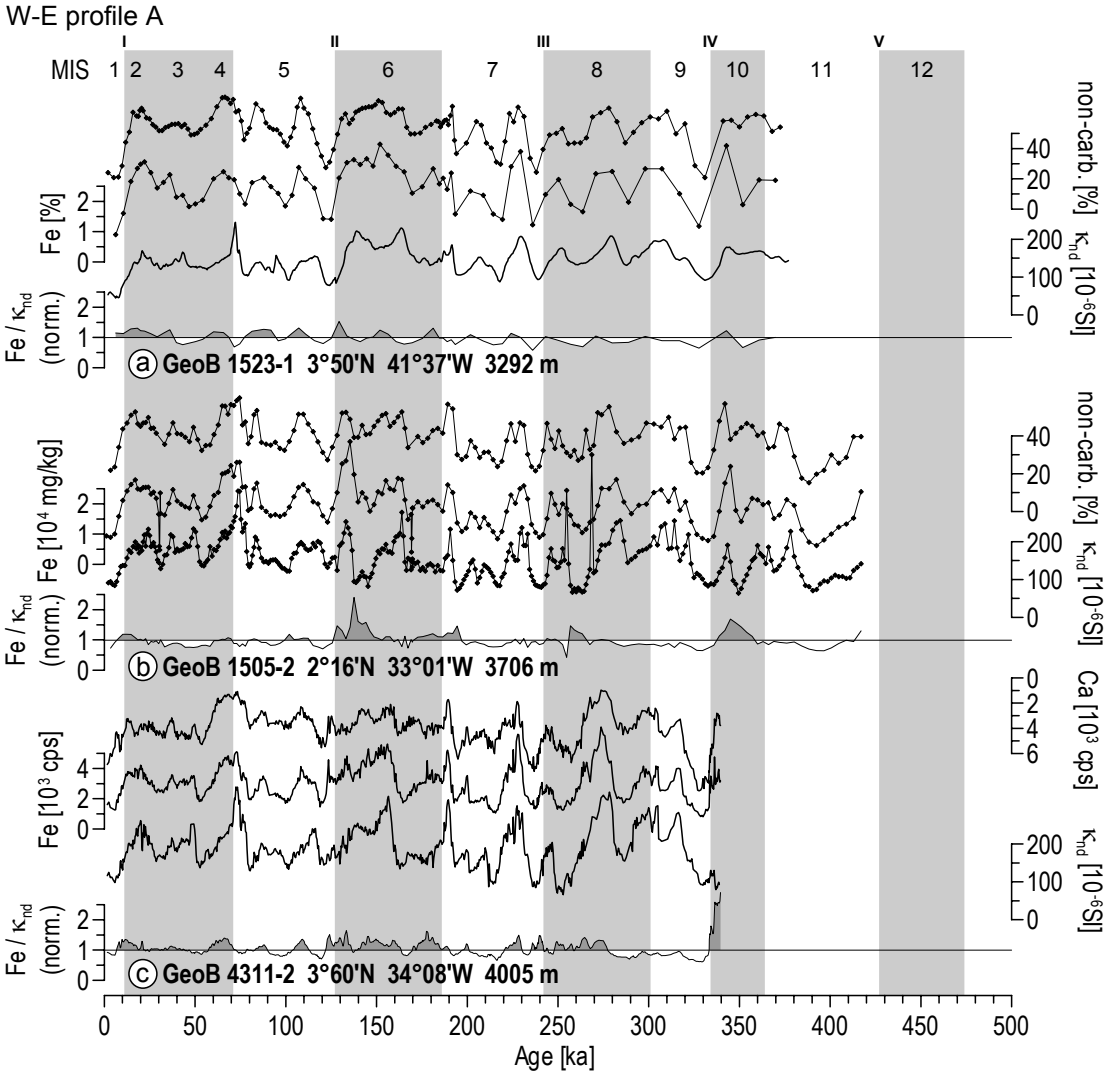

Fig.6. Variations in non-carbonate content (100%-$CaCO_3$%), iron content (Fe) and non-diamagnetic susceptibility (κ_{nd}) of W-E profile A. Where non-$CaCO_3$ content was not available, an inverse Ca record was used instead. The three parameters show excellent correspondence in unaltered sections, while susceptibility deviates in diagenetically affected layers. This is particularly good to see in cores GeoB 4315-2 and 4317-2 (MIS 6, 10 and 12) as indicated by the magnetite dissolution proxy Fe/κ_{nd}.

pervasive diagenesis. In comparison, W-E trends are subordinate and not as easily discernable from this compilation.

In the diagenetically unaltered sections the patterns of non-$CaCO_3$, Fe and κ_{nd} along each of the two latitudinal profiles correspond well. All three parameters basically measure terrigenous content and are therefore mirror images of the complementary carbonate contents. Previous remarks on the signal characteristics of the carbonate record therefore apply as well to Fe and κ_{nd} records, albeit in the reverse sense. Sedimentologically and mathematically conjugated by mutual dilution, biogenous and terrigenous components cannot be readily interpreted in terms of flux variations. Calculated accumulation rate records suffer visibly from an insufficient number of absolute age tie points and are therefore not shown here. However, average glacial and interglacial accumulation rates can be determined with higher precision; they are compiled and discussed below.

At closer inspection of each signal triplet (Figs. 6a,b and 7), it can be seen, that susceptibility recurrently deviates from non-$CaCO_3$ and Fe, in

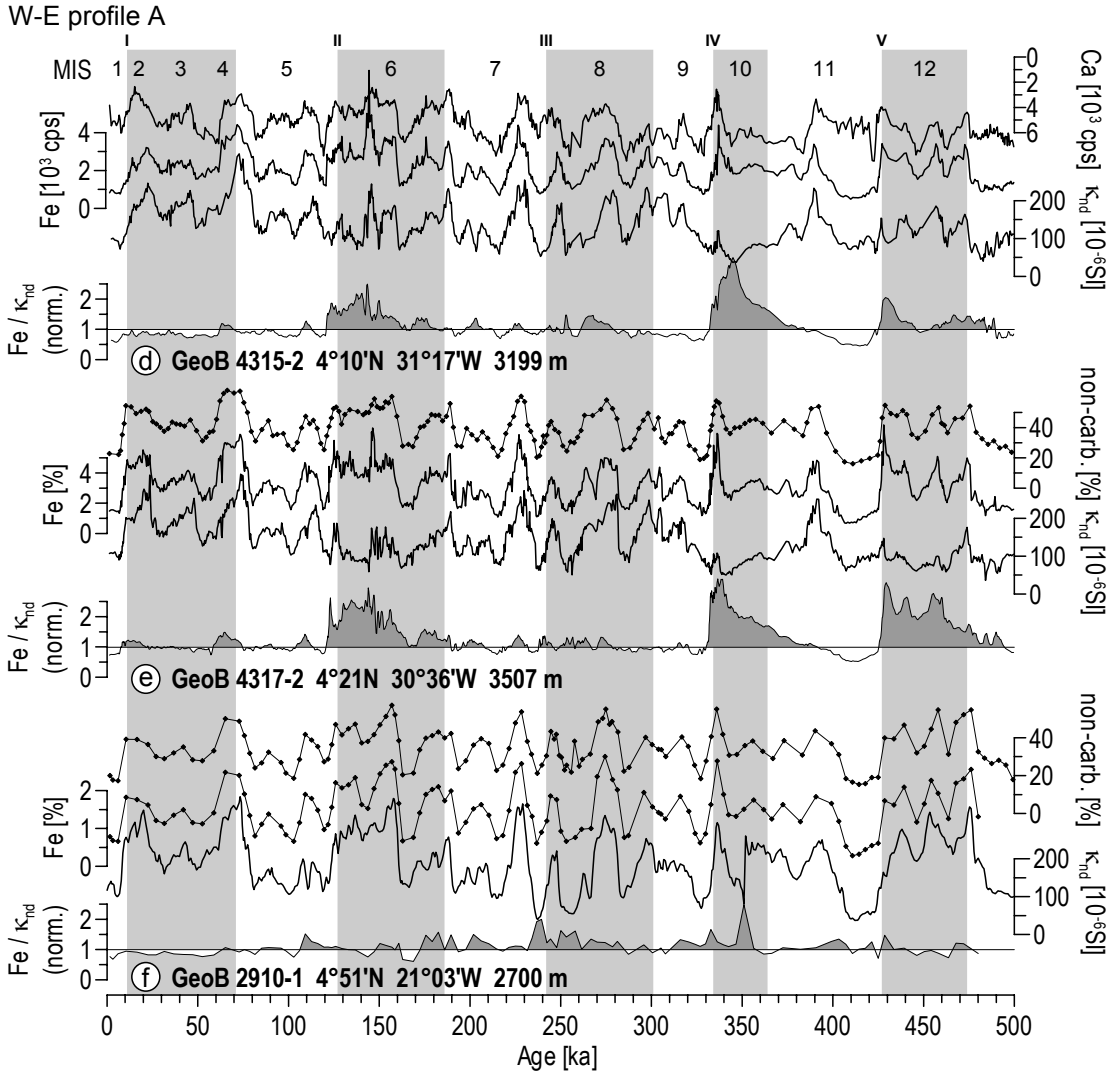

Fig.6.cont.

particular at glacial terminations and within glacials (e.g. MIS 6, 10 and 12). In general, these offsets in the susceptibility signal show lower and less modulated values and occur almost simultaneously in every core of each transect. The Fe/κ_{nd} ratio clearly pinpoints this behavior as magnetic mineral dissolution layers. Although dissolution layers in profiles A and B are basically synchronous, they occur more frequently at 0° than at 4° N.

Along the northern profile A situated at 4° N in a recently oligotrophic area (Fig. 6b) a fairly constant baseline value alternates with elevated Fe/κ_{nd} values (gray shaded sections) around major climate transitions, in particular after MIS 6, 10, and 12. These sections coincide well with TOC enrichments shown in Fig. 4. Especially in cores GeoB 4317-2

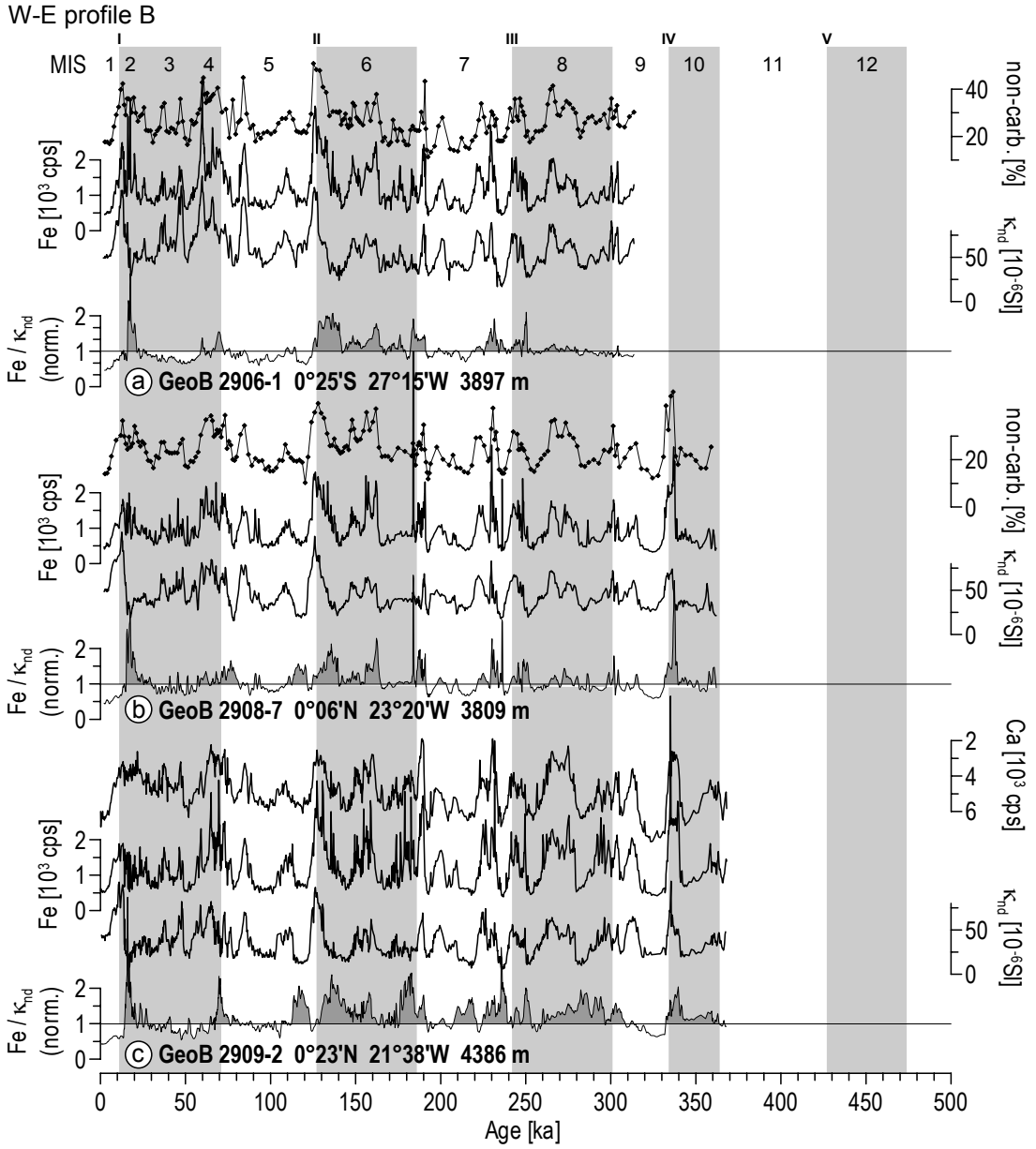

Fig.7. Variations in non-carbonate content (100%-$CaCO_3$%), iron content (Fe) and non-diamagnetic susceptibility (κ_{nd}) of W-E profile B. Differences of the two profiles A and B are explained in detail in the text.

and 4315-2 the magnetite dissolution peaks form broad sawtooth patterns with steep flanks at the terminations encompassing sediment sections of about 100 cm in thickness. In MIS 2, 4 and 8 dissolution peaks are faint or absent.

Along profile B (Fig. 7) at 0° at the northern margin of the Equatorial Divergence Fe/κ_{nd} peaks are shorter, mostly less intense, but much more frequent. Such a pervasive overprint hampers the use of magnetic signals for chronostratigraphic purposes here. As indicated by pronounced peaks in Fe/κ_{nd}, κ_{nd} goes through extreme minima in late MIS 2 (Termination I) and all preceding climate analogues. Dissolution signatures appear in all glacials and even in some interstadials (5.4, 7.2, 7.4); they respond preferentially to a precessional rhythm (Fig.7). The Fe/κ_{nd} peaks are generally steeper and more symmetric.

With respect to the previously discussed anti-correlation of $CaCO_3$ and C_{org} content, it does not come as a surprise that magnetite dissolution, reduced carbonate content and thereby enhanced terrigenous content go along in organic carbon enriched sections. Subsequent oxic and suboxic degradation of organic matter results in coincident carbonate and magnetite losses. We clearly see this effect in sections deposited during high glacials and terminations, most notably at the terminations II and IV of profile B (Fig. 7).

The high signal conformity of terrigenous contents finds an explanation in a largely similar carbonate dilution regime exerted by uniform, ocean-wide mechanisms of supra- and sub-lysoclinal carbonate dissolution. Vertical lysoclinal displacement was found to be entirely responsible for the equally high similarity of susceptibility records from the oligotrophic Subtropical Atlantic (Schmieder et al. 2000).

Magnetogranulometric and -mineralogical Records

So-called 'relational' rock magnetic parameters compare the concentrations of magnetically discernible magnetic mineral and particle size fractions. They are by definition independent of biogenous and terrigenous content and often react very sensitive to changes in source rock geology and transport pathways (Frederichs et al. 1999). Two well established and easily measurable relational parameters are investigated here: the magnetogranulometric M_{ar}/M_{ir} ratio and the magneto-mineralogical $S_{-0.3T}$ ratio, together with their respective basis parameters, M_{ar}, M_{ir} and M_{hir} presented in the following chapter. Details on the expression of redoxomorphic diagenesis in these parameters are described in the complementary paper by Funk et al. (this volume).

M_{ar}/M_{ir} records of the northern profile A (Fig. 8) have the general appearance of ice volume records and correlate highly to the oxygen isotope 'low latitude stack' (Bassinot et al. 1994) in most of their parts (Fig. 8i). These patterns are clear and uniform and lend themselves ideally to cyclostratigraphic purposes. Core mean M_{ar}/M_{ir} values of profile A level around 0.06 (0.055 to 0.08) It is interesting to regard the systematic W-E trend of the total data range. The plateau-like glacial signal sections assume low and therefore 'coarse' levels of 0.04 to 0.05. All interglacial maxima (e.g. MIS 5.5) are well developed and reach their largest, thus ‘finest’ values of about 0.10 at the westernmost end of profile A. To the east, they take increasingly lower, less fine peak values of 0.07 to 0.08. The individual interglacials are well isolated and extremely spiky; they highly resemble respective $CaCO_3$ records (Fig. 2) and coincide with carbonate-rich layers deposited during periods of sea level high stands, shallow nutricline and hence higher productivity in the west and reduced upwelling with lower productivity in the east. This analogy of M_{ar}/M_{ir} and $CaCO_3$ records cannot be extended to the warm stadials of glacial periods, where magnetogranulometry shows a smaller variance than carbonate content.

Some glacial sections of the M_{ar}/M_{ir} records exhibit traits of reductive magnetite dissolution similar to those already detected and described for the magnetic susceptibility records. Some extremely peaked M_{ar}/M_{ir} minima within ORLs sharply protrude from the prevalent climate patterns signaling an abrupt coarsening of the magnetic particle assemblage. These features strongly disturb certain sections of cores GeoB 1505-2, 4311-2, 4312-2, 4315-2 and 4317-2, in particular during MIS 8, 10 and 12. Such changes in magnetic grain-size distribution are due to chemical depletion of the finer

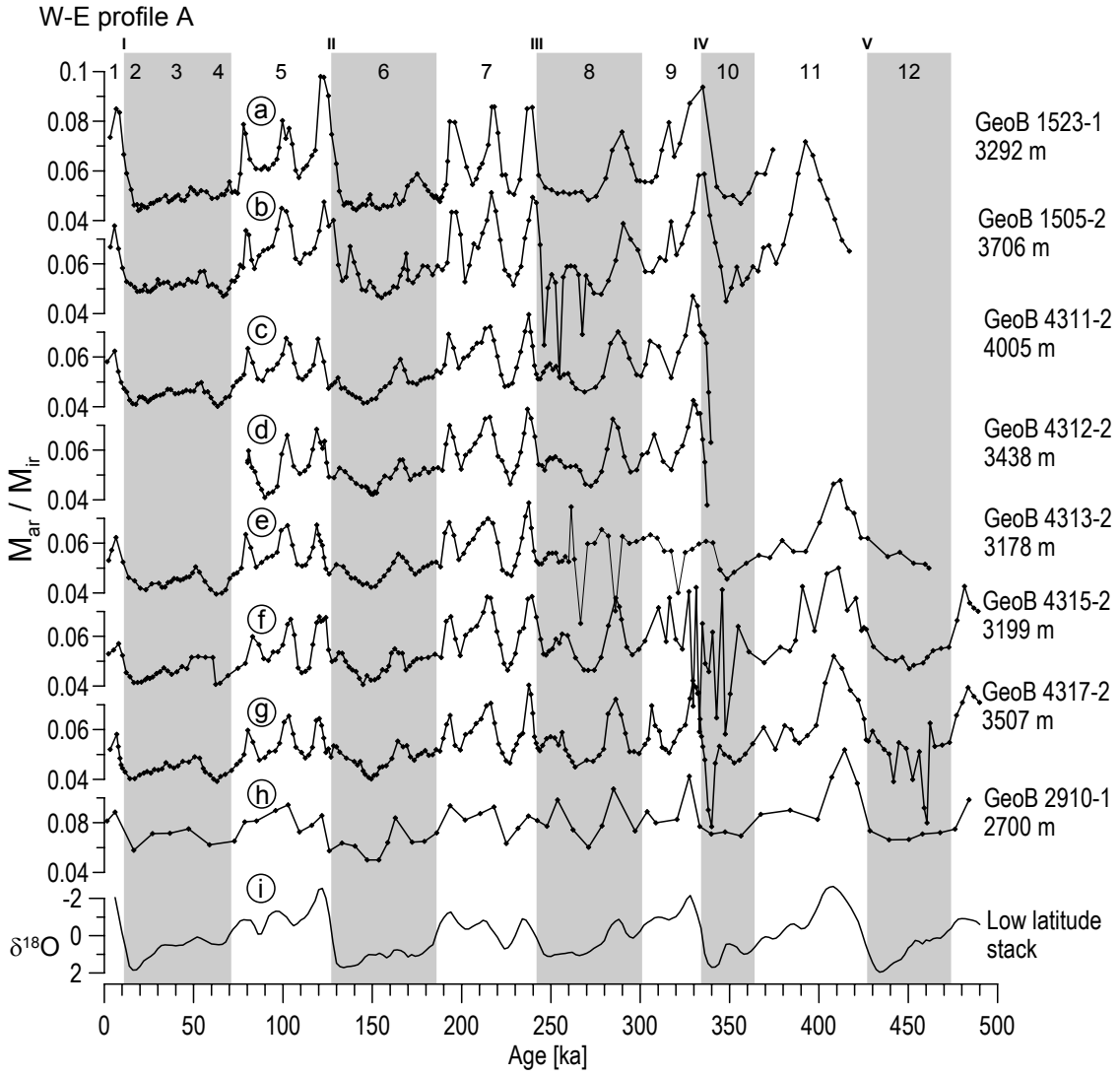

Fig.8. The magnetic grain size index M_{ar}/M_{ir} exhibit a uniform signal signature along W-E profile A (4°N) with a high correlation to the $\delta^{18}O$ latitude stack (**i**, Bassinot et al. 1994). Sharp signal minima portend to magnetically depleted zones and fall into glacial periods.

ferrimagnetic grains, which are more quickly dissolved owing to their large specific surface/volume ratio. This fine particle loss entails a relative enrichment of residual coarser particles and thereby an effective 'coarsening' – even if every grain actually lost volume (Karlin 1990).

In profile B, mean M_{ar}/M_{ir} values vary between 0.068 and 0.079 including altered sections (Fig. 9) and indicate a higher relative proportion of fine magnetic grains in comparison to profile A sediments. At a much higher frequency and pervasiveness, reductive dissolution events interrupt the primary signal with extremely deviating and 'coarse' M_{ar}/M_{ir} values around 0.02. In consequence, a primary signature can only be attributed to short, intermittent signal sections. These, nevertheless, seem to correlate to profile A records and the low latitude $\delta^{18}O$ stack. All diagenetically affected intervals show elevated Fe/κ_{nd} values (Figs. 6a,b and 7).

The $S_{-0.3T}$ ratio (Bloemendal et al. 1992) relates hematite to magnetite. In practice, this parameter primarily traces variations between various sources and erosional regimes. The major hematite source

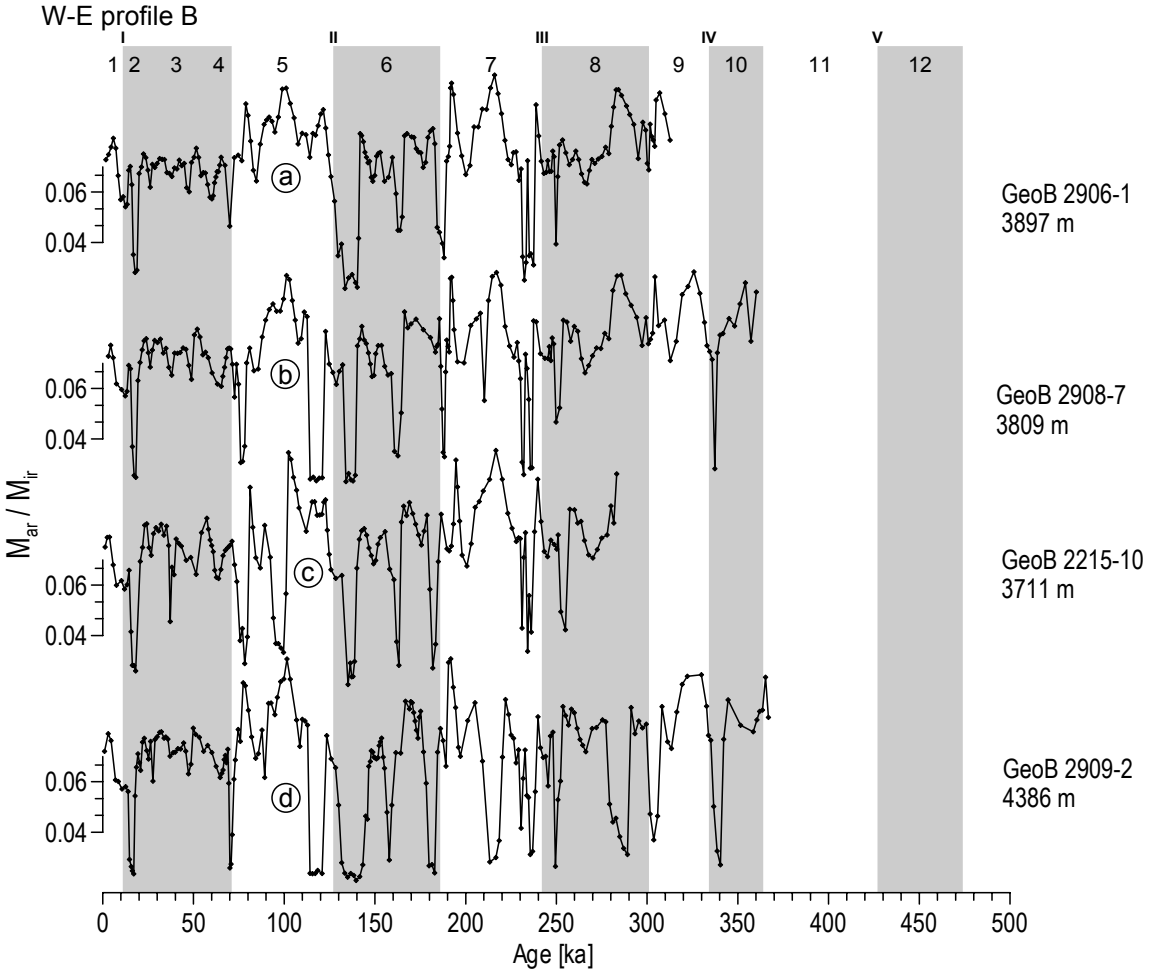

Fig.9. Along W-E profile B (0°) the M_{ar}/M_{ir} ratio is considerably stronger affected than to the north. The pristine signal is nearly complete masked by extremely deviating 'coarser' values caused by magnetite dissolution.

of the Equatorial Atlantic region is dust from the arid northwest Africa, followed by an Amazonian influx distributed eastwards by the Northequatorial Countercurrent (Bleil and von Dobeneck, this volume).

As mentioned earlier, the compilation of available $S_{-0.3T}$ records of profiles A and B (Fig. 10) includes data sets produced with different pulse magnetizers and settings. These records follow comparable patterns, but their absolute numbers are not entirely consistent. It is evident at first sight, that all four records of profile A equally represent global climate cycles. Other than the M_{ar}/M_{ir} ratio, they follow glacial more than interglacial dynamics (compare MIS 5 and 6). This precession-dominated, typically 'tropical' signal clearly contrasts with the eccentricity-dominated M_{ar}/M_{ir} pattern. $S_{-0.3T}$ amplitudes and relative hematite content seem to increase from GeoB 1523-1 (a) in the west to GeoB 4317-2 (c) at the eastern flank of the mid-Atlantic ridge pointing to a growing influence of Saharan dust. Surprisingly, the record of the easternmost Sierra Leone Rise core GeoB 2910-1 (d) does not continue this trend, but returns to values similar to those of the westernmost Ceará Rise core.

Diagenesis comes again into play at all the previously described dissolution intervals. Its traits are extremely low, seemingly 'hematite-rich' values, which deform the primary signal around termination IV, in MIS 12, and, less significantly, also around termination II. The equatorial core GeoB 2908-7

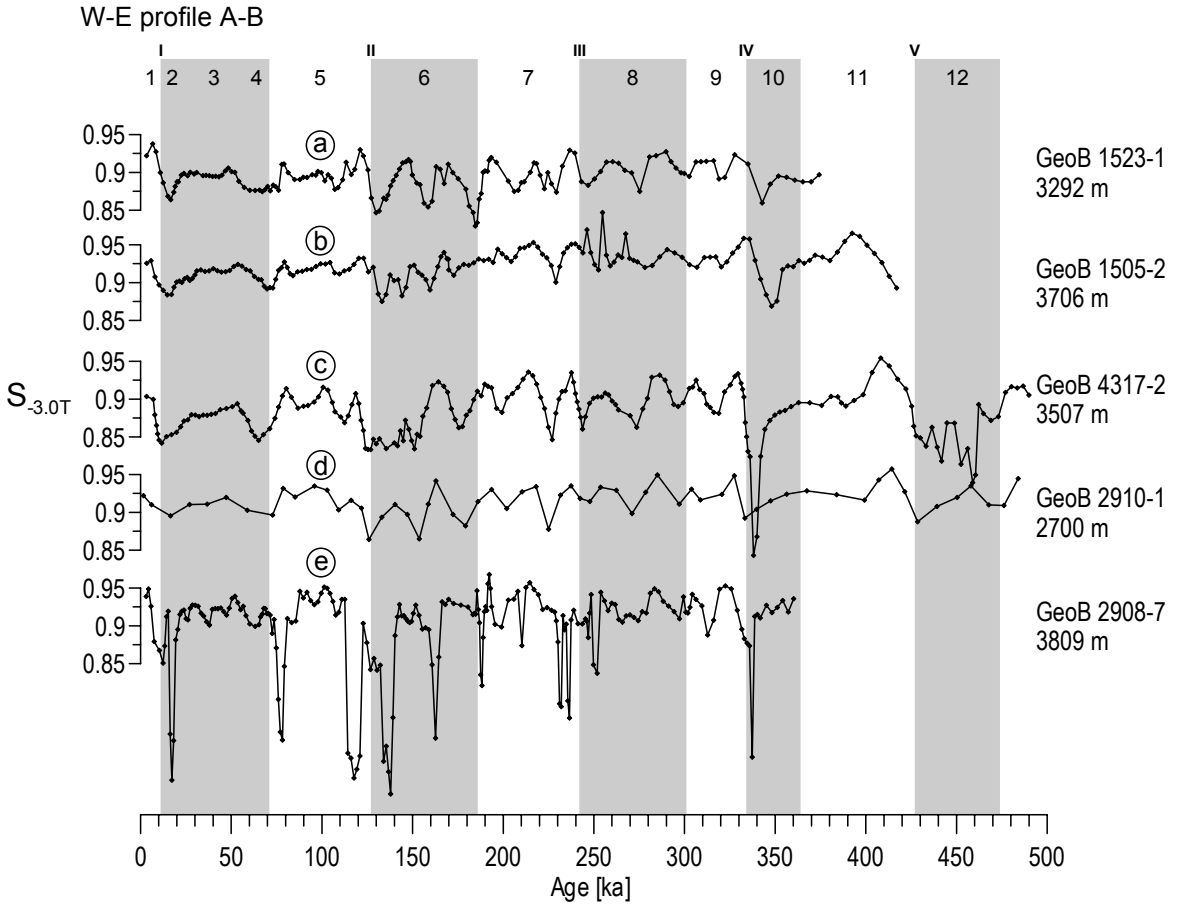

Fig.10. Compilation of $S_{-0.3T}$ records of profiles A and B. For explanation see text.

(**e**) shows again stronger and more frequent overprinting in all the numerous ORLs at terminations I, II, III and IV as well as in MIS 4 and 6. This change in magnetic composition is primarily related to magnetite depletion by reductive dissolution, leaving the more reduction-resistant, probably also coarser hematite phases behind as a relict mineral.

Selective Rock Magnetic Records

In order to resolve the climatic controls responsible for the signal characteristics of the two rock magnetic proxies M_{ar}/M_{ir} and $S_{-0.3T}$, it is necessary to take a look at their three defining curves M_{ar}, M_{ir} and M_{hir}, tracking fine-particle (SD) magnetite, total magnetite and hematite content, respectively. The co-compilation of these three parameters (Fig. 11) raises evidence for a regional interpretation.

A detailed inspection of all curves shows, that their patterns are essentially quite similar. However, their dynamics and signal levels vary considerably. These properties are most easily compared on basis of some statistical quantities compiled in Table 2, comprising arithmetic means, relative standard deviations and interparametric Pearson's correlation coefficients. Signal sections severely affected by diagenesis were excluded from this calculation. Three main trends can be observed:

1. Comparing relative standard deviations of all parameters and sites, we find that hematite variance systematically exceeds coarse magnetite variance and nearly doubles fine magnetite variance. We also note, that all these variances increase from west to east.

2. Correlation coefficients between hematite and coarse magnetite records are always higher than those between fine and coarse magnetite records. Correlations improve from west to east,

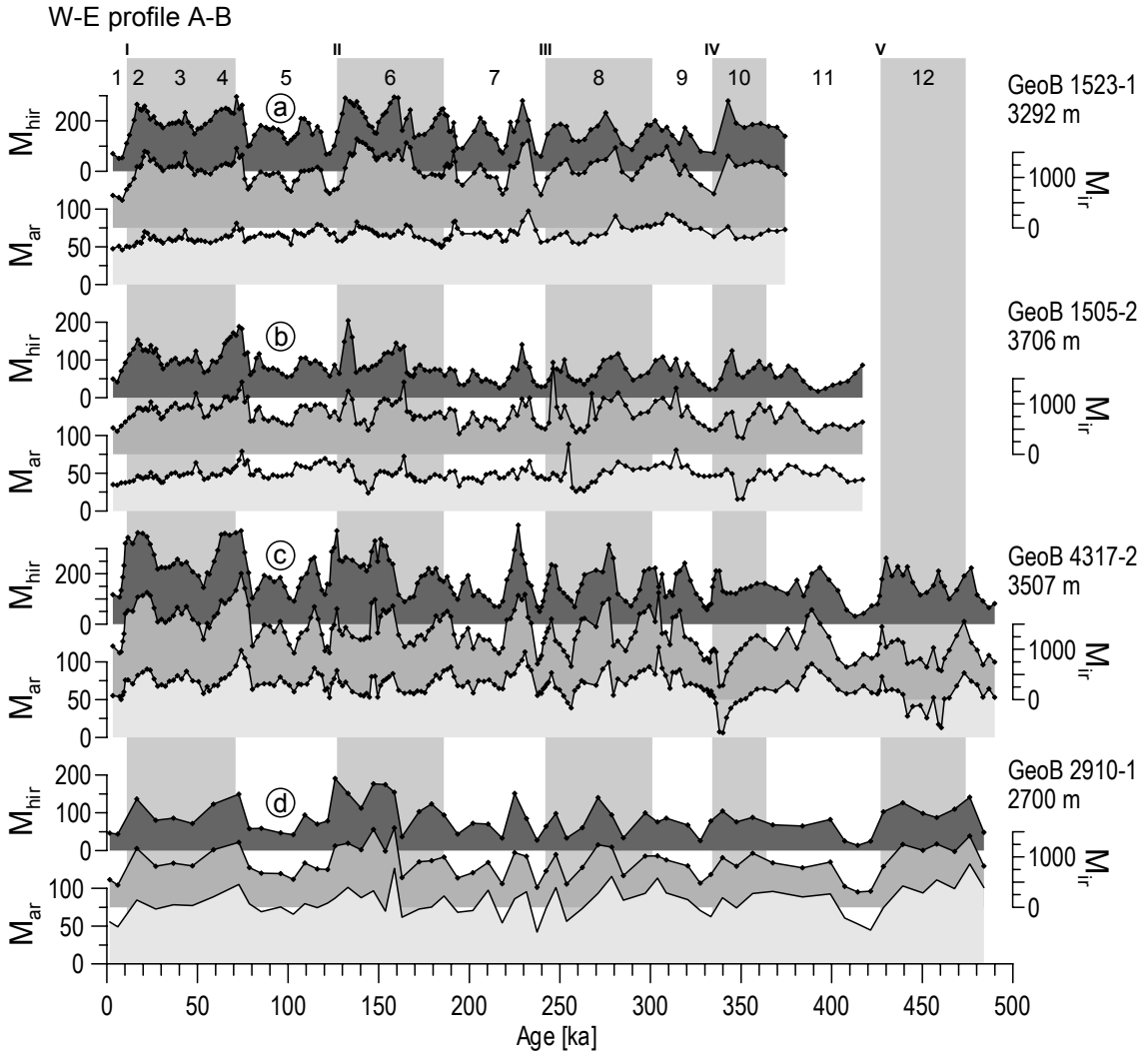

Fig.11. Compilation of the three rock magnetic parameters M_{ar} (light gray), M_{ir} (gray) and M_{hir} (dark gray) tracking fine-particle (SD) magnetite, total magnetite and hematite content, respectively.

where both coefficients seem to converge to a single value.

3. While there is no systematic W-E trend with regard to mean values (partly due to variable carbonate dilution), the averages for fine magnetite are regionally more stable than those of hematite and coarse magnetite.

From all three trends it follows, that the fine-grained magnetite phase is to be regarded as a spatially and temporarily more stable phase than hematite and coarse magnetite, which show much higher climatic modulation. According to an environmental magnetic case study of site GeoB 1505-2 by von Dobeneck (1998) and Frederichs et al. (1999), the latter parameters track terrigenous input from continental origin, while the fine-grained magnetite signal is probably of bacterial origin, or, alternatively, a faint, detrital background signal. In consequence, the magnetogranulometric M_{ar}/M_{ir} ratio deals not with a unimodal magnetic phase changing grain-size over time, but rather with a bimodal system of a coarse detrital and a fine, probably bacterial phase of which only the coarse phase is climate-controlled. The increasing variance of fine magnetite and its correlation to coarse magnetite towards the east implies, that the Saharan dust flux progressively contributes to and thereby modulates this fine magnetite fraction. At

Parameter	GeoB 1523-1	GeoB 1505-2	GeoB 4317-2	GeoB 2910-1
$\mu(M_{hir})$ [10^{-3} A/m]	**179**	**83**	**195**	**84**
$\sigma(M_{hir})$ [%]	*32*	*44*	*43*	*50*
$\mu(M_{ir})$ [10^{-3} A/m]	**1183**	**810**	**1426**	**873**
$\sigma(M_{ir})$ [%]	*22*	*28*	*26*	*34*
$\mu(M_{ar})$ [10^{-3} A/m]	**66**	**49**	**73**	**66**
$\sigma(M_{ar})$ [%]	*14*	*22*	*19*	*23*
$\rho(M_{hir}, M_{ir})$	**0.74**	**0.81**	**0.84**	**0.90**
$\rho(M_{ar}, M_{ir})$	**0.57**	**0.74**	**0.83**	**0.85**

Tab. 2. This compilation of the arithmetic means (***μ***), relative standard deviations (***σ***) and interparametric Pearson's correlation coefficients (***ρ***) gives an overview of dynamics and signal levels of the three basic magnetic parameters M_{ar}, M_{ir} and M_{hir} along the W-E profile A. Signal sections severely affected by diagenesis were excluded from this calculation.

the western side, only the coarse magnetite fraction of Amazonian origin shows noticeable climate control, while the fine magnetite fraction barely varies with time. The very high, i.e. fine interglacial values of the M_{ar}/M_{ir} ratio at and near the Ceará Rise imply, that the Amazon particle flux to the pelagial realm is extremely reduced at sea level high-stands. It finds other sinks in that time, in particular the newly eroded depocenters on the broad north Brazilian shelf (Milliman et al. 1975; Damuth 1977).We conclude, that the climatic information of the M_{ar}/M_{ir} ratio in the Equatorial Atlantic is essentially controlled by the denominator M_{ir}, hence, the terrigenous particle flux, while the more biogenous numerator M_{ar} compensates for carbonate dilution and diagenesis effects. The diminishing amplitudes of the M_{ar}/M_{ir} ratio to the east result from a growing influence of the Saharan source over the fine magnetite fraction. This coupling of coarse and fine magnetite fractions effectively stabilizes their mutual M_{ar}/M_{ir} ratio and reduces its amplitudes.

The mathematical controls of hematite and magnetite on the magnetomineralogical $S_{-0.3T}$ ratio are most easily recognized when expressing it as $S_{-0.3T} = M_{ir}/(M_{ir}+M_{hir})$. We find from the statistical analysis, that the hematite phase consistently shows stronger climate modulation than the magnetite phase. Again the term M_{hir} in the denominator takes a lead in this ratio and overcompensates coherent variations of M_{ir}, while carbonate dilution again cancels out. In other words, we see here a dominance of hematite over magnetite flux variations.

From a sedimentological perspective, this finding suggests, that glacial hematite fluxes were relatively enhanced, either by larger Saharan influence or by different weathering conditions. The lack of a consistent trend in average $S_{-0.3T}$ ratios along profile A is puzzling and possibly an expression of internal variability within the Saharan dust falls in the study area, in particular at their southeastern margins. Records from more northerly locations along the main dust trajectory are needed to study the genuine signature of the southern Saharan magnetic mineral assemblage (Bloemendal et al. 1988).

Synopsis of Glacial/Interglacial Accumulation Rate Averages

For paleoclimate research we need to know individual material fluxes and budgets, which can only be resumed from accumulation rates (AR).In awareness of the known difficulties involved in estimating accumulation rates from records with cyclostratigraphic, i.e. relative age models we decided to follow the approach of Ruddimann (1997) and Wagner (2000), who limited AR errors resulting from dating uncertainties by averaging over larger time intervals. Here we determined ARs over extended glacial (MIS 2+3+4, 6) and interglacial (MIS 1, 5, 7) periods of the 100 kyr cycle. That this approach largely cancels out precessional variations. An additional problem was encountered with the two western cores of profile A, which suffer from noticeable coring induced compression in their lower parts. This problem is often encountered when coring porous, clay-rich and therefore easily deformable sediments. A modest compression has little effect on concentration records if these have been correctly transposed into the time domain. However, the deformation of accumulation records is by far more problematic and not tolerable, when it comes to compare absolute AR values. As a conservative but firm approach, all AR averages of profile A were therefore exclusively derived from the last 200 kyr, where compression (Bleil and von Dobeneck, this volume) and early diagenesis seem to have done little damage. Each region is represented by a single sediment core.

For most of the W-E profile (Fig. 12), total sedimentation rates (a) amount to some 2.5 cm/kyr and show little or no consistent glacial/interglacial variability. As sole exception, the Sierra Leone Rise record GeoB 2910-1 has a 40% lower sedimentation rate of about 1.4 cm/kyr. In terms of biogenous (d) and terrigenous (f) content, the latter decreases from about 55% in the west to around 35% in the east. Since AR averages of $CaCO_3$ (e) of roughly 1 g/cm^2 kyr do not show large zonal or temporal gradients, the glacial/interglacial shifts in non-$CaCO_3$ AR averages (g) are largely responsible for lithological variability. We notice a W-E decrease from 1.2 over 0.78 and 0.75 down to 0.35 g/cm^2 kyr. This trend is obviously inverse to the trade wind direction and, unless we take atmospheric focusing of the Saharan dust fall into consideration, also to existing opinions on Saharan prevalence in the central Equatorial Atlantic.

In particular the very low eastern detrital ARs are astonishing and raise some suspect that winnowing may have come into play at this topographic height of the Sierra Leone Rise. On the other hand, we find also the largest, i.e. finest average M_{ar}/M_{ir} ratios at this eastern site (Fig. 9). Magnetic 'fining', however, is contradictive to elevated bottom current velocities. Furthermore, we find also the highest and most climate dependent susceptibilities (h) at this site, in spite of the lower terrigenous contents.

The governing W-E trend from lower to higher carbonate-free susceptibilities is only interrupted by GeoB 4317-2, the only core with relatively lower susceptibility and magnetite AR during glacials (i). This is clearly an effect of the large magnetite losses during glacial MIS 6 as suggested by highest glacial TOC averages (0.30%) among all cores of profile A (b).

Comparing TOC contents (b) and ARs (c), we find, that some subtle shifts towards higher glacial TOC contents observed in the three western cores are at least partly due to carbonate dilution. In reality, TOC accumulation at the Ceará Rise even drops slightly during glacials as to be expected from the shear wind driven seesaw mechanism, which disequilibrates glacial Equatorial Atlantic productivity by lifting the eastern and lowering the western nutricline. Indeed, glacial C_{org} burial rates were some 19% higher on the western and 36% higher on the eastern flanks of the MAR, most likely due to larger W-E gradients in ocean productivity.

AR averages of glacial/interglacial C_{org} and $CaCO_3$ shift inversely like the earlier shown signal patterns. GeoB 4317-2, the core with the highest glacial TOC increase and magnetite loss, also features the largest drop to glacial $CaCO_3$ accumulation rates. This drop in carbonate sedimentation is also seen at the shallow Ceará Rise core GeoB 1523-1 (2845 m) whereas the deepest core GeoB 1505-2 (3706 m) shows nearly balanced glacial/interglacial $CaCO_3$ contents and ARs. This again is strong evidence for a lead of sedimentary diagenesis over CCD oscillation in controlling supra-

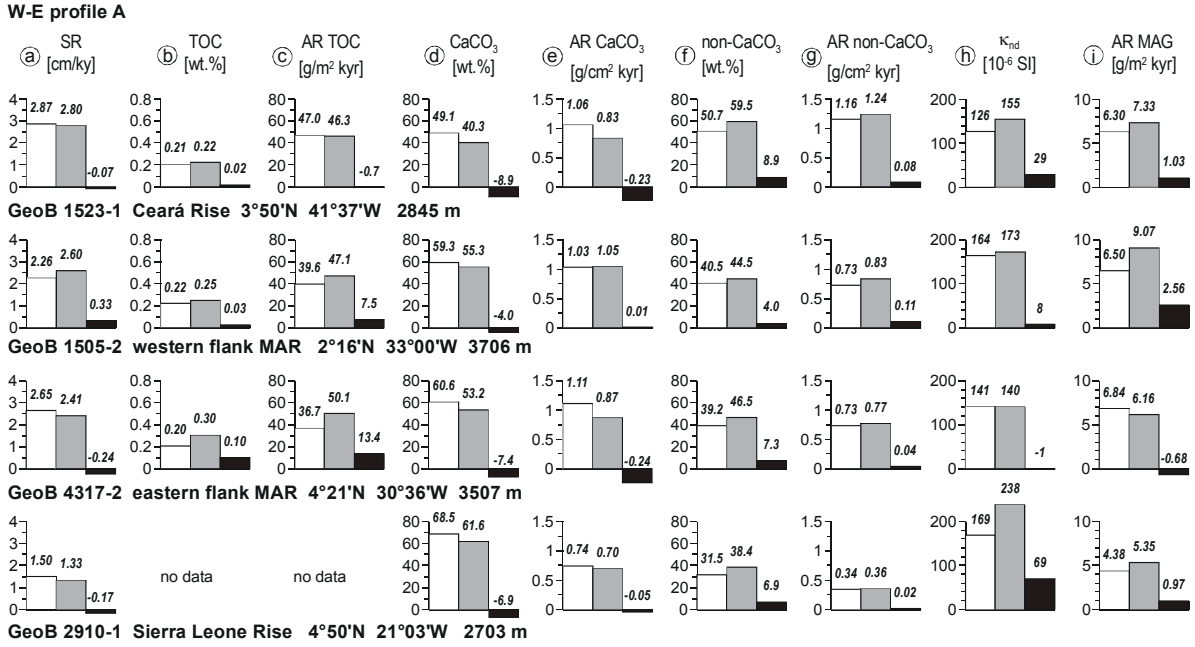

Fig.12. The 200 ka to present means of sedimentation rates **a**), TOC content **b**) and accumulation **c**), $CaCO_3$ content **d**) and accumulation **e**), non-$CaCO_3$ content **f**) and accumulation **g**), non-diamagnetic susceptibility **h**) and magnetite accumulation **i**) of W-E profile A. White bars denote averages over interglacial (MIS 1, 5, 7) and gray bars over glacial (MIS 2+3+4, 6) periods, while black bars show their difference.

lysoclinal Equatorial Atlantic carbonate contents.

We now change perspective and proceed to the meridional NW-SE cross profile stretching over an equatorial latitude zone from 4°N to 5°S with an outpost at 15°S (Fig. 13). Here, the interglacial and glacial averages were drawn from total record lengths.

The subtle meridional rise and fall in mean sedimentation rates from some 2.5 cm/kyr (GeoB 4317-2) up to 3.5 cm/kyr (GeoB 2908-7, 1117-2) and back to about 2.5 cm/kyr (GeoB 1041-3, 1112-4) unveils merely a glimpse at the lithological contrasts hidden in this profile (Fig. 13). From the separate compilations of biogenous and terrigenous components and their ARs (b-g), it can be easily inferred, that two large, but mutually opposed meridional trends exist, which counterbalance each other in total sedimentation rates.

The $CaCO_3$ percentages (d) start with merely 57% (GeoB 4317-2) at the northern oligotrophic margin, rise to 76%, 84% and 82% (GeoB 2908-7, 1117-2, 1041-3) in the mesotrophic Equatorial Divergence region and reach nearly pure calcareous values of 94% and 96% at the southern oligotrophic gyre. Consequently, non-$CaCO_3$ content (f) decreases by one order of magnitude from 43% to 4% from north to south. This large gradient results from non-$CaCO_3$ ARs (g), which show vastly decreasing numbers of 0.75, 0.65, 0.33, 0.24, 0.12 and 0.06 g/cm² kyr over cross profile D while respective $CaCO_3$ ARs (e) do not vary by more than a factor of two (1-2 g/cm² kyr).

Combining profiles A and D we may conclude, that the major regional trends in Equatorial Atlantic lithology are primarily caused by the heterogeneous distribution of continental source regions and transport pathways. Regional productivity variations are clearly subordinate. However, for the temporal trends, i.e. glacial-interglacial variability, we have the opposite regime:

The general trend to lower glacial $CaCO_3$ contents (d) has statistically more to do with lower glacial $CaCO_3$ ARs (e) than with higher glacial non-$CaCO_3$ ARs (g). It should be noted, that the ratio of glacial and interglacial $CaCO_3$ ARs is of nearly equal proportion at 3500, 3800, and 4000 m water

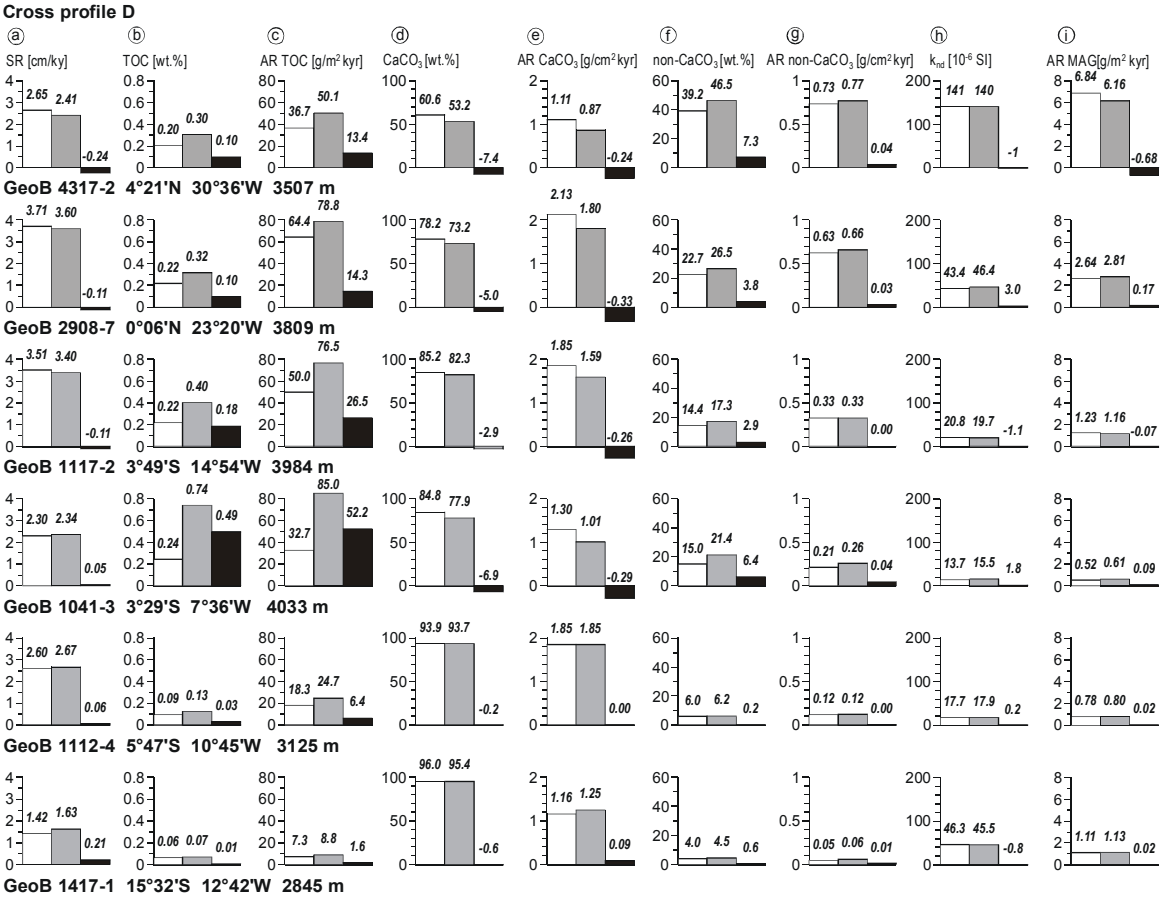

Fig.13. Total core means of sedimentation rates **a**), TOC content **b**) and accumulation **c**), $CaCO_3$ content **d**) and accumulation **e**), non-$CaCO_3$ content **f**) and accumulation **g**), non-diamagnetic susceptibility **h**) and magnetite accumulation **i**) of NW-SE cross profile D. White bars denote averages over interglacial, gray bars over glacial periods, while black bars show their difference.

depths. Only at the two southernmost and shallowest (3125 m and 2845 m water depth) stations do we see balanced or even slightly enhanced glacial $CaCO_3$ ARs. As shown earlier for cross profile D (Figs. 4, 5), between 50 and 200% more organic carbon has on average been preserved in glacial than in interglacial sediment sections. The related much higher glacial C_{org} burial rates have left a syndepositional diagenetic overprint in the $CaCO_3$ records as well as a postdepositional signature in the magnetic mineral records. Averaged susceptibilities (h) and magnetite ARs (i) decay at an even steeper rate from N to S than the related non-$CaCO_3$ contents (f) and ARs (g), most likely by an increasingly higher tribute to reductive diagenesis.

In this context, it is interesting to note, that the ratio of C_{org} and $CaCO_3$ ARs is surprisingly high at the northernmost location GeoB 4317-2. Neither productivity nor bottom water chemistry can be hold responsible for this finding, but these superproportional C_{org} contents go along with remarkably heavy losses in glacial magnetite accumulation. We may conclude from this situation, that scavenging, i.e. accelerated downward transport by flocculation of organic material with (magnetite-bearing) dust particles, could explain this situation. Intimate contact of particles with a redox partnership within such clusters may lead to particularly high reductive magnetite losses. This would also explain some untypically broad ORLs in the northernmost studied sediments of core GeoB 4317-2.

Specific Signatures of Early Diagenetic Processes

Berner (1987) showed that organic carbon enrichment and degradation is responsible for the early diagenesis of sedimentary iron minerals and resulting changes of rock magnetic signals. The quantity of preserved organic carbon in sediments depends on the organic matter supply from the surface layer of the ocean, water depth, bulk sedimentation rate, and its oxidation by bottom water oxygen and other oxidants (Müller et al. 1988). Subsequent to deposition the organic material is subject to degradation by microorganisms. Froelich et al. (1979) proposed a conceptual model for these microbially mediated processes: Accordingly, the oxidation of organic matter follows a sequential series of terminal electron acceptors in descending order of free energy gain. The oxidants are: dissolved oxygen, nitrate, Mn oxyhydroxides, Fe oxyhydroxides, and sulfate. Oxyhydroxide is a frequently used term for -oxides, -hydroxides, and everything in between these two end – members (van Santvoort et al. 1997). The extent of the reaction sequence depends on the availability and reactivity of both organic matter and reductants and the competitive efficiency of microbial populations (Karlin and Levi 1983). If the amount of organic matter in a sediment is such that suboxic diagenesis involves Fe-reducing bacteria (Froelich et al. 1979), reductive dissolution of detrital iron oxides occurs (Bloemendal et al. 1992) altering the bulk magnetic properties of the sediment (Robinson et al. 2000).

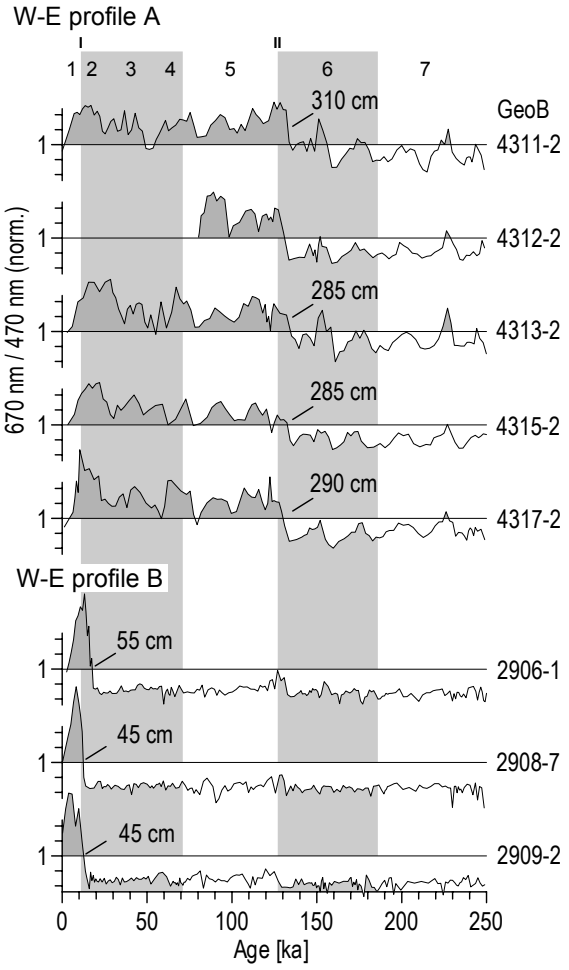

Fig.14. Reflectance ratio 670nm/470nm along the W-E profiles A and B. The Fe^{2+}/Fe^{3+} redox boundary is indicated by an abrupt color change represented by a drop to values below 1. Note the very different depths of this transition at 4°N and 0°.

Subsurface Color Transition

Reductive dissolution of Fe oxides has not only a consequence on magnetic properties, but, due to their important role as pigments, strongly influences the color aspect of a sediment. The prominent subsurface color transition found in all investigated Equatorial Atlantic sediment cores (Fig. 14) represents the modern iron redox boundary (Lyle 1983). Illustrated on the basis of core pictures (Fig. 15a,i) and color reflectance data the change from hues of reddish browns to greenish grays appears at different depths in cores GeoB 4317-2 (transect A) and 2908-7 (transect B). The oxidized layer is indicated by higher 670 nm/470 nm (red/blue) reflectance ratios (Fig. 15b,j, gray shaded). The color transition in core GeoB 4317-2 (4°N, Fig. 15a) marked by an abrupt drop to values <1 is situated at a depth of 2.9 m, just beneath termination II. Core GeoB 2908-7 (0°) exhibits the redox boundary below termination I at the substantially shallower depth of 0.45 m (Fig. 15b). Remarkably, the color change is almost located at the same depth interval along each longitudinal transect, but varies considerable between profiles A and B. Along profile A the thickness of the oxidized layer (gray shaded) ranges down to sediment depths between 2.85 m and 3.10 m (Fig. 14). In the cores of tran-

sect B the depth of the color change is located at only 0.50 m below the sediment surface indicating a remarkable shallowing of the boundary towards the Equatorial Divergence.

(Lyle 1983) used the depth position of the transition from Fe(III) to Fe(II) as a measure of the relative supply and degradation rate of organic carbon. He mapped the thickness of the oxidized Fe(III)-bearing surface sediment layer in the eastern tropical Pacific Ocean and correlated thin brown layers to a high accumulation and consumption of organic carbon. (Müller et al. 1988) have also demonstrated a correlation between the thickness of the upper oxidized layer and the productivity of surface waters, organic fluxes and bulk sedimentation rates. In the eastern tropical Pacific they linked hemipelagic sediments dominated by reducing conditions to highly productive waters, and pelagic sediments formed under oxic conditions to less fertile surface waters. On the basis of magnetic hysteresis data Tarduno and Wilkison (1996) defined a progressive downward shift of the modern iron redox boundary due to a decrease in organic carbon input.

Present-day productivity, however, cannot be made responsible for the different depth positions of the iron redox boundary observed in the Equatorial Atlantic. This holds true for all interglacial sections of crossprofile D cores (Fig. 4), where no obvious differences in the sedimentary TOC contents between the north and south are observed. Significant regional variability of TOC is confined to the greatly enhanced glacial productivity, which still today determines the depth position of the redox boundary by forming the topmost ORL (Colley et al. 1984). Upper surfaces of the ORLs therefore coincide both with color and major climate transitions. In the cores under study the iron redox boundary also corresponds to the uppermost magnetite dissolution zone.

The depth of the modern redox boundary is determined by the latest preserved organic carbon enrichments. In profile A at 4°N no productivity pulses are indicated for MIS 2 and 4 (Fig. 15c, GeoB 4317-2). Accordingly, the modern iron redox boundary is located beneath termination II coinciding with the upper limit of the youngest ORL which in turn coincides with the uppermost major magnetite dissolution zone (Fig. 15e). The same holds true for sediments at 0° (Fig. 15B, GeoB 2908-7). Here, the presumable ultimate productivity pulse led to enhanced TOC accumulation during MIS 2 (Fig. 15k). As documented by enhanced Fe/κ_{nd} ratios (Fig. 15m) and earlier shown rock magnetic proxies the topmost magnetically altered section clearly corresponds to the respective ORL. Accordingly, the redox boundary is located beneath termination I (Fig. 15B). These conditions forbid to draw simple links between the color transition depth and modern regional productivity patterns. Nevertheless, this position can be used to estimate the historical lateral expansion of the Equatorial upwelling system.

Oxidation of Organic Carbon

At the climate transitions organic matter accumulation decreased and bottom water conditions changed. In a second stage of early diagenesis the oxidative degradation of organic matter proceeded as a descending oxidation front into the sediment (Wilson et al. 1985; Wilson et al. 1986), owing to downward diffusion of O_2 from the overlying bottom water. At the investigated sites, reoxygenation was favoured by O_2 rich North Atlantic Bottom Water at the onset of interglacial periods. In glacial periods pronounced minima in $CaCO_3$ content are attributed to emplacement of corrosive Circumpolar Deep Water (de Menocal et al. 1993; Bickert and Wefer 1996) (Fig. 15f,n). As documented by comparison of TOC profiles with detailed XRF single sample barium measurements the youngest ORLs in cores GeoB 4317-2 and 2908-7 seemingly became progressively thinner during decomposition. The refractory element barium is likewise enriched in the sediment at times of enhanced productivity (Bishop 1988) and considered to be a more reliable proxy for productivity. It is therefore used to reconstruct the original TOC profile (Mercone et al. 2000). Methods and limitations of this application were described by Gingele et al. (1999). The total barium content has to be corrected for the detrital fraction by using the following equation:

$$Ba_{\text{excess}} = Ba_{\text{total}} - \left(Al \cdot Ba / Al_{\text{average}}\right)$$

An average Ba/Al ratio of 0.0045 for detrital aluminosilicates as suggested by Kasten et al. (2001) is used here. The Ba_{excess} profiles of cores GeoB 4317-2 and 2908-7 (Fig. 15d,l) do not match the TOC records (Fig. 15c,k). The upper boundaries of the ORLs were probably steepened by burn-down as described by Thomson et al. (1995) in sapropels and lie now somewhat below their original position. A distinct Ba maximum is found just above the major climate transition II in core GeoB 4317-2 (Fig. 15d) and delineates a relatively higher organic matter input at the onset of interglacial conditions. Remarkably, the Ba_{excess} profiles coincide much better with variations of the Fe/κ_{nd} ratio (Fig. 15e). This indicates that the degradation of the today 'missing' TOC was accompanied by dissolution of magnetic minerals. Obviously, the partial magnetite depletion still witnesses the prior TOC accumulation. Also in core GeoB 2908-7 (Fig. 15B) the comparison of the TOC and barium profiles suggests a partial oxidative burn-down of the TOC record (Fig. 15k,l). Again, the former extension of the ORL is still documented by the irreversible reductive loss of detrital magnetite (Fig. 15m).

In the suboxic ORLs below the oxidation front, Mn^{2+} and Fe^{2+} are released by reductive dissolution of Mn and Fe oxides through bacterially mediated degradation of organic matter. These released Mn^{2+} and Fe^{2+} ions diffused upwards and precipitated as Mn and Fe (hydr)oxides at the downward moving oxidation front above the youngest ORLs (Fig. 15g,h,o,p).

Scanning electron microscope investigations of core GeoB 2908-7 provide further information about the stage of diagenesis reached in the ORL in MIS 6. Authigenesis of framboidal and octahedral pyrite respectively implies intermittent anoxic conditions of this section (Fig. 16a). In this case, the flux of organic matter to the sediment exceeds the oxygen flow and the degradation proceeds by bacterial sulfate reduction. Diffusive fluxes of Fe, liberated by dissolution of iron oxides such as magnetite, resulted in the formation of pyrite, which was partly oxidized by an oxidation front at later stage (Fig. 16b).

Authigenesis of Magnetic Minerals above the Iron Redox Boundary

Three susceptibility patterns of crossprofile D hold evidence for authigenic magnetic enhance-ment above the active iron redox boundary (Fig. 17b-d). The initially inverse pattern of magnetic susceptibility and carbonate clearly deviates in a positive direction within a relatively narrow depth range. In core GeoB 4317-2 the expected correlation between the non-$CaCO_3$ fraction and magnetic susceptibility is obvious. Yet, in core GeoB 2908-7, and more sharply defined in cores GeoB 1117-2 and 1041-3, deviations of the two parameters are indicated above the color transition and at termination I respectively. Distinct maxima in the magnetic susceptibility profiles indicate the presence of ferrimagnetic components of probably secondary origin as described by Tarduno et al. (1998). Karlin et al. (1987) reported evidence of metabolic authigenesis of fine-grained magnetite crystals by Fe(II)-oxidizing magnetotactic bacteria close to the color change marking the Fe(III)/Fe(II)-redox transition (Lyle 1983). Magnetotactic bacteria, which may find this optimal zone with greater efficiency by using the inclination of the earth's

Fig.15. Comparison of the uppermost sections of cores GeoB 4317-2 (transect A) and 2908-7 (transect B). The oxidized layer and the depth position of the color change, indicative for the iron redox boundary, identified by eye **(a,i)** and by the ratio of 670 nm to 470 nm **(b,j,** gray shaded**)**. Please note the particular relation to major climate transitions. The color contrast results from the presence of both Fe(II) and organic material. In each case the youngest ORL is located just below the redox boundary **(c,k)**. Comparison of the productivity indices TOC and Ba_{excess} indicates **(d,l)** burn down of the upper reaches of the ORLs. After formation of the ORLs suboxic conditions led to dissolution of magnetite documented by enhanced Fe/κ_{nd} ratios **(e,m**, gray shaded**)**. Pronounced minima in $CaCO_3$ content may also provoked by oxidation of organic matter and metabolically mediated CO_2 **(f,n)**. Downward moving oxidation fronts have oxidized the upper part of the ORLs and have brought into contact with upward diffusing Mn^{2+} and Fe^{2+} ions. This produces Mn and Fe (hydr)oxides at the top of the ORLs **(g,h,o,p,** gray shaded**)**.

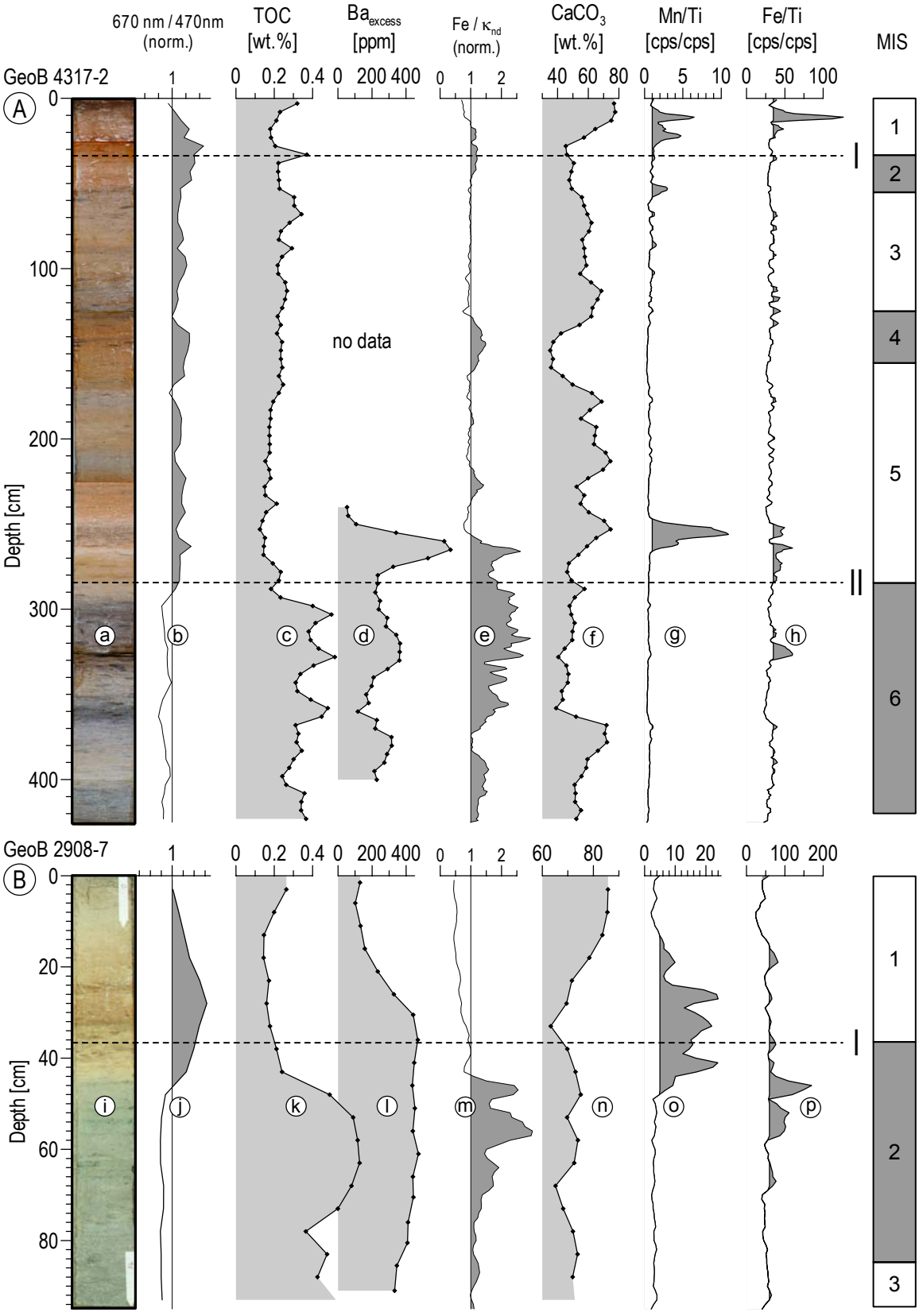
670 nm / 470nm (norm.)
TOC [wt.%]
Ba excess [ppm]
Fe / κnd (norm.)
CaCO3 [wt.%]
Mn/Ti [cps/cps]
Fe/Ti [cps/cps]
MIS
GeoB 4317-2
A
Depth [cm]
no data
a
b
c
d
e
f
g
h
I
II
1
2
3
4
5
6
GeoB 2908-7
B
i
j
k
l
m
n
o
p

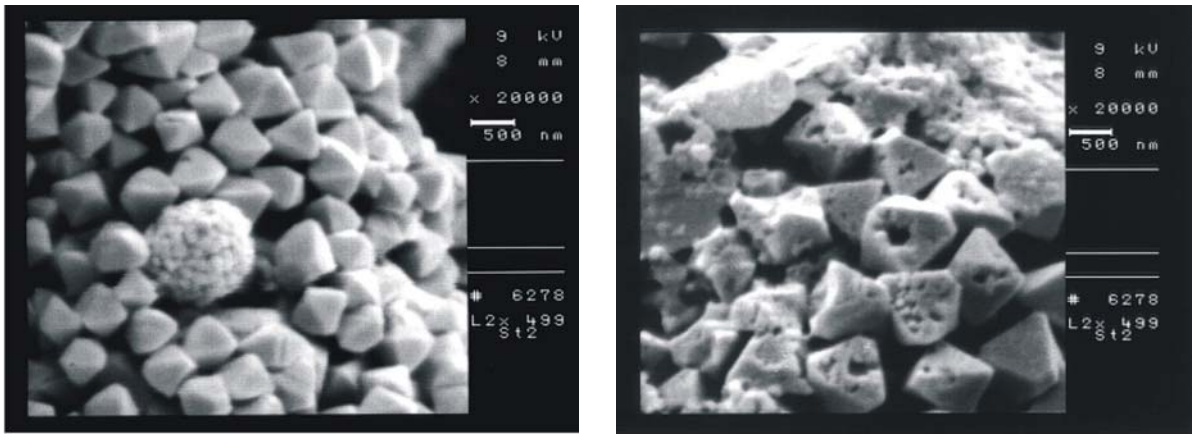

a) **b**)

Fig.16. Scanning electron microscopy (SEM) micrographs of authigenic pyrite formation in an ORL of core GeoB 2908-7 (MIS 6). **a)** Octahedral and framboidal pyrite indicate intermittent anoxic conditions in the ORL. **b)** Partially dissolved octahedrons mark more oxic conditions at a later time.

magnetic field (Stolz 1992) precipitate ultrafine-grained crystals of single domain, ferro-magnetic minerals intracellulary, which become a stable carrier of remanent magnetization. In sediments of the eastern South Atlantic Petermann and Bleil (1993) found highest concentrations of magnetotactic bacteria in a well-defined narrow subsurface layer. The depth of this layer was found to depend on the input and turnover of organic matter, linking a high flux of organic matter with high numbers of living magnetotactic bacteria. This relation is also found here along the NW-SE cross profile C. At the less productive location GeoB 4317-2 no authigenic maximum is indicated by magnetic susceptibility due to a more expanded oxic/anoxic transition zone. Towards the center of Equatorial Divergence increasingly larger magnetite precipitation peaks in the susceptibility signal of cores GeoB 2908-7, 1117-2 and 1041-3 (Thießen 1993) mirror a narrower zonation of terminal electron acceptors (Froelich et al. 1979) due to higher input of organic matter. Biomineralization seems to be restricted to the oxic/anoxic transition zone where iron is available in its soluble form.

Conclusions

As a contribution to the reconstruction of Late Quaternary material budgets and current systems in the Equatorial Atlantic Ocean, we co-interpret basin-wide spatio-temporal stratigraphic information contained in rock magnetic, sedimentological and geochemical records to gain deeper insight into the nature and relevance of the sediment accumulation and diagenetic alteration processes. Four profiles made up of 16 cores dissect the Equatorial Divergence high productivity region, the Saharan dust and the Amazon suspension plume. All investigated C_{org}, $CaCO_3$ and, to some extent, even terrigenous records were shaped or at least overprinted by diagenetic effects. According to our study, early diagenesis in the central Equatorial Atlantic is a leading issue for material flux and budget calculations and a serious problem for productivity and primary deposition estimates.

As oxygen isotope records were not available for the more recently collected cores, our ocean-spanning stratigraphic network was based on the variations of Ca and/or $CaCO_3$ content, which were found to be reasonably coherent throughout the entire region. Interestingly, not just the lysoclinal but even the permanently supra-lysoclinal locations show similar carbonate signatures. All $CaCO_3$ records are inversely correlated to the respective C_{org} records with increasing coherency towards the center of the Equatorial Divergence Zone. Both phenomena are likely to be the effect of synsedimentary carbonate dissolution which is driven by free CO_2 released by aerobic bacterial metabolism in the subsurface sediment. Over time, sufficient

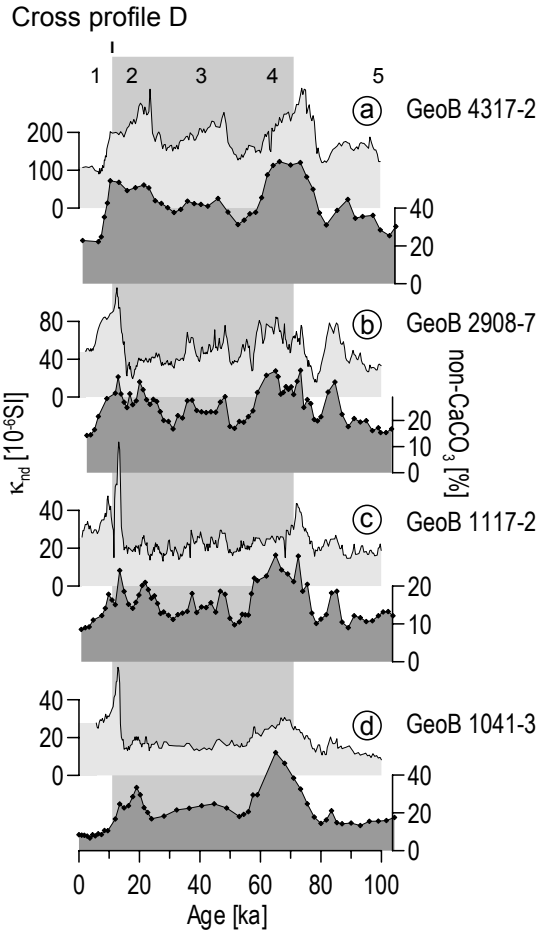

Fig.17. Non-$CaCO_3$ and magnetic susceptibility records of cross profile D. Sharp maxima in magnetic susceptibility above the Fe^{3+}/Fe^{2+} redox boundary are attributed to bacterial magnetite **(b-d,** not present in **a)**.

quantities of C_{org} are available for this process since typical benthic Equatorial Atlantic $C_{org}/CaCO_3$ rain rate ratios of about 1:1 transform into $C_{org}/CaCO_3$ accumulation rate ratios of only 1:100 to 1:1000 - this difference offers an enormous potential for subsurface carbonate diagenesis. $C_{org}/CaCO_3$ ratios averaged over glacial periods were found to be up to three times higher than those averaged over interglacials. The systematic glacial increase in C_{org}% is certainly a consequence of enhanced productivity, quicker burial and lower bottom water oxygenation. The fact that even supralysoclinal $CaCO_3$ accumulation rates systematically decrease in glacial periods is clear evidence for the lead of dissolution over productivity in shaping the $CaCO_3$% records.

Non-carbonate, i.e. terrigenous content is spatially controlled by source distance and shows a strong N-S decline. The temporal variations, however, have apparently more to do with dilution effects of a varying carbonate deposition than with changes in terrigenous accumulation rates. We found non-carbonate (100% - $CaCO_3$%), iron and susceptibility records to be highly collinear down to fine pattern details. Susceptibilities were partly overprinted by reductive diagenesis of magnetite. Magnetically depleted and organically enriched layers coincide perfectly and identify the two solid-state redox reaction partners. The iron to susceptibility ratio Fe/κ proved to be a sensitive proxy for suboxic magnetite diagenesis, indicating pervasive postsedimentary iron reduction within organic rich layers formed during cold periods throughout the Equatorial Divergence region. At the Ceará and Sierra Leone Rises, magnetite dissolution is barely detectable. On both flanks of the Mid-Atlantic ridge we find intense iron reduction during marine oxygen isotope stages 6, 10 and 12, in particular at the terminations. Towards the equator, the diagenesis-affected zones become narrower, but also more frequent and finally reflect a full precessional rhythm until individual diagenesis peaks merge into broader magnetite-depleted zones.

Magnetogranulometric and –mineralogical proxies show highly uniform, SPECMAP type climate signals throughout the study region except for overprinted sections. Interglacials have relatively finer magnetite grain size and relatively lower hematite content. The climate signature is generally better expressed in M_{ar}/M_{ir} as in $S_{-0.3T}$. The amplitude of M_{ar}/M_{ir} variations decreases from west to east as a result of the differing contributions of Amazon and Sahara. We can infer from the three selective rock magnetic parameters M_{ar}, M_{ir}, M_{hir}, that the above discussed magnetic ratios and their climatic variations are determined by mixing of individual sources with specific characteristics. The fine-grained, potentially bacterial or fine detrital magnetite phase has a very stable flux through time, particularly in the western part. The flux of the coarse grained magnetite phase varies strongly with Amazon discharge into the open ocean, with peaks corresponding to glacial sea level fall and low stand. Hematite fluxes show even higher varia-

bility. Peaks indicate intensified Saharan dust fall during glacial periods.

A detailed quantitative synopsis of glacial and interglacial accumulation rate averages with regard to total sediment, C_{org}, $CaCO_3$, non-$CaCO_3$, and susceptibility was carried out in order to detect zonal and meridional trends. By far the most prominent features are the 4°N to 4°S decrease in terrigenous accumulation (6:1) and the Equatorial Divergence high in glacial C_{org} accumulation, which decays much faster south- than northwards. The glacial increase in C_{org} and proportional decrease in $CaCO_3$ accumulation clearly reflects sedimentary carbonate diagenesis. This trend does not continue into the supralysoclinal oligotrophic South Atlantic.

A common feature of the Equatorial Atlantic sediment column is a sharp color change from reddish brown to greenish gray hues located at about 3 m depth at 4°N and at about 0.5 m depth at 0°. These transitions mark the modern Fe^{3+}/Fe^{2+} redox boundary and are typically located just above the uppermost ORL. Their depth is obviously not defined by the steady supply and degradation rate of organic carbon. Instead, it appears to be stabilized by the C_{org} reservoir of the topmost preserved productivity pulse. At 4°N, this 'sapropelic' layer coincides with glacial stage 6, at 0° with glacial stage 2. These Fe^{3+}/Fe^{2+} redox depth positions may have previously been shallower than suggested by the present color reflectance and carbon records. An interesting case is core GeoB 4317-2 from a 4°N Mid-Atlantic Ridge location. Not just barium content, but also our magnetite dissolution index indicate, that the productivity pulse in glacial stage 6 lasted longer than indicated by the C_{org} profile. The record was later depressed by 'burn-down', i.e. organic carbon depletion by a downward diffusing oxidation front. Traces of magnetite dissolution during glacials 2 and 4 even suggest, that the Fe^{3+}/Fe^{2+} redox boundary may have been as shallow as 0.35 m during the termination period, before it stepwise retreated to the present depth of 2.85 m with time and increasing bottom water oxygenation. Solid phase records of subsurface Fe^{3+} and Mn^{4+} precipitates agree with this assumption. Authigenic precipitates of relocated ferrous iron can often be detected by magnetic methods. In all sediment cores from the Equatorial Divergence region, a susceptibility spike appears just above the modern redox boundary, always corresponding to an age of about 14 ka. According to rock magnetic characteristics, this magnetite phase is probably constituted of fossil bacterial magnetosomes. Northerly cores with a more expanded redox zonation do not exhibit this magnetic enhancement.

Acknowledgements

We thank officers and crews of RV *Meteor* for their efficient support during cruises M 29/3 and M 38/1. U. Röhl made the XRF scanner measurements possible and was very helpful. This study was funded by the Deutsche Forschungsgemeinschaft (Sonderforschungsbereich 261 at Bremen University, contribution No. 386). J.A. Funk was supported by the Deutsche Forschungsgemeinschaft in the framework of Graduiertenkolleg 221. T. von Dobeneck is a visiting research fellow at Utrecht University supported by the Netherlands Research Center for Integrated Solid Earth Science (ISES). The two peer reviewers, D. Rey and M. Urbat, have greatly improved this manuscript and are gratefully acknowledged.

References

Archer D, Maier-Reimer E (1994) Effect of deep-sea sedimentary calcite preservation on atmospheric CO_2 concentration. Nature 367: 260-263

Bassinot FC, Labeyrie LD, Vincent E, Quidelleur X, Shakelton NJ, Lancelot Y (1994) The astronomical theory of climate and the age of the Brunhes-Matuyama magnetic reversal. Earth Planet Sci Lett 126: 546-559.

Bickert T (1992) Rekonstruktion der spätquatären Bodenwasserzirkulation im östlichen Südatlantik über stabile Isotope bentischer Foraminiferen. Ber Fachber Geowiss Univ Bremen 27, pp 1-205

Bickert T, Wefer G (1996) Late Quaternary deep water circulation in the South Atlantic: Reconstruction from carbonate dissolution and benthic stable isotopes. In: Wefer G, WH Berger, Siedler G and Webb DJ (eds) The South Atlantic: Present and Past Circulation, Springer-Verlag, Berlin, pp 599-620

Bishop JKB (1988) The barite-opal-organic carbon association in oceanic particulate matter. Nature 332: 341-343

Bloemendal J, King JW, Hall FR, Doh S-J (1992) Rock magnetism of late Neogene and Pleistocene deep-sea sediments: Relationship to sediment source, diagenetic processes, and sediment lithology. J Geophys Res 97: 4361-4375

Bloemendal J, Lamb B, King J (1988) Paleoenvironmental implications of rock - magnetic properties of late Quaternary sediment cores from the eastern equatorial Atantic. Paleoceanography 3: 61 -87

Bonifay D, Giresse P (1992) Middle to Late Quaternary sediment flux and post- depositional processes between the continental slope off Gabon and the Mid-Guinean margin. Mar Geol 106: 107-129

Boyle EA, Keigwin LD (1982) Deep circulation of the North Atlantic over the last 200,000 years: Geochemical evidence. Science 218: 784-787

Boyle EA, Keigwin LD (1985) Comparison of Atlantic and Pacific paleochemical records for the last 215,000 years: Changes in deep ocean circulation and chemical inventories. Earth Planet Sci Lett 76: 135-140

Broecker WS, Denton GH (1989) The role of ocean-atmosphere reorganisations in glacial cycles. Geochim Cosmochim Acta 53: 2465-2501

Brummer GJA, Van Eijden AJM (1992) 'Blue-ocean' paleoproductivity estimates from pelagic carbonate mass accumulation rates. Mar Micropaleontol 19: 99-117

Canfield DE, Berner RA (1987) Dissolution and pyritization of magnetite in anoxic marine sediments. Geochim Cosmochim Acta 51: 645-659

Colley S, Thomson J, Wilson TRS, Higgs NC (1984) Post-depositional migration of elements during diagenesis in brown clay and turbidite sequences in the North East Atlantic. Geochim Cosmochim Acta 48: 1223-1235

Curry WB, Lohmann GP (1986) Late Quaternary sedimentation at the Sierra Leone Rise (eastern equatorial Atlantic Ocean). Mar Geol 70: 223-250

Curry WB, Lohmann GP (1990) Reconstructing past particle fluxes in the tropical Atlantic Ocean. Paleoceanography 5: 487-506

Curry WB (1996) Late Quaternary deep circulation in the western Equatorial Atlantic. In: Wefer G, Berger WH, Siedler G, Webb D (eds) The South Atlantic: Present and Past Circulation. Springer, Berlin, pp 577-598

Damuth JE (1977) Late Quaternary sedimentation in the western equatorial Atlantic. Geol Soc Amer Bull 88: 695-710

deMenocal PB, Ruddiman WF, Pokras EM (1993) Influences of high- and low- latitude processes on African terrestrial climate: Pleistocene eolian records from equatorial Atlantic ocean drilling program Site 663. Paleoceanography 8: 209-242

Dunlop DJ (1973) Superparamagnetic and single-domain threshold sizes in magnetite. J Geophys Res 78: 1780–1793

Duplessy J C, Labeyrie L, Paterne M, Hovine S, Fichefet T, Duprat J, Labracherie M (1996) High latitude deep water sources during the Last Glacial Maximum and the intensity of the global oceanic circulation. In: Wefer G, Berger WH, Siedler G, Webb D. (eds) The South Atlantic: Present and Past Circulation. Springer, Berlin, pp 445-460

Dupont LM, Jahns S, Marret F, Ning S (2000) Vegetation change in equatorial West Africa: Time-slices for the last 150 ka. Palaeogeogr Palaeoclimatol Palaeoecol 155: 95-122

Fischer G and participants (1998) Report and preliminary results of METEOR cruise M38/1, Las Palmas - Recife, 25.1.-1.3.1997. Ber Fachber Geowiss Univ Bremen 94, pp 1-178

François R, Bacon MP (1991) Variations in terrigenous input into the deep Equatorial Atlantic during the past 24,000 years. Science 251: 1473-1475

François R, Bacon MP, Suman DO (1990) Thorium 230 profiling in deep-sea sediments: High-resolution records of flux and dissolution of carbonate in the equatorial Atlantic during the last 24000 years. Paleoceanography 5: 761–787

Frederichs T, Bleil U, Däumler K, von Dobeneck T, Schmidt A (1999) The magnetic view on the marine paleoenvironment: Parameters, techniques, and potentials of rock magnetic studies as a key to paleoclimatic and paleoceanographic changes. In: Fischer G, Wefer G (eds) Use of Proxies in Paleoceanography: Examples from the South Atlantic. Springer Berlin, pp 575-599

Froelich PN, Klinkhammer GP, Bender ML, Luedtke NA, Heath GR, Cullen D, Dauphin P, Hammond D, Hartman B, Maynard V (1979) Early oxidation of organic matter in pelagic sediments of the eastern equatorial Atlantic: Suboxic diagenesis. Geochim Cosmochim Acta 43: 1075-1090

Gardner JV, Burkle LH (1975) Upper Pleistocene Ethmodiscus rex from the eastern equatorial Atlantic. Micropaleontology 21: 236-242

Gingele F, Dahmke A (1994) Discrete barite particles and barium as tracers of paleoproductivity in South Atlantic sediments. Paleoceanography 9: 151-168

Gingele FX, Zabel M, Kasten S, Bonn WJ, Nürnberg CC (1999) Biogenic barium as a proxy for paleoproductivity: Methods and limitations of application. In: Fischer G, Wefer G (eds) Use of proxies in paleoceanography: Examples from the South Atlantic.

Springer, Berlin, pp 345-364
Haese RR, Petermann H, Dittert L, Schulz HD (1998) The early diagenesis of iron in pelagic sediments: A multidisciplinary approach. Earth Planet Sci Lett 157: 233-248.
Higgs HC, Thomson J, Wilson TRS, Croudace IW (1994). Modification and complete removal of eastern Mediterranean sapropels by postdepositional oxidation. Geology 22: 423 - 426
Jansen JHF, Van der Gaast SJ, Koster AJ (1998) CORTEX, a shipboard XRF-scanner for element analyses in split sediment cores. Mar Geol 151: 143-153
Johns WE, Schott FA, Zantopp RJ, Evans RH (1990) The North Brazil Current retroflection: Seasonal structure and eddy variability, J Geophys Res 95: 22103-22120
Karlin R, Levi S (1983) Diagenesis of magnetic minerals in recent haemipelagic sediments. Nature 303: 327-330
Karlin R, Levi S (1985) Geochemical and sedimentological control of the magnetic properties of hemipelagic sediments. J Geophys Res 90: 10,373-10,392
Karlin R, Lyle M, Heath GR (1987) Authigenic magnetic formation in suboxic marine sediments. Nature 326: 490-493
Karlin R (1990) Magnetite diagenesis in marine sediments from the Oregon continental margin. J Geophys Res 95: 4405-4419
Kasten S, Haese RR, Zabel M, Rühlemann C, Schulz HD (2001) Barium peaks at glacial terminations in sediments of the equatorial Atlantic Ocean - relicts of deglacial productivity pulses? Chemical Geology 175: 635-651
Kidd RB, Cita MB, Ryan WBF (1978) Stratigraphy of eastern Mediterranean sapropel sequences recovered during DSDP Leg 42A and their paleoenvironmental significance. In: Hsü KJ et al. (eds) Initial Reports of the Deep Sea Drilling Project. US Government Printing Office, Washington: pp 421-443
Kumar N, Embley RW (1977) Evolution and origin of Ceará Rise: An aseismic rise in the western equatorial Atlantic. Geol Soc Amer Bull 88: 683-694
Kutzbach JE (1981) Monsoon climate of the early Holocene: Climatic experiment with the Earth's orbital parameters for 9000 years ago. Science 214: 59-61
Lutjeharms JRE (1996) The exchange of water between the South Indian and South Atlantic Oceans. In: Wefer G, Berger WH, Siedler G, Webb D (eds) The South Atlantic: Present and Past Circulation. Springer, Berlin, pp 125-162
Lyle M (1983) The brown-green color transition in marine sediments: A marker of the Fe(III)-Fe(II) redox boundary. Limnol Oceanogr 28: 1026-1033
Lyle M (1988) Climatically forced organic carbon burial in equatorial Atlantic and Pacific Oceans. Nature 335: 529-532
Maher BA (1988) Magnetic properties of some synthetic submicron magnetites. Geophys J 94: 83-96
Martin WR, Sayles FL (1996) CaCO3 dissolution in sediments of the Ceara Rise, western equatorial Atlantic. Geochim Cosmochim Acta 60: 243-263
Maslin M, Mikkelsen N (1997) Amazon fan mass-transport deposits and underlying interglacial deposits: Age estimates and fan dynamics. Proc ODP Sci Results 155: 353-365
Meinecke G (1992) Spätquartäre Oberflächenwassertemperaturen im östlichen äquatorialen Atlantik. Ber Fachber Geowiss Univ Bremen 29, pp 1-181
Mercone D, Thomson J, Croudace IW, Siani G, Paterne M, Troelsta S (2000) Duration of S1, the most recent sapropel in the eastern Mediterranean Sea, as indicated by accelerator mass spectrometry radiocarbon and geochemical evidence. Paleoceanography 15: 336 - 347
Milliman JD, Summerhayes CP, Barretto HT (1975) Quaternary sedimentation on the Amazon continental margin: A model. Geol Soc Amer Bull 86: 610-614
Milliman JD (1993) Production and accumulation of calcium carbonate in the ocean: Budget of a non-steady. Glob Biochem Cycl 7: 927-957
Mix AC, Rugh W, Pisias N G, Veirs S (1992) Color reflectance spectroscopy: A tool for rapid charakterization of deep-sea sediments. Proc ODP, Initial Reports 138: 67-77
Müller PJ, Erlenkeuser H, v Grafenstein R (1983) Glacial - interglacial cycles in oceanic productivity inferred from organic carbon contents in eastern north Atlantic sediment cores. In: Thiede J, Suess E (eds) Coastal Upwelling Part B. Plenum Press, New York, USA: pp 365 - 398
Müller PJ, Hartmann M, Suess E (1988) The chemical environment of pelagic sediments. In: Halbach P, Friedrich G, von Stackelberg U (eds) The manganese nodule belt of the Pacific Ocean. Enke, Stuttgart, 254 p.
Oppo DW, Fairbanks RG (1987) Variability in the deep and intermediate water circulation of the Atlantic Ocean during the past 25,000 years: Northern Hemisphere modulation of the Southern Ocean. Earth Planet Sci Lett 86: 1-15
Parry LG (1965) Magnetic properties of dispersed magnetite powders. Philosophical Magazine 11: 303–312
Passier HF, Dekkers MJ, de Lange GJ (1998) Sediment chemistry and magnetic properties in an anomalously reducing core from the eastern Mediterranean

Sea. Chem Geol 152: 287-306

Passier HF, Dekkers MJ (2002) Assessment of the formation of iron oxides in the active oxidation front above sapropel S l in the eastern Mediterranean Sea by low- temperature magnetic properties. Geophys J Int, In press

Petermann H, Bleil U (1993) Detection of live magnetotactic bacteria in South Atlantic deep-sea sediments. Earth Planet Sci Lett 117: 223-228

Pfeifer K, Hensen C, Adler M, Wenzhöfer F, Weber B, Schulz HD (2002) Modeling of subsurface calcite dissolution - including the respiration and re-oxidation processes of marine sediments in the region of the equatorial upwelling off Gabon. Geochim Cosmochim Acta 66: 4247-4259

Pickard GL, Emery WJ (1990) Descriptive Physical Oceanography. Pergamon Press Oxford UK, 320 p

Rath S, Wagner T, Henrich S (1999) Pleistozäne Schwankungen im Staubeintrag und in der Karbonaterhaltung im äquatorialen Atlantik (ODP Site 663) zwischen 480 und 390 Ka: Hinweise aus Korngrößenanalysen. Zentralblatt Geologie-Paläontologie Teil I H 7-10: 1-19

Ratmeyer V, Balzer W, Bergametti G, Chiapello I, Fischer G, Wyputta U (1999a) Seasonal impact of mineral dust on deep-ocean particle flux in the eastern subtropical Atlantic Ocean. Mar Geol 159: 241-252

Ratmeyer V, Fischer G, Wefer G (1999b) Lithogenic particle fluxes and grain size distributions in the deep ocean off northwest Africa: Implications for seasonal changes of aeolian dust input and downward transport. Deep Sea Research 46: 1289-1337

Raymo ME, Ruddiman WF, Shakleton NJ, Oppo DW (1990) Evolution of Atlantic - Pacific $\delta^{13}C$ gradients over the last 2.5 m.y. Earth Planet Sci Lett 97: 353-368

Raymo ME, Oppo DW, Curry W (1997) The mid-Pleistocene climate transition: A deep-sea carbon isotopic perspective. Paleoceanography 12: 546-559

Rhein M, Schott F, Fischer J, Send U, Stramma L (1996) The deep water regime in the Equatorial Atlantic. In: Wefer G, Berger WH, Siedler G, Webb D (eds) The South Atlantic: Present and Past Circulation, Springer Berlin: pp 261-271

Robinson SG, Sahota JTS, Oldfield F (2000) Early diagenesis in North Atlantic abyssal plain sediments characterized by rock magnetic and geochemical indices. Mar Geol 163: 77-107

Röhl U, Abrams LJ (2000) High-resolution, downhole, and nondestructive core measurements from Sites 999 and 1001 in the Caribbean Sea: Application to the Late Paleocene thermal maximum. In: Leckie RM, Sigurdsson H, Acton GD, Draper G (eds) Proc ODP Sci Results. College Station Texas, pp 191-203

Rossignol-Strick M, Nesteroff W, Olive P, Vergnaud-Grazzini C (1982) After the deluge: Mediterranean stagnation and sapropel formation. Nature 295: 105-110

Ruddiman WF (1997) Tropical Atlantic terrigenous fluxes since 25,000 yrs B.P. Mar Geol 136: 189-207

Ruddiman WF, Janecek TR (1989) Pliocene-Pleistocene biogenic and terrigenous fluxes at equatorial Atlantic Sites 662, 663, and 664. In: Ruddiman W, Sarnthein M (eds) Proc ODP Sci Results. College Station, Texas pp 211-240

Rühlemann C, Frank M, Hale W, Mangini A, Mulitza S, Müller PJ, Wefer G (1996) Late Quaternary productivity changes in the western equatorial Atlantic: Evidence from 230Th-normalized carbonate and organic carbon accumulation rates. Mar Geol 135: 127-152

Sahota JTS, Robinson SG, Oldfield F (1995) Magnetic measurements used to identify paleoxidation fronts from the Madeira abyssal plain. Geophys Res Lett 22: 1961-1964

Sarnthein M, Tetzlaff G, Koopmann B, Wolter K, Pflaumann, U 1981. Glacial and interglacial wind regimes over the eastern subtropical Atlantic and North-West Africa. Nature 293: 193-196

Sarnthein M, Thiede J, Pflaumann U, Erlenkeuser H, Fütterer D, Koopmann B, Lange H, Seibold E (1982) Atmospheric and oceanic circulation patterns off Northwest Africa during the past 25 million years. In: von Rad U, Hinz K et al. (eds) Geology of the Northwest African Continental Margin. Springer-Verlag Berlin: pp 545-604

Sarnthein M, Winn K, Jung SJA, Duplessy J-C, Labeyrie L, Erlenkeuser H, Ganssen G (1994) Changes in east Atlantic deepwater circulation over the last 30,000 years: Eight time slice reconstructions. Paleoceanography 9: 209-267

Schmieder F, von Dobeneck T, Bleil U (2000) The Mid-Pleistocene climate transition as documented in the deep South Atlantic Ocean: Initiation, interim state and terminal event. Earth Planet Sci Lett 179: 539-549

Schneider RR, Schulz HD, Hensen C (2000) Marine carbonates: Their formation and destruction. In: Schulz HD, Zabel M (eds) Marine Geochemistry. Springer, Berlin, pp 283-307

Schulte S, Bard E (2003) Past changes of biologically mediated dissolution of calcite above the chemycal lysocline documented in Indian Ocean sediments. Quater Sci Rev 22 (15-17), 1757-1770

Schulz, HD and participants (1991) Report and

preliminary results of *Meteor* cruise M16/2, Recife - Belem, 28.4.-20.5.1991. Ber Fachber Geowiss Univ Bremen 19, pp 1-149

Showers WJ, Angle DG (1986) Stable isotopic characterization of organic carbon accumulation on the Amazon continental shelf. Continent Shelf Res 6: 227-244

Stolz JF (1992) Magnetotactic Bacteria: Biomineralization, Ecology, Sediment Magnetism, Environmental Indicator. In: Skinner HGW, Fitzpatrick RW (eds) Biomineralization processes of iron and manganese. Catena-Verl Cremlingen-Destedt, pp 133-145

Street-Perrott FA, Perrott RA (1990) Abrupt climate fluctuations in the tropics: The influence of Atlantic Ocean circulation. Nature 343: 607-612

Tarduno JA (1994) Temporal trends of magnetic dissolution in the pelagic realm: Gauging paleoproductivity? Earth Planet Sci Lett 123: 39-48

Tarduno JA, Tian W, Wilkison S (1998) Biogeochemical remanent magnetization in pelagic sediments of the western equatorial Pacific Ocean. Geophys Res Lett 25: 3987-3990

Tarduno JA, Wilkison SL (1996) Non-steady state magnetic mineral reduction, chemical lock-in, and delayed remanence acquisition in pelagic sediments. Earth Planet Sci Lett 144: 315-326

Thießen W (1993) Magnetische Eigenschaften von Sedimenten des östlichen Südatlantiks und ihre paläozeanographische Relevanz. Ber Fachber Geowiss Univ Bremen 4, pp 1-170

Thomson J, Higgs NC, Wilson TRS, Croudace IW, de Lange GJ, van Santvoort, PJM (1995) Redistribution and geochemical behaviour of redox - sensitive elements around S 1, the most recent eastern Mediterranean sapropel. Geochim Cosmochim Acta 59: 3487-3501

Tiedemann R, Sarnthein M, Shackleton NJ (1994) Astronomic timescale for the Pliocene Atlantic $\delta^{18}O$ and dust flux records of Ocean Drilling Program Site 659. Paleoceanography 9: 619-638

Tiedemann R, Sarnthein M, Stein R (1989) Climatic changes in the western Sahara: Aeolo-marine sediment record of the last 8 million years (Sites 657-661) In: Ruddimann W, Sarnthein M et al. (eds) Proc ODP Sci Results. Vol 108, pp 241-277

van Kreveld SA, Knappertsbusch M, Ottens J, Ganssen GM, van Hinte JE (1996) Biogenic carbonate and ice-rafted debris (Heinrich layer) accumulation in deep-sea sediments from a Northeast Atlantic piston core. Mar Geol 131: 21-46

van Santvoort PJM, de Lange GJ, Thomson J, Cussen H, Wilson TRS, Krom MD, Ströhle K (1996) Active post-depositional oxidation of the most recent sapropel (S1) in sediments of the eastern Mediterranean Sea. Geochim Cosmochim Acta 60: 4007-4024

van Santvoort PJM, de Lange GJ, Langereis CG, Dekkers MJ, Paterne M (1997) Geochemical and paleomagnetic evidence for the occurence of 'missing' sapropels in eastern Mediterranean sediments. Paleoceanography 12: 773-786

Verardo DJ, McIntyre A (1994) Production and destruction: Control of biogenous sedimentation in the tropical Atlantic 0-300,000 years BP. Paleoceanography 9: 63-86

von Dobeneck T (1996) A sytematic analysis of natural magnetic mineral assemblages based on modelling hysteresis loops with coercivity-related hyberbolic basis functions. Geophys J Int 124: 675-694

von Dobeneck T (1998) The concept of 'partial susceptibilities'. Geologica Carpathica 49: 228-229

von Dobeneck T, Schmieder F (1999) Using rock magnetic proxy records for orbital tuning and extented time series analyses into the Super- and Sub-Milankovitch bands. In: Fischer G, Wefer G (eds) Use of Proxies in Paleoceanography: Examples from the South Atlantic. Springer; Berlin, pp 601-633

Wagner T (2002) Organic sedimentation in the Equatorial Atlantic: Evolution from Cretaceous to early Quaternary depositional environments. Palaeogeogr Palaeoclimatol Palaeoecol 179: 113-147

Wagner T (2000) Control of organic carbon accumulation in the late Quaternary equatorial Atlantic (Ocean Drilling Program sites 664 and 663): Productivity versus terrigenous supply. Paleoceanography 15: 181-199

Wagner T, Dupont LM (1999) Terrestrial organic matter in marine sediments: Analytical approaches and eolian-marine records in the Central Equatorial Atlantic. In: Fischer G, Wefer G (eds) Use of Proxies in Paleoceanography: Examples from the South Atlantic. Springer, Berlin, pp 547-574

Wefer G, Berger W H, Bickert T, Donner B, Fischer G, Kemle-von Mücke S, Meinecke G, Müller P J, Mulitza S, Niebler H-S, Pätzold J, Schmidt H, Schneider R R, Segl M (1996) Late Quaternary surface circulation in the South Atlantic: The stable isotope record and implications for heat transport and productivity. In: Wefer G, Berger WH, Siedler G, Webb D (eds) The South Atlantic: Present and Past Circulation, Springer Berlin: pp 461-502

Wefer G and participants (1988) Report and preliminary results of *Meteor* cruise M6/6, Libreville - Las Palmas, 18.2.-23.3.1988. Ber Fachber Geowiss Univ Bremen 3, pp 1-97

Wefer G and participants (1989) Report and preliminary

results of *Meteor* cruise M9/4, Dakar - Santa Cruz, 19.2.-16.3.1989. Ber Fachber Geowiss Univ Bremen 7, pp 1-103

Wefer G and participants (1991) Report and preliminary results of *Meteor* cruise M16/1, Pointe Noir - Recife, 27.3.-25.4.1991. Ber Fachber Geowiss Univ Bremen 18, pp 1-120

Wefer G and participants (1994) Report and preliminary results of *Meteor* cruise M23/3, Recife - Las Palmas, 21.3.-12.4.1993. Ber Fachber Geowiss Univ Bremen 44, pp 1-71

Wilson TRS, Thomson J, Colley S, Hydes DJ, Higgs NC, Sorensen J (1985) Early organic diagenesis: The significance of progressive subsurface oxidation fronts in pelgic sediments. Geochim Cosmochim Acta 49: 811-822

Wilson TRS, Thomson J, Hydes DJ, Colley S, Culkin F, Sörensen J (1986) Oxidation fronts in pelagic sediments: Diagenetic formation of metal-rich layers. Science 232: 972-975

Wilson TRS, Thomson J (1998) Calcite dissolution accompanying early diagenesis in turbiditic deep ocean sediments. Geochim Cosmochim Acta 62: 2087-2096

Zabel M, Bickert T, Dittert L, Haese RR (1999) Significance of the sedimentary Al:Ti ratio as an indicator for variations in the circulation patterns of the equatorial North Atlantic. Paleoceanography 14: 789-799

Chapter 4

Integrated Rock Magnetic and Geochemical Proxies for Iron Mineral Dissolution and Precipitation in Marine Sediments Based on Single Sample and New Split Core Scanning Techniques

Tilo von Dobeneck and Jens A. Funk

Universität Bremen, Fachbereich Geowissenschaften, Postfach 33 04 40,
D-28334 Bremen, Germany
(e-mail): dobeneck@uni-bremen.de

Numerous paleoenvironmental studies on suboxic to anoxic sediments have combined rock magnetic and chemical data to identify iron mineral alteration by *redoxomorphic diagenesis* (Dapples, 1962), a 'collective noun for processes of early diagenesis involving both reductive and oxidative stages' (Robinson et al., 2000). Redox reactions inducing dissolution, depletion, relocation and precipitation of iron take place in and around sapropels, turbiditic sequences and organically enriched sediments deposited under conditions of upwelling, reduced bottom water circulation or eutrophication. The geochemical settings for redoxomorphic diagenesis are alike in all mentioned situations: The (bacterially mediated) oxidation of embedded organic matter follows a declining energy yield sequence of terminal electron acceptors from interstitial oxygen and nitrate to Mn (IV), Fe (III) and sulfate (Froelich et al., 1979). At the stage of iron reduction organic carbon mineralization leads to a gradual dissolution of ferric iron minerals such as magnetite, maghemite and hematite.

This process is exemplified in Figure 1 by rock magnetic and geochemical single sample data of an active iron redox boundary in an Equatorial Atlantic sediment core (GeoB 2908-7, 0-100 cm) marked by a sharp brown-gray color transition at about 45 cm depth (Fig. 1a). Further characteristic diagenesis features related with an organically enriched layer (Fig. 1b) are a local minimum in magnetic mineral concentration (Fig. 1c) and a relative decrease of the finer vs. coarser magnetite fractions (Fig. 1d) caused by preferential dissolution of finer particles. Thereby produced ferrous iron precipitates in situ as paramagnetic phase or diffuses upwards to the active iron redox front forming authigenic, generally paramagnetic Fe^{3+} oxihydroxides and biogenic magnetite. An iron enrichment due to this relocation is detected by peaks in the element ratio of (mobile) iron and (stable) aluminum (Fig. 1e).

This short and relatively simple section shows that intense diagenesis is well detected by co-interpreting the shown standard rock magnetic and chemical data sets. However, these diagnostics are semi-quantitative at best, ambiguous with respect to changes in primary lithology and not sensitive enough to detect mild forms of diagenesis. For ample resolution of the fine-scaled signal these single sample measurements have to be performed at 1-2 cm spacing - a rather laborious task for longer sections. We have therefore developed more selective and quantitative proxy parameters for iron oxide diagenesis based entirely on data acquired by half core logging systems. Applied to a longer sequence as Central Equatorial Atlantic core GeoB 4317-2 (Fig. 2) the gain in affordable resolution and information from single sample (Figs. 2a-c,e,f,h) to scanning measurements (Figs. 2d,g,i-l) is obvious.

Spot readings of magnetic susceptibility ê (Figs. 1f, 2d) cumulate all iron minerals with high emphasis of ferrimagnetic species. Sharp signal minima of susceptibility deviating from the general trend of other climate proxies, e.g. $\%CaCO_3$ (Fig.2e), are indicative, but not specific of magnetite dissolution. This is unfortunate as susceptibility logs can be easily acquired at rates of some 100 data points per hour. At half that speed runs a new logging device capable of measuring total iron concen-

From SAGNOTTI L and ROBERTS AP (eds), 2002, *Fundamental Rock Magnetism and Environmental Application*
Quaderni di Geofisica No 26, pp 183-185

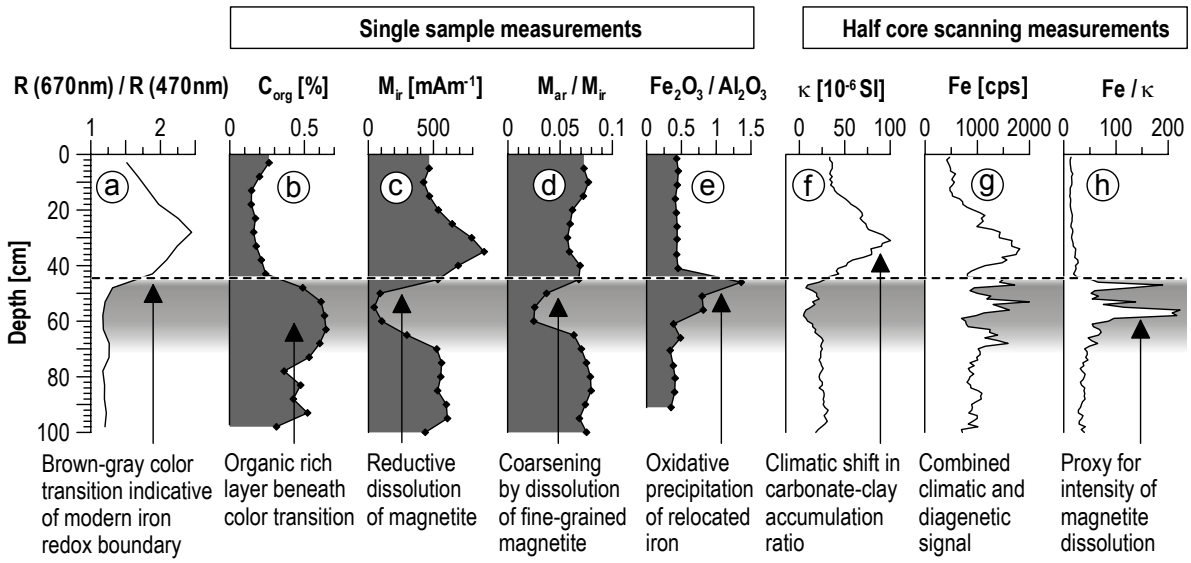

Fig.1. Characteristic signatures of redoxomorphic iron mineral diagenesis at the active Fe^{3+}/Fe^{2+} redox boundary (dotted line) exemplified by equatorial Atlantic gravity core GeoB 2908-7. Curves represent **(a)** ratio of red and blue reflectance, **(b)** organic carbon content, **(c)** isothermal remanent magnetization, **(d)** magnetogranulometric ratio, **(e)** iron/aluminum ratio, **(f)** magnetic susceptibility, **(g)** iron content, **(h)** iron/susceptibility ratio. Gray curve fillings represent single sample, white fillings half core scanning measurements. The horizontal band symbolizes the magnetite dissolution layer.

trations, the X-ray fluorescence (XRF) core scanner (Jansen et al., 1998). This automated instrument developed and built at the Netherlands Institute for Sea Research (NIOZ, Texel) is available at our department and can detect K, Ca, Ti, Mn, Fe, Cu and Sr contents down to concentrations of around 0.1%.

In most parts of the exemplary record, Fe counts (Figs. 1g, 2g) mimic respective susceptibility signals as both parameters largely delineate the terrigenous content. However, XRF data are largely unbiased by mineralogy and do not follow susceptibility lows caused by conversion of ferri- into paramagnetic iron species. The Fe/κ ratio of both logs (Figs. 1h, 2i) therefore highlights exactly those intervals, where such alterations occur. Combining both scanning techniques, diagenetically altered sediments can be detected at a hitherto unprecedented speed and precision - provided that the primary composition of the terrigenous sediment fraction has been fairly constant through time. An alternative entirely hysteresis-based proxy is the ratio of high-field to low-field susceptibility, here abbreviated as χ_{nf}/χ_{tot} (Fig. 2h). Both proxy signals reveal a succession of three zones of intense reduction linked to glacial oxygen stages 6, 10 and 12. Less pervasive diagenesis is indicated during all other glacials,

Fig.2(right). Geochemical and rock magnetic records of equatorial Atlantic gravity core GeoB 4317-2. Curves (single sample data: dotted line, scanned data: solid line) represent **(a)** organic carbon content, **(b)** magnetogranulometric ratio of anhysteretic and isothermal magnetization, **(c)** $S_{-0.3T}$ ratio of low- and high-coercive minerals, **(d)** non-diamagnetic susceptibility κ_{nd} (= $\kappa + 15 \cdot 10^{-6}$ to avoid zero value), **(e)** non-carbonate (terrigenous) content, **(f)** non-ferrimagnetic (hysteretic high field) susceptibility χ_{nf}, **(g)** XRF iron content, **(h)** hysteresis-based magnetite dissolution proxy χ_{nf}/χ_{tot}. Newly proposed iron diagenesis proxies (normalized to baseline value of 1) for **(i)** magnetite dissolution Fe/κ_{nd}, **(j)** iron enrichment by relocation Fe/Ti, **(k)** magnetic mineral precipitation κ_{nd}/Ti, **(l)** relative magnetite content κ_{nd}/Fe. Labels DL I to III indicate layers of intense magnetite dissolution. Background shading marks degree of magnetite dissolution based on Fe/κ_{nd}. Magnetic mineral precipitation zones based on κ_{nd}/Ti are hatched. The right column delimits warm (white) and cold (gray) oxygen isotope stages.

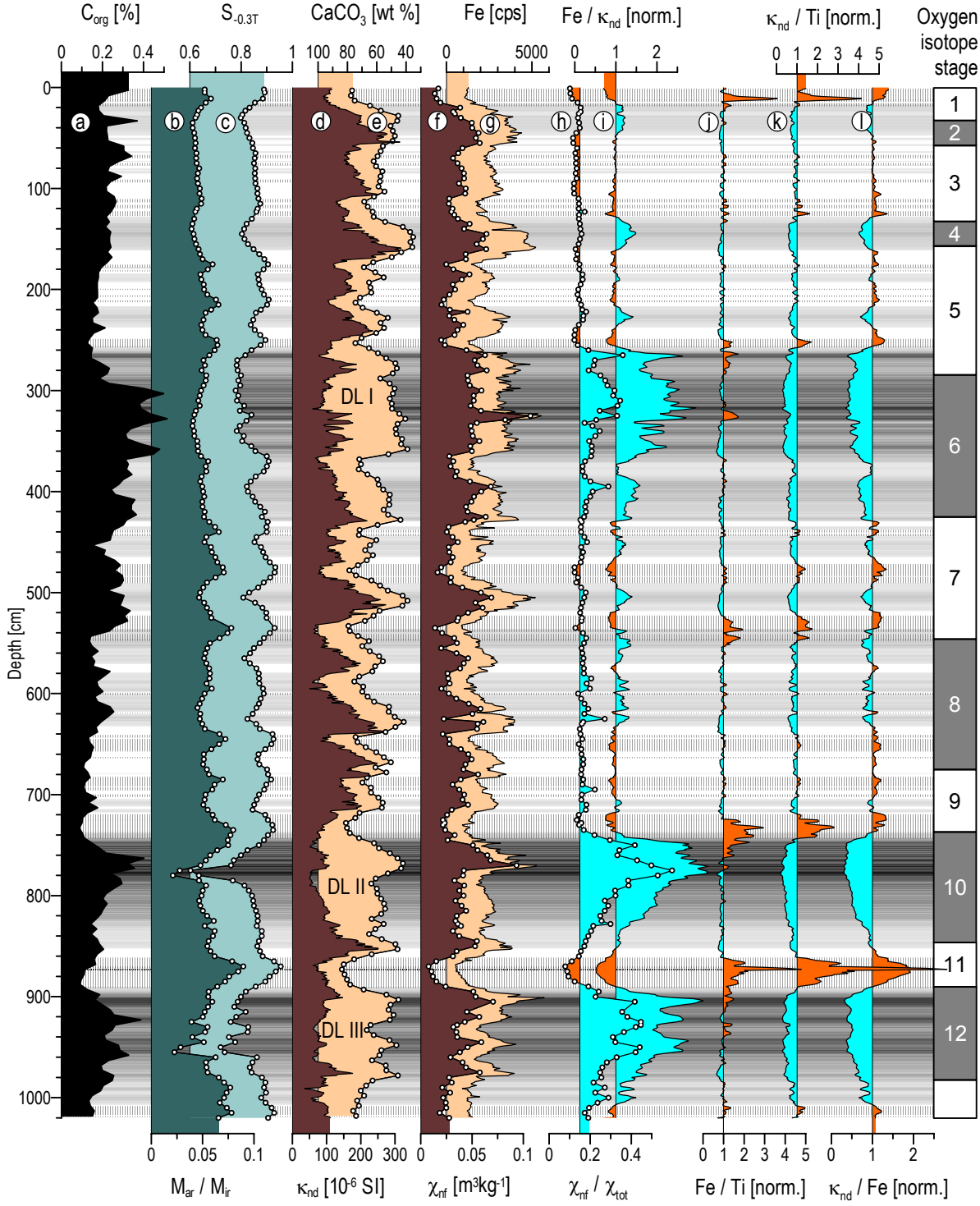
C_org [%]
S_-0.3T
CaCO3 [wt %]
Fe [cps]
Fe / κnd [norm.]
κnd / Ti [norm.]
Oxygen isotope stage
Depth [cm]
DL I
DL II
DL III
Mar / Mir
κnd [10-6 SI]
χnf [m3kg-1]
χnf / χtot
Fe / Ti [norm.]
κnd / Fe [norm.]

in spite that the corresponding C_{org} contents (Fig. 2a) are not always elevated. It is very likely, that the C_{org} concentrations in these layers were originally larger and have been later diminished by prograding oxidation. The reductive loss of magnetite is therefore a useful indicator of former suboxic events.

Sedimentary Ti^{4+} is like Al^{3+} an inert and insoluble, hence conservative ion of terrigenous origin. Primary titanium accumulation is mostly highly correlated with that of iron. XRF-based Ti logs can therefore be used as normalizers for κ and Fe logs. This yields two additional proxy ratios for ferrimagnetic iron precipitation (κ_{nd}/Ti, Fig. 2k) and total iron enrichment (Fe/Ti, Fig. 2j).

In total, the mutual proportionalities of Fe, Ti and magnetite concentrations in unaltered sediment sections enable us to define quantitative proxy parameters for magnetite depletion (Fe/κ_{nd}) below and precipitation (κ_{nd}/Ti) above the modern and numerous fossil redox boundaries, while iron relocation is detected on basis of the Fe/Ti ratio. All three ratios were calibrated internally by setting the baseline value to 1. It is possible to reconstruct and quantify primary deposition and secondary change of magnetite as well as total Fe by using linear Ti-based transfer functions derived in pristine core sections. All necessary raw data sets can be measured by combining non-destructive split core surface scanning techniques with a cumulative data acquisition time of less than two minutes per sample.

References

Dapples, EC (1962) Stages of diagenesis in the development of sandstones. Geological Society of America Bulletin, 73, 913-934

Froelich, PN, Klinkhammer GP, Bender ML, Luedtke NA, Heath GR, Cullen D, Dauphin P, Hammond D, Hartman B, Maynard V (1979) Early oxidation of organic matter in pelagic sediments of the eastern equatorial Atlantic: suboxic diagenesis. Geochimica et Cosmochimica Acta, 43, 1075-1090.

Jansen JHF, Van der Gaast SJ and Koster AJ (1998) CORTEX, a shipboard XRF-scanner for element analyses in split sediment cores. Marine Geology, 151,143-153.

Robinson SG, Sahota JTS and Oldfield F (2000) Early diagenesis in North Atlantic abyssal plain sediments characterized by rock magnetic and geochemical indices. Marine Geology, 163, 77-107.

Chapter 5

A combined geochemical and rock-magnetic investigation of a redox horizon at the last glacial/interglacial transition

A. Reitz[1*], C. Hensen[2], S. Kasten[3], J.A. Funk[3] and G.J. deLange[1]

[1]*Geochemistry Department, Faculty of Earth Sciences, Utrecht University, P.O. Box 80021, 3508 TA Utrecht, The Netherlands*
[2]*GEOMAR – Research Centre for Marine Geosciences, Marine Environmental Geology Wischhofstr. 1-3, D-24148 Kiel, Germany*
[3]*Universität Bremen, Fachbereich Geowissenschaften, Postfach 33 04 40, D-28334 Bremen, Germany*
[*] *corresponding author (e-mail): A.Reitz@geo.uu.nl*

Abstract: A high-resolution study of an active Fe^{2+}/Fe^{3+} redox horizon has been carried out on sediments of the central equatorial Atlantic. The multidisciplinary approach combining geochemical and rock-magnetic parameters gives evidence of the interrelation of the redox horizon with the last change from glacial to interglacial conditions (T1). Distinct enrichments of redox-sensitive elements (Mn, Fe, V, and U) reveal a characteristic depth-sequence, indicating non-steady-state diagenetic conditions caused by a decrease in productivity and an increase in oxygen content in the bottom water during T1 and a reversal during the Holocene. Thus, the redox boundaries first moved down into the sediment and subsequently upwards. The movement of the redox boundaries led to the development of conspicuous double peaks for Fe and Mn. The reconstruction based on geochemical data is supported by susceptibility and magnetization measurements of the sediments displaying well-defined anomalies in the vicinity of active and paleo redox boundaries. The combination of geochemical and rock-magnetic parameters, like the ferrimagnetic susceptibility, and total Fe concentration (χ_f/Fe) are suitable for characterizing distinct zones of dissolution and precipitation of ferromagnetic mineral phases (e.g. magnetite). Moreover, the small scale movement of the Fe^{2+}/Fe^{3+}redox-boundary, could be traced in detail by overlaying the peak-shape pattern of V/Al and of χ_f/χ_{tot}.

Keywords: Equatorial Atlantic Ocean, high resolution investigation, geochemistry, rock-magnetics, non-steady state diagenesis, Fe^{2+}/Fe^{3+} redox-boundary

1. Introduction

During the Quaternary the interaction of atmospheric and oceanic circulation patterns, which controls the productivity and preservation of organic matter, changed repeatedly in response to orbitally forced glacial/interglacial cycles (Wagner, 1999; Berger et al., 1994; Imbrie and Palmer Imbrie, 1998). Deep-ocean sediments are archives for such climate variations, which can be revealed by the analysis of various properties determined by geochemical, geophysical or sedimentological methods (cf. Fischer & Wefer, 1999). In particular, geochemical and rock-magnetic investigations of marine sediments can give useful information on long-term variation of a number of climate-driven processes (e.g. accumulation of organic carbon, oxygen content in bottom water etc.).

Abrupt changes of organic matter input and/or the oxygen level in the bottom water are shown to generate transient conditions of early diagenetic processes (Wilson et al., 1985). Diagenetic processes may not only overprint primary sedimentary signals, but can also generate secondary diagenetic

signals contributing valuable information about the magnitude and type of the driving processes (e.g. Wilson et al., 1985). Evidence for changes in the sedimentary and depositional environment are particularly pronounced in the following sediment sequences: (1) turbidites (e.g. Prahl et al., 1989; Thomson et al., 1993), (2) sapropels of the Mediterranean Sea (e.g. de Lange et al., 1989; Thomson et al., 1995; van Santvoort et al., 1996), and (3) glacial/interglacial transitions (e.g. Thomson et al., 1996).

Environmental changes like increases in productivity and sedimentation rate and/or a reduction in deep-water circulation may result in oxygen deficiency in the bottom, water thus enhancing the burial and preservation of non-oxidized organic matter in deep-sea sediments (Arthur et al., 1984; Emerson and Hedges, 1988; Tyson and Pearson 1991). Primary productivity and the preservation of organic matter in sediments of the modern equatorial Atlantic is influenced by changes in oceanic and atmospheric circulation patterns. In sediments of the tropical and equatorial Atlantic cyclic formations of organic-rich layers were formed from Pleistocene to recent during glaciations by enhanced primary productivity and better preservation of organic matter due to the reduction of bottom water exchange (see summary by Funk et al., 2004a, and references therein).

The diagenetic remineralisation of the buried organic matter occurs via a sequence of pathways catalyzed by different types of microorganism, which use dissolved oxygen followed by a sequence of secondary oxidants. In order of decreasing energy supply these are nitrate and/or Mn-oxides, Fe-oxides and sulfate (Froelich et al., 1979; Curtis, 1983), and their use creates a change in redox conditions. This change in redox conditions is usually accompanied by a change in sediment color from brown to grey. In the following, we present a brief overview of the characteristic geochemical and rock-magnetic patterns that result from this diagenetic sequence.

Geochemical and rock-magnetic characteristics as proxies for diagenetic overprinting

In marine sediments Lyle (1983), König et al. (1997, 1999), and Robinson et al. (2000) attribute the color change from reddish/brownish in the oxic part to grayish/greenish in the anoxic part to a redox change of iron, which is bound to clay minerals. The enrichment and distribution of redox-sensitive elements around the color transition is controlled by the type and course of the diagenetic processes. Consequently, the element enrichments in the vicinity of a color change represent secondary authigenic formations. The behavior of redox-sensitive elements is thought to be indicative for the oxygen content of the bottom water during the formation of the facies (Calvert and Pedersen, 1993).

The penetration depth of oxygen into the sediment is controlled by the accumulation rate and reactivity of organic carbon and the oxygen content of the bottom water. A change in any of these parameters will result in a change of redox conditions in the sediment. Under oxic conditions manganese and iron form insoluble oxides, whereas vanadium and uranium are present as soluble anions. Under anoxic conditions the latter two are reduced to insoluble species of lower charge (Mangini et al., 2001), but the former two are mobilized.

Variations in the rock-magnetic characteristics of marine sediments are mostly climate-driven (Bloemendal et al., 1988; Frederichs et al., 1999). Changes in concentration and composition of magnetic materials are mainly a result of a change in the source area and transport mechanism but are also affected by secondary processes like reductive diagenesis and production of biogenic magnetite (Bloemendal et al., 1989, 1992; van Hoof et al., 1993; Tarduno and Wilkison, 1996; Passier et al., 1998). Since the amount of magnetic minerals in marine sediments is very low, they have a high potential to display even the slightest changes in the geochemical environment.

In this study we compare the depth of the color transition and the glacial/interglacial transition in a core from the central equatorial Atlantic. We use a high resolution multidisciplinary approach, combining

geochemical and rock-magnetic results. This has enabled us to determine the fixation of the Fe-redox transition at the last glacial/interglacial transition. In addition, we have reconstructed the development and the movement of the Fe^{2+}/Fe^{3+}-redox boundary in response to climate change. By the aforementioned reconstruction we developed a better knowledge of the climate-induced environmental changes effective to sediments located on the border of an upwelling area.

2. Materials and methods

2.1 Core location and stratigraphy

Gravity core GeoB 2908-7 with a total length of 10.94 m was recovered during Meteor cruise M29/3 in the central equatorial Atlantic (00°06.4'N, 23°19.6'W) in the area of the Central Equatorial Fracture Zone from 3809 m water depth (Fig. 1). The Central Equatorial Fracture Zone System is known as the current pathway for the Antarctic Bottom Water (AABW) from the western to the eastern Atlantic Ocean (Mercier et al., 1994). The core station is located in the Equatorial Divergence zone, a region of intensified productivity due to northeast trade wind controlled surface currents. Additionally, this area receives a strong eolian input from the Saharan dust plume, raining out within the ITCZ (Inter Tropical Convergence Zone; Fig. 1). According to Sarnthein et al. (1981) and Bloemendal et al. (1992) the Saharan dust plume is the predominant source of magnetic minerals and detrial iron in the Equatorial Atlantic.

The sediment core consists mainly of undisturbed pelagic sediments (Baumann et al., 1995) principally foraminiferal/nannofossil oozes (Wagner and Klemd, 1995). The first 95 cm of the sediment core represent the last 26.19 ky (age model after Funk et al., 2004a). The colour change from light olive (anoxic) to light brown (oxic) is located at 46 cm (Fig. 2). Below 46 cm the sediment is grey to olive-green. The distinct colour change is located at about 10 cm below the midpoint of T1 (13.5 kyr, Raymo, 1997; ablation phase at the oxygen isotope boundary 2/1).

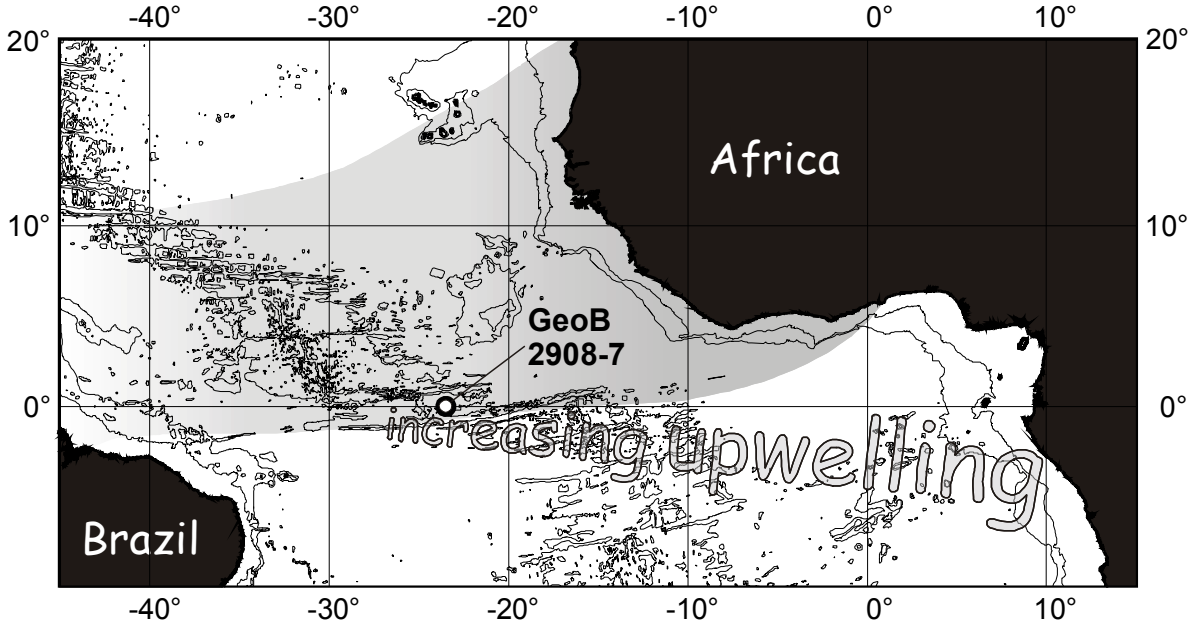

Fig. 1. Map of the equatorial Atlantic Ocean with the site of gravity core GeoB 2908-7. Upwelling related to the Equatorial Divergence intensifies eastward increasing productivity and organic matter accumulation. The shaded area indicates the region of Saharan dust fall for the boreal winter situation.

2.2 Geochemical analysis

Bulk element analyses of the sediment sequence 0-95 cm were performed by Inductively Coupled Plasma-Atomic Emission Spectrometry (*Perkin-Elmer* optima 3300 RL ICP-AES) and Inductively Coupled Plasma-Mass Spectrometry (*Finnigan* Sola ICP-MS) in 1 cm resolution after a 3-step total digestion in a microwave device (Ethos 1600 and Mega 2, MLS). (1) Digestion of 50 mg of freeze-dried sediment in a mixture of 3 mL HNO_3 (65% s.p.), 2 mL HF (48% s.p.) and 2 mL HCl (30% s.p.) at 200°C; (2) evaporation of the solution close to dryness; (3) dissolution and homogenisation of the residual in a solution of 0.5 mL HNO_3 (65% s.p.) and 4.5 mL MilliQ-water, finally the solution was filled up to 50 mL with MilliQ-water. To each batch of 10 samples, one blank and a reference standard (MAG-1, USGS; Gladney and Roelandts, 1988) have been added and treated in the same way as the sediments. Each sample solution was analyzed in 3 replicates, and a deviation of less than 3% was accepted for ICP-AES and less than 10% for ICP-MS.

Dissolution effects (e.g. calcium carbonate) should be minimized by normalizing the measured elements to aluminum (Al). It is assumed that Al is exclusively bound to the alumosilicate phase (Calvert and Petersen, 1993) and behaves as a conservative element with respect to diagenetic overprinting (Thomson et al., 1998). Hence this technique emphasizes the effects of diagenetic element mobilization (Brown et al., 2000).

2.3 Rock-magnetic analysis

Hysteresis measurements were carried out at a 1 cm resolution with a *PMC* M2900 alternating gradient force magnetometer (AGM). For the measurements < 50 mg miniature samples as described by von Dobeneck (1996) have been prepared. The 3 step hysteresis analysis started with the determination of the minor loop applying a maximum field strength of 300 mT and a field increment of 2 mT. In the second step the backfield curve was determined by first magnetizing the sample and subsequently magnetizing it in the opposite direction. Finally, the major loop was determined applying a maximum field strength of 1000 mT and a field increment of 5 mT in the third step. The hysteresis measurements were processed with the program HYSTEAR (von Dobeneck, 1996) to acquire the basic hysteresis parameters, which are (1) the saturation magnetization M_s, (2) the remanent saturation magnetization M_{rs}, (3) the coercivity B_c, and (4) the remanent coercivity B_{cr}. Accordingly, the magnetization (i.e. magneto-granulometric M_{rs}/M_s ratio by Day et al., 1977), and magnetic stability of a sample can be derived. The hysteresis based total susceptibility χ_{tot} (per mass unit) integrates all induced magnetization signals; the non-ferromagnetic susceptibility χ_{nf} represents exclusively the paramagnetic (iron-bearing silicates and clays) and the diamagnetic (biogenic carbonate and opal) sediment matrix. The difference between them is given by the ferromagnetic susceptibility χ_f, which is a quantitative measure of the abundance of ferromagnetic and antiferromagnetic minerals.

3. Results

3.1 Geochemical characteristics

Down-core variations of element/Al-ratios are plotted in Figure 2. A conspicuous depth sequence of redox-sensitive element enrichments around the color transition is distinctively visible. The sequence starts with a broad Mn/Al double-peak above the color change that is followed downward by an Fe/Al double-peak of which the upper one is located directly at the color change. Just below the upper Fe/Al peak, increasing values of V/Al occur, followed in turn by increasing values of U/Al.

The productivity-related Ba/Al ratio shows increasing values below the glacial to interglacial transition (TI). These increased values form a broad peak extending over at least 30 cm; in addition, there is a slight but distinct increase from about 5 to 15 cm depth. The Sr/Al plot displays higher values from about 0 to 15 cm depth followed by a distinct broad depletion between 15 and about 40 cm. Below that depth mean values prevail.

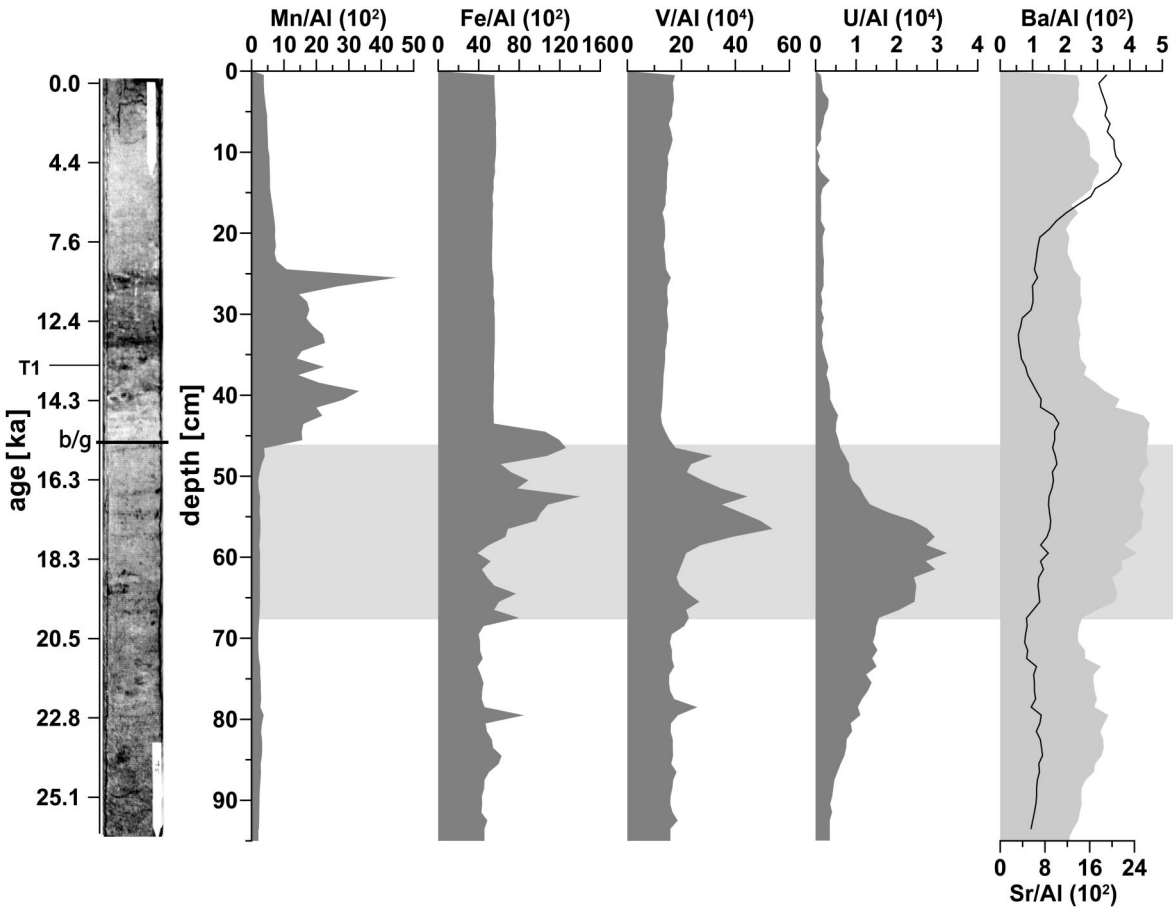

Fig. 2. Results of geochemical, solid phase analyses within the first meter segment of gravity core GeoB 2908-7. The sediment age on the left hand side of the core picture is given after Funk et al. (2003a). The midpoint of the termination is represented by the horizontal light grey line labeled as T1. The color change from brownish/reddish (0-46 cm) to greenish/grayish (47-95 cm) is marked by the horizontal grey line labeled b/g (brown/grey). From the left to the right the enrichment sequence of redox-sensitive element to aluminum ratios are depicted. The last plot to the right displays the productivity related Ba/Al ratio and the $CaCO_3$ accumulation related Sr/Al ratio. The horizon of diagenetic mineral dissolution is shown as a light grey background rectangle.

3.2 Rock-magnetic and combined rock-magnetic/geochemical characteristics

Concentration-dependent parameters

The ratio of ferrimagnetic susceptibility to total susceptibility (χ_f/χ_{tot}; Fig. 3) shows a pronounced drop at about 47 cm followed by a gradual recovery to its original level at about 66 cm. This reduction in χ_f/χ_{tot} correlates with the visible color change from brown to gray. Other rock magnetic anomalies also occur in this part of the core. These are reductions in the total susceptibility to iron-ratio (χ_f/Fe), and in the remanent magnetism to aluminum-ratio (M_{rs}/Al). The non-ferrimagnetic susceptibility (χ_{nf}) shows three main peaks. One pronounced peak is located above TI and two smaller ones are found within the marked redox horizon.

Grain size sensitive parameters

The profile of B_c being indicative for the presence of stable magnetite shows a peak-shaped enrichment within the zone of the color change (Fig.3). Down core to about 65 cm this enrichment is

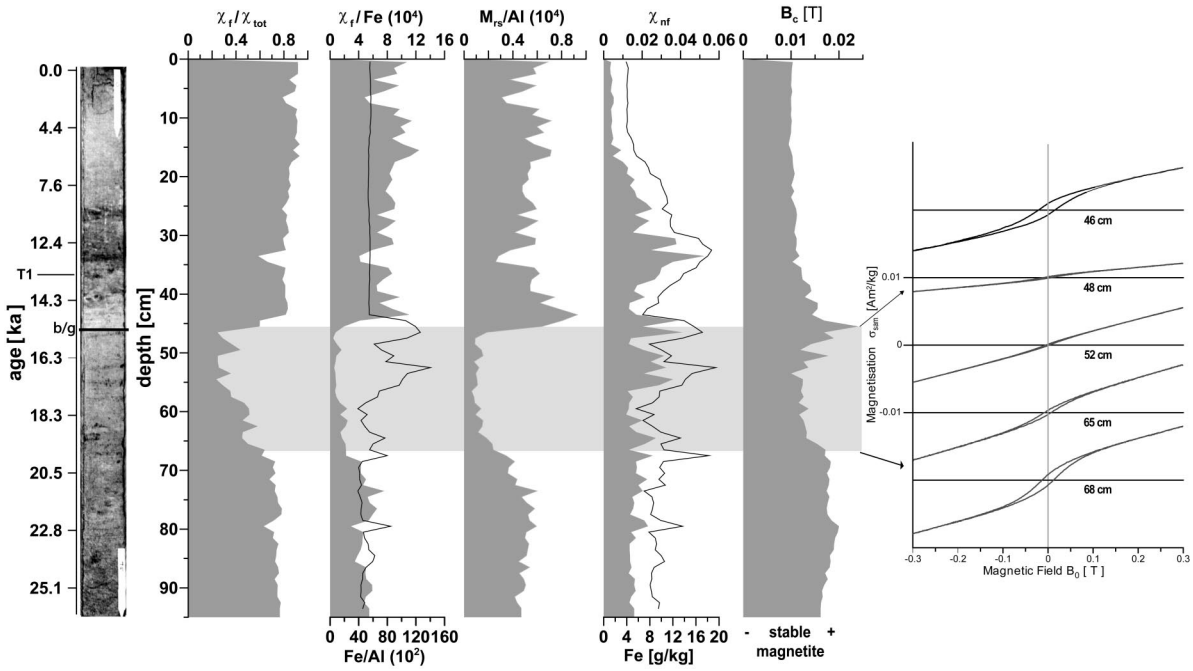

Fig. 3. Rock-magnetic and combined rock-magnetic/geochemical results of the first meter segment of gravity core GeoB 2908-7. The first three plots (χ_f/χ_{tot}, χ_f/Fe, and M_{rs}/Al) indicate diagenetic magnetic mineral dissolution. The Fe/Al ratio as an indicator for secondary iron mineral precipitation is superimposed. The χ_{nf} displays the non-ferrimagnetic susceptibility and is correlated with the concentration of total Fe. The B_c is supposed to be an indicator for the occurrence of stable magnetite. On the right hand side hysteresis loops are shown from the vicinity of the horizon of diagenetic mineral dissolution.

followed by a horizon with depleted values. The quotients of the magnetogranulometric M_{rs}/M_s (saturation remanence to saturation magnetization) and B_{cr}/B_c (remanent coercivity to coercivity) enable the quantitative characterization of the magnetite grain-size spectrum (Day et al., 1977; modified by Dunlop, 2002a,b; Fig. 4). The inscribed fields of the diagram represent (a) magnetically stable single-domain particles (SD), (b) pseudo-single-domain particles (PSD), and (c) magnetically less stable multi-domain particles (MD). The samples of this study show a distinct dominance of PSD particles (0.1 – 10 μm).

4. Discussion

4.1 Development of the redox-horizon from the last glacial to Holocene times

Productivity changes over time

The Ba/Al ratio (Fig. 2), which is considered to be an indicator paleo-productivity (e.g. Dymond et al., 1992; Gingele and Dahmke, 1994; François et al., 1995), displays relative changes in productivity over the last 26 kyr. During the glacial (from about 50 cm downward), which had its midpoint at about 21 kyr (Rühlemann et al., 1999a), productivity was relatively high. In upwelling areas like the region of the core site, productivity is about 10 times higher than in oligotrophic areas (Reading and Levell, 1996). Accordingly, the oxygen content of the

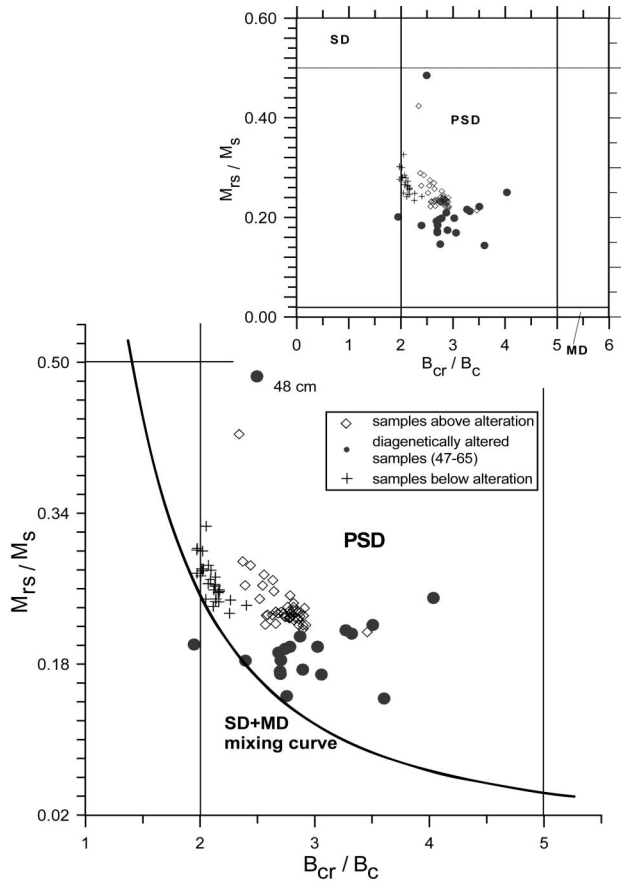

Fig. 4. Day plot representation of the quotients of M_{rs}/M_s and B_{cr}/B_c to characterize the magnetite grain size spectrum including the theoretical SD+MD mixing curve (after Dunlop 2002b). Upper right corner: Day plot including grain size spectra of SD (single domain), PSD (pseudo-single domain), and MD (multi domain). The enlarged PSD section shows more clearly that the two groups of sample points above and below the interval of diagenetically induced magnetite dissolution are paralleling the SD + MD mixing curve. Samples from the altered interval indicate coarser grain sizes and do not follow the mixing curve.

bottom water was relatively low, and thus the preservation of organic matter was increased (Verardo and McIntyre, 1994). Hence, the upper part of the broad Ba/Al ratio enrichment interfaces into the early stage of T1 starting between 19 and 16 cal. kyr. BP (Rühlemann et al., 1999a). The current asymmetry of the tropical Atlantic Ocean, with high productivity in eastern upwelling regions and oligotrophy in the westerly region, has been predominant over the last 300 kyr (Rühlemann et al., 1999b).

The depletion of Ba/Al is most obvious at the mid-point of T1 (13,5 kyr BP) and clearly indicates that the major shift to more oligotrophic conditions had already occurred by that time. According to Lototskaya (1999), T1 lasted for about 7 kyr. A re-establishment of higher productivity conditions starts at about 7 kyr BP (Fig.2). This was most likely driven by the movement of the intertropical convergence zone (ITCZ) into its recent position, which encompasses the core site at its southern flank. These observations are supported by the downcore variations of the Sr/Al ratio, indicating simultaneous variations in the $CaCO_3$ content. The obvious change in productivity (from glacial to T1) are also reflected in the distinct increase in sedimentation rate (4.3 and 2.3 cm/kyr for glacial and interglacial, respectively; Funk et al., 2004a).

Such a strong shift in the environmental conditions as observed at the transition from glacial to

T1 – probably associated with an increase of the oxygen level of the bottom water – is likely to have caused variations in the diagenetic sequence and the redox conditions in paleo-surface sediments (Wallace et al., 1988; Thomson et al., 1984, 1996). A typical observation for such an environment is a downward prograding redox front (Colley et al., 1984) developing conspicuous solid phase enrichments. Over time, the downward progression usually decelerates and finally stops as the O_2 supply becomes limited due to the increasing distance from the sediment surface (Wilson et al., 1985). In the following, the observed metal enrichments are discussed in the context of the proposed redox boundary relocation.

Mn and Fe enrichments

The maximum depth of the formerly progressing oxidation front is presumably marked by the top of the lower Fe peak (at 54 cm; Fig. 2). Most likely the oxidation front remained for a prolonged time at this position due to stable diagenetic conditions (i.e. a balance between the upward flux of reducing and downward flux of oxidizing constituents). A supplementary indicator for the depth limit of the oxidation front is the uranium enrichment, since it only forms under permanently and strongly reducing conditions (Shaw et al., 1990). The main process that leads to an uranium enrichment is the diffusion of $[UO_2(CO_3)_3]^{4-}$ from the bottom water into the sediment, followed by a reduction and precipitation as uraninite (UO_2) below the Fe-remobilization depth (Klinkhammer and Palmer, 1991; Crusius et al., 1996). Accordingly, the maximal penetration depth of the Fe^{2+}/Fe^{3+} redox boundary is indicated by the plateau-like top of the U-enrichment (Fig. 2). The upward U-tailing conversely developed during the upward trend of the oxidation front and the element-redox-boundaries, respectively. The recent position of the redox-front can be recognized by the distinct color change (at 45 cm) as described by Lyle (1983).

The zone of the upper Fe-peak (color transition) coincides with the lower limit of elevated Mn-concentrations (25-46 cm). Even though pore water data are not available at this depth, the recent to sub-recent formation of the Fe-peak can be explained by the oxidation of Fe^{2+} by MnO_2 following Eq. 1 (e.g. Burdige, 1993):

$$2Fe^{2+}_{aq} + MnO_2 + 2H_2O \rightarrow 2FeOOH + Mn^{2+}_{aq} + 2H^+ \qquad (1)$$

This hypothesis of Fe-oxidation by Mn-reduction is further supported by magnetite formation at this depth as it will be shown below. A transitory Fe^{3+} phase ($Fe(OH)_3$) is thought to form due to the reaction of Fe^{2+} with Mn-oxides (e.g. Tarduno and Wilkison, 1996). The required Fe^{2+} is most likely released in association with the degradation of organic material from underlying sedimentary units involving the reduction of Fe-oxides, as described for Mediterranean sapropel S1 (Passier et al., 1996). Diffusing upward, this Fe^{2+} will react with MnO_2, thus releasing Mn^{2+} while being immobilized as $Fe(OH)_3$. Subsequently, this Mn^{2+} is diffusing upwards, where it is typically oxidized above the oxygen penetration depth. This process has formed a Mn-enrichment zone between 25 and 46 cm. The distinct peak at 25 cm represents, however, the most dramatic change to higher productivity from T1 to the Holocene. As the oxygen penetration depth in that region is estimated to be <10 cm at present (Wenzhöfer et al., 2002), it is unlikely that the Mn-peak at 25 cm is still actively forming. Moreover, the shape of the upper 25 cm of the Mn/Al profile shows a distinct decrease towards the top (Fig. 2) indicating a continuing upward movement of the Mn-redox-boundary.

This statement can be substantiated by a simple model calculation supposing that the Fe of the lower Fe-peak is the source of Fe^{2+} that has been generated via C_{org} degradation (Fig. 2 and 5). Assuming that the major part of the upwardly diffusing Mn^{2+} has originally been oxidized at the upper Mn-peak, the amount of Fe in the upper Fe peak should be equal to twice the amount of Mn in the upper Mn peak (Eq. 1). The calculation is based on the average amount of Mn respective to Fe in the peak surface area minus the corresponding background concentration, assuming a porosity of 0.7 and a grain density of 2.65 g/cm^3. Based on an area of 1 cm^2, the total amount of Mn in the upper peak is 0.01g (188 mol) and that of Fe in the upper peak is 0.021g (376 mol)

corresponding to the assumption made. According to Fick's first law a build-up of the upper Mn-peak would last for about 6 kyr assuming a diffusion coefficient of 118.26 dm^2/yr, a δ Mn concentration of 50 µmol/dm^3 and a δ distance of 19 cm (Fig. 5).

However, it is most likely that the upper Fe peak still forms in the described way whereas the Mn-oxidation level moved upwards during the last 4 to 5 kyr due to the relocation of the oxygen penetration depth in the sediment. Since pore water data are lacking to unambiguously identify active reaction horizons, further evidence is required to substantiate the proposed development of the redox fronts. In the following we demonstrate that careful evaluation of rock-magnetic data can help to overcome this problem to a certain degree.

4.2 Characterization of diagenetic dissolution of magnetic minerals

The χ_f/χ_{tot} ratio (Fig. 3) is thought to represent the proportion of mainly ferro- (magnetite) to antiferro- (haematite/goethite) magnetic minerals. Since magnetite is the main carrier of the magnetization, the χ_f/Fe_{tot} ratio (ferrimagnetic susceptibility to total Fe) indicates potential changes in the magnetite abundance that are related to variations in the Fe-content of the sediment. The comparison of this ratio to the Fe/Al ratio provides a good way of identifying diagenetic dissolution and precipitation processes of Fe-oxides. The diagenetic destruction of the terrigenous magnetic fraction is displayed by the M_{rs}/Al (remanent saturation magnetization to aluminum; Fig. 3) ratio. The zone where major dissolution of magnetic minerals has occurred and partly still occurs extends from 47 to 66 cm indicated by the plots of χ_f/χ_{tot}, χ_f/Fe_{tot}, and M_{rs}/Al (Fig. 3). This depth interval appears also in the hysteresis loops (Fig. 3) as the diagenetically overprinted interval. The limbs of the hysteresis curve within the diagenetically overprinted interval are almost linear, which points to the absence of single domain grains. Conversely, the hysteresis loops above and below that interval affected by dissolution, are typical of single-domain magnetite (Frederichs et al., 1999).

Reductive dissolution of ferrimagnetic minerals is considered to be a grain-size selective process

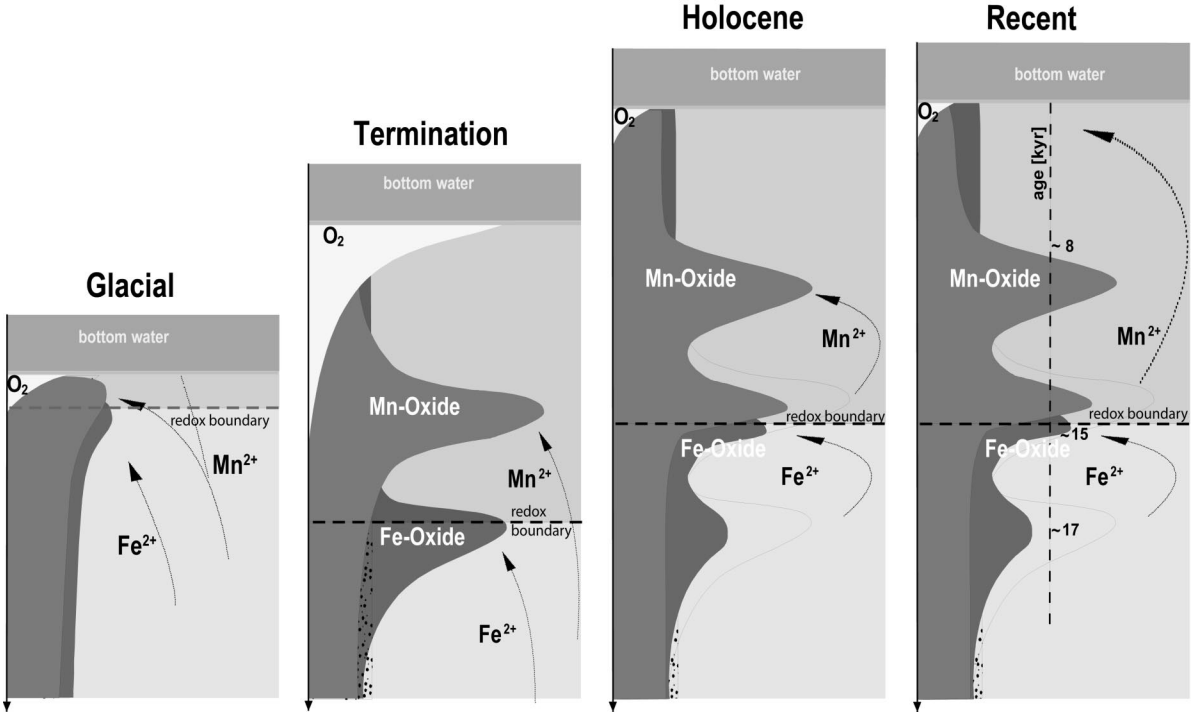

Fig. 5. Model sketch for the development of the Fe^{2+}/Fe^{3+} redox boundary movement from the glacial to the recent situation including simplified solid phase Mn, Fe and C_{org} profiles, estimated O_2 pore water penetration, and supposed Fe^{2+} and Mn^{2+} fluxes.

(Karlin et al., 1987; Robinson et al. 2000). The ultrafine (<0.1 ìm) particles have a larger specific surface area and are thus the first to be dissolved. Accordingly, there will be a shift to coarser residual grain sizes. The fine-grained material is characterized by SD and MD particles (Day et al., 1977). Dunlop (2002a,b) modified the Day plot in order to estimate grain-size trends and distinguish MD from SP (super paramagnetic) mixtures. From the PSD grain-size spectrum it is obvious that the samples from the diagenetically overprinted interval (black circles; Fig. 4) reveal coarser grain-sizes than those above and below. The latter two can be subdivided into two groups, namely (1) below the horizon of alteration with a slightly smaller PSD grain size (grey crosses) and (2) above with a mid-PDS grain size (open grey rhombs). These two groups represent a narrow size distribution of smaller grains and a parallelism with the SD+MD mixing curve introduced by Dunlop (2002b) due to magnetite associated with magnetosomes from magnetotactic bacteria. Dunlop (2002b) concluded that the Day plot is sufficient to locate the exact position of the redox boundary in the sediment column. In the present study such a precise distinction is not possible because the interval of dissolution of magnetic minerals - leaving behind magnetite with coarser grain sizes extends over about 20 cm. Consequently, it is not clear from the Day plot if the redox boundary is located at the upper or lower limit of this latter group.

In the upper zone of dissolution an enrichment of fine stable magnetite is indicated by its B_c-distribution (Fig. 3). Karlin et al. (1987) discussed the authigenesis of fine-grained magnetite crystals in close proximity to a color-boundary and the redox-transition from Fe^{2+} to Fe^{3+} in marine sediments, similar to that observed in gravity core GeoB 2908-7 at about 46 cm. This observation can be explained by the metabolic activity of Fe^{2+} oxidizing magnetotactic bacteria, which are known as nitrate reducers (Karlin et al., 1987; Rhoads et al., 1991; Robinson et al., 2000), but which might also be able to use MnO_2 as an electron acceptor. This appears to be a likely process since the geochemical data from the same depth interval show that Fe^{2+} is oxidized by MnO_2 to Fe-hydroxides. According to Tarduno and Wilkison (1996) the ephemeral ferric iron phase that is formed due to the reaction with MnO_2 can further be used in bacterial reduction producing magnetite. This also explains the existence of sample "48 cm" in the Day-diagram (Fig. 4), which in contrast to all other samples of the dissolution interval is located in the finer PSD sector and is most likely secondary magnetite.

In agreement with the geochemical evidence, these observations support the hypothesis that the restricted horizon is rather a secondary signal of early diagenesis than a primary signal of climatic change which has also been shown for the sapropel setting (e.g. Passier et al., 1998). In consideration of the anomalies of particularly χ_f/χ_{tot}, χ_f/Fe, and M_{rs}/Al it can be stated that these parameters reflect in the first instance the dissolution processes of the magnetic mineral phase which are primarily the magnetic iron-titanium-oxides supplied to the sediment by terrigenous input (Funk et al., 2004b) . The correlation of χ_{nf} and Fe (total) illustrates the subordinate part of the magnetic iron particles with respect to the total iron concentration. The fluctuations, particularly in the plots of χ_f/Fe and χ_f/χ_{tot}, near the redox-horizon correspond to "non-steady state" diagenetic conditions.

4.3 Relation between the shape of the peaks and the movement of the redox-front

The shapes of selected geochemical and rock-magnetic concentration profiles (i.e. χ_f/χ_{tot} and V/Al) can give additional information concerning the course of the proposed movement of the redox boundary. From the results so far it is obvious that the Fe^{2+}/Fe^{3+} redox front reached its relatively deepest penetration during T1 and is moving upwards at present. However, due to the significant enrichment of MnO_2 between 25-46 cm which acts as an effective long-term sink for Fe^{2+}, the upward movement of the Fe^{2+}/Fe^{3+} front is probably very slow. The abundance of MnO_2 in this horizon will thus guarantee ongoing formation of Fe-oxide enrichments which means a more permanent situation of non steady-state.

Since the upward movement of the redox front more or less overprinted the signatures of the downward movement, the latter signal is now partly

obscured. However, the V/Al and χ_f/χ_{tot} ratios are suitable to partly identify some details of the upward movement of the redox boundary related to the change from T1 to Holocene. At least three abrupt steps of the upwards movement are visible.

The V/Al ratio (Fig. 6) shows a distinct enrichment below the upper Fe-peak in the suboxic to anoxic zone. According to Shaw et al. (1990) and Hastings et al. (1996) vanadium can be enriched by in-situ reactions and under nearly anoxic conditions of the bottom water due to pentrations from the overlying water. They postulate the extraction of vanadium out of the pore water and enrichment into the sediment just below the reduction zone of Fe-oxyhydroxides. Hence, anoxic events can be identified by a distinct increase of V-accumulation. The shape of the V-peak displays the gradual upwards migration of the oxidation-front and consequently the vanadium redox boundary.

In the case of the subordinate enrichment the front may have remained for a prolonged time at that location forming a distinct vanadium peak, before moving upwards until conditions again became favorable for a V enrichment. The tailing upwards form of the curve can be viewed as an indicator for its predisposition for slightly reducing conditions. Accordingly, it was a discontinuous upward movement, which reflects the sensitivity of redox conditions during the climatic transition from T1 to the Holocene. By plotting the χ_f/χ_{tot} over the V/Al (Fig. 6) the aforementioned process becomes more obvious. The χ_f/χ_{tot} shows small peaks in between the V/Al peaks. Hence, there are still peaks of elevated magnetic susceptibility even in the zone of magnetite dissolution.

Presumably, the redox front moved down relatively rapidly. On its discontinuous, stepwise upward movement the magnetic signal was dissolved almost entirely in those horizons where the redox front remained for a prolonged time and formed a zone of V/Al enrichment. During periods of more rapid upward movement only a small part of the magnetic susceptibility was lost, as indicated by the two small peaks within the zone of dissolution.

5. CONCLUSIONS

The combination of high resolution geochemical and rock-magnetic results displays unambiguously the horizon of diagenetic overprinting in terms of the occurrence of magnetic mineral dissolution and secondary redox-sequential element enrichments (Mn, Fe, V and U). The changes in the redox-environment that lead to non-steady state diagenesis, have been the result of changing environmental conditions between the last glacial and the Holocene. A direct comparison of the shape of selected geochemical and rock-magnetic parameter-depth plots in the vicinity of the redox horizon, especially for χ_f/χ_{tot} and V/Al, has enabled us to trace the later redox-boundary relocation (from

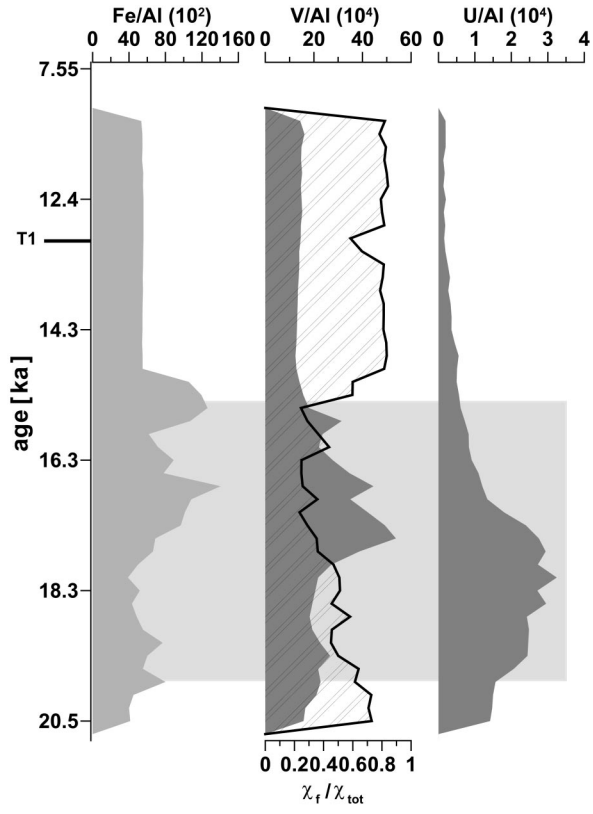

Fig. 6. Detailed geochemical and rock-magnetic solid phase profiles in the vicinity of the color change (redox boundary). Particularly V/Al and χ_f/χ_{tot} clearly trace the stepwise upward movement of the iron-redox boundary from T1 to Holocene.

T1 to Holocene) in detail.

This study has shown that a multidisciplinary high resolution analysis of diagenetically overprinted sediments is required to record the exact shape of characteristic geochemical and rock-magnetic enrichments and dissolution, respectively. By means of these records it is possible to trace the relocation of element redox boundaries. Moreover, the combination of geochemical and rock-magnetic methods appears to be a promising tool to identify and trace the processes of early diagenesis, which are particularly effective to sediments located on the boundary of high productivity areas that have been subject to climate-induced geochemical changes. On the other hand our results show, that the use of rock-magnetic parameters as a climatic indicator in sediments with strong diagenetic overprinting might be limited.

Acknowledgments – We greatly thank Mark Dekkers for extensive revision of an earlier version of the manuscript. Jan Bloemendal and an anonymous reviewer are thanked for their critical and constructive suggestions. We thank Marcus Schmidt and Anke Dreizehner for their contribution to the sample preparation. This work was founded by NWO/ALW (Aard- en Levenswetenschappen) via the project SAPS (NSG contribution No. 2004.03.02), and by Deutsche Forschungsgemeinschaft – Research Centre Ocean Margins (contribution No. RCOM0126).

References

Arthur, M.A., Dean, W.E., Stow, D.A.V., 1984. Models for the deposition of Mesozoic-Cenozoic fine-grained, organic-carbon-rich, sediment in the deep-sea. In: Stow, D.A.V., Piper, D.J.W. (Eds.), Fine-Grained Sediments: Deep-water Processes and Facies. Geol. Soc. London, Spec. Publ. 15, 527-560.

Baumann, K.-H., Henning, R., Meggers, H., 1995. Carbonate Contents. In: Schulz, H., Bleil, U., Henrich, R., Segl, M. (Eds.). Geo Bremen SOUTH ATLANTIC 1994, Cruise No. 29, 17 Juni – 5 September 1994. METEOR-Berichte, Universität Hamburg, pp. 248-252.

Berger, W.H., Herguera, J.C., Lange C.B., Schneider, R., 1994. Paleoproductivity: Flux proxies versus nutrient proxies and other problems concerning the Quaternary productivity record. In: Zahn, R., Pedersen T.F., Kaminski M.A., Labeyrie, L. (Eds.), Carbon Cycling in the Glacial Ocean: Constraints on the Ocean's Role in Global Change. NATO ASI Series 17, Springer, Berlin, Heidelberg, pp. 385-412.

Bloemendal, J., Lamb, B., King, J.W., 1988. Palaeoenvironmental implications of rock-magnetic properties of late Quaternary sediment cores from the eastern equatorial Atlantic. Paleoceanography 3, 61-87.

Bloemendal, J., King, J.W., Tauxe, L., Valet, J.P., 1989. Rock magnetic stratigraphy of Leg 108 (eastern tropical Atlantic) Sites 658, 659, 661 and 665. Proc. ODP, Sci. Results 108, 415-428.

Bloemendal, J., King, J.W., Hall, F.R., Doh, S.-J., 1992. Rock magnetism of late Neogene and Pleistocene deep-sea sediments: relationship to sediment source, diagenetic processes, and sediment lithology. J. Geophys. Res. 97, 4361-4375.

Brown, E.T., Callonnec, L.L., German, C.R., 2000. Geochemical cycling of redox-sensitive metals in sediments from Lake Malawi: A diagnostic paleotracer for episodic changes in mixing depth. Geochim. Cosmochim. Acta 64, 3515-3523.

Burdige, D.J., 1993. The biogeochemistry of Mn and Fe reduction in marine sediments. Earth Sci. Rev. 35, 249-284.

Calvert, S.E., Pedersen, T.F., 1993. Geochemistry of Recent oxic and anoxic marine sediments: Implications for the geological record. Mar. Geol. 113: 67-88.

Colley, S., Thomson J., Wilson, T.R.S., Higgs, N.C., 1984. Post-depositional migration of elements during diagenesis in brown clay and turbidite sequences in the North East Atlantic. Geochem. Cosmochim.

Acta 48, 1223-1235.

Crusius, J., Calvert, S., Pedersen, T., Sage, D., 1996. Rhenium and molybdenum enrichments in sediments as indicators of oxic, suboxic and sulfidic conditions of deposition. Earth. Planet. Sci. Lett. 145, 65-78.

Curtis, C., 1983. Microorganisms and diagenesis of sediments. In: Krumbein, W.E. (Ed.), Microbial Geochemistry. Blackwell, Oxford, pp. 263-286.

Day, R., Fuller, M., Schmidt, V.A., 1977. Hysteresis Properties of Titanomagnetites: Grain-Size and Compositional Dependence. Physics of the Earth and Planetary Interiors 13, 260-267.

de Lange, G.J., Middelburg, J.J., Pruysers, P.A., 1989. Discussion: Middle and Late Quaternary depositional sequences and cycles in the Eastern Mediterranean. Sedimentology 36, 151-158.

Dunlop, D.J., 2002a. Theory and application of the Day plot (M_{rs}/M_s versus H_{cr}/H_c) 1. Theoretical curves and tests using titanomagnetite data. J. Geophys. Res. 107, 10.1029/2001JB000486.

Dunlop, D.J., 2002b. Theory and application of the Day plot (M_{rs}/M_s versus H_{cr}/H_c) 2. Application to data for rocks, sediments, and soils. J. Geophys. Res. 107, 10.1029/2001JB000487.

Dymond, J., Suess, E., Lyle, M., 1992. Barium in deep-sea sediments: a geochemical proxy for paleoproductivity. Paleoceanography 7, 163-181.

Emerson, S., Hedges, J.I., 1988. Processes controlling the organic carbon content of open ocean sediments. Paleoceanography 3, 621-634.

Fischer, G., Wefer. G. (Eds.), 1999. Use of Proxis in Paleoceanography: Examples from the South Atlantic. Springer-Verlag, Berlin, Heidelberg, 735 pp.

François, R., Honjo, S., Manganini, S.J., Ravizza, G.E., 1995. Biogenic barium fluxes to the deep sea: implications for paleoproductivity reconstruction. Global Biogeochem. Cycles 9, 289-303.

Frederichs, T., Bleil, U., Däumler, K., von Dobeneck, T., Schmidt, A.M., 1999. The Magnetic View on the Marine Paleoenvironment: Parameters, Techniques and Potentials of Rock Magnetic Studies as a Key to Paleoclimatic and Paleoceanographic Changes. In: Fischer, G., Wefer, G. (Eds.), Use of Proxies in Paleoceanography: Examples from the South Atlantic. Springer-Verlag, Berlin, Heidelberg, pp. 575-599.

Froelich, P.N., Klinkhammer, G.P., Bender, M.L., Luedtke, N.A., Heath, G.R., Cullen, D., Dauphin, P., Hammond, D., Hartman, B., Maynard, V., 1979. Early oxidation of organic matter in pelagic sediments of the eastern equatorial Atlantic: suboxic diagenesis. Geochim. Cosmochim. Acta 43, 1075-1090.

Funk, J.A., von Dobeneck, T., Wagner, T., Kasten, S., 2004a. Late Quaternary Sedimentation and Early Diagenesis in the Equatorial Atlantic Ocean: Patterns, Trends and Processes Deduced from Rock Magnetic and Geochemical Records. In: Wefer, G., Mulitza, S., Ratmeyer, V. (Eds.), The South Atlantic in the Late Quaternary: Reconstruction of Material Budget and Current Systems. Springer-Verlag, Berlin, pp 461-497.

Funk, J.A., von Dobeneck, T., Reitz, A., 2004b. Integrated Rock Magnetic and Geochemical Quantification of Redoxomorphic Iron Mineral Diagenesis in Late Quaternary Sediments from the Equatorial Atlantic. In: Wefer, G., Mulitza, S., Ratmeyer, V. (Eds.), The South Atlantic in the Late Quaternary: Reconstruction of Material Budget and Current Systems. Springer-Verlag, Berlin, pp 237-260.

Gingele, F., Dahmke A., 1994. Discrete barite particles and barium as tracers of paleoproductivity in South Atlantic sediments. Paleoceanography 9, 151-168.

Gladney, E.S., Roelandts, I., 1988. 1987 compilation of elemental concentration data for USGS BHVO-1, MAG-1, QLO-1, RGM-1, SCO-1, SDC-1, SGR-1 and STM-1. Geostandards Newsletters 12, 253-362.

Hastings, D., Emerson, S., Mix, A., 1996. Vanadium in foraminiferal calcite as a tracer for changes in the areal extent of reducing sediments. Paleoceanography 11, 665-678.

Imbrie, J., Palmer Imbrie, K., 1998. Ice Ages: Solving the Mystery. Seventh printing. Harvard University Press, Cambridge Massachusetts London, 224 pp.

Karlin, R., Lyle, M., Heath, G.R., 1987. Authigenic magnetite formation in suboxic marine sediments. Nature 326, 490-493.

Klinkhammer, G.P., Palmer, M.R., 1991. Uranium in the oceans: where it goes and why. Geochim. Cosmochim. Acta 55, 1799-1806.

König, I., Drodt, M., Suess, E., Trautwein, A.X., 1997. Iron reduction through the tan-green color transition in deep-sea sediments. Geochim. Cosmochim. Acta, 61, 1679-1683.

König, I., Haeckel, M., Drodt, M., Suess, E., Trautwein, A.X., 1999. Reactive Fe(II) layers in deep-sea sediments. Geochim. Cosmochim. Acta 63: 1517-1526.

Lototskaya, A.A., 1999. Mid-latitude North Atlantic climate between 150,000 and 100,000 years BP. Amsterdam University, PhD thesis, 171 pp.

Lyle, M., 1983. The brown-green colour transition in marine sediments: a marker for the Fe(III)-Fe(II) redox boundary. Limnol. Oceanogr. 28, 1026-1033.

Mangini, A., Jung, M., Laukenmann, S., 2001. What do we learn from peaks of uranium and of manganese in deep sea sediments? In: Kasten, S. and Hensen,

C. (Eds.), Mar. Geol. 177, 63-78.

Mercier, H., Speer, K.G., Honnorez, J., 1994. Flow pathways of bottom water through the Romanche and Chain Fracture Zones. Deep-Sea Res. I 41, 1457-1477.

Passier, H.F., Middelburg, J.J., van Os, B.J.H., de Lange, G.J., 1996. Diagenetic pyritisation under eastern Mediterranean sapropels caused by downward sulphide diffusion. Geochim. Cosmochim. Acta 60, 751-763.

Passier, H.F., Dekkers, M.J., de Lange, G.J., 1998. Sediment chemistry and magnetic properties in an anomalously reducing core from the eastern Mediterranean Sea. Chem. Geol. 152, 287-306.

Prahl, F.G., de Lange, G.J., Lyle, M., Sparrow, M.A., 1989. Post-depositional stability of long-chain alkenones under oxic and suboxic conditions. Nature 341, 434-437.

Raymo, M.E., 1997. The timing of major climate terminations. Paleoceanography 12, 577-585.

Reading, H.G., Levell, B.K., 1996. Controls on the sedimentary rock record. In: Reading, H.G. (Ed.), Sedimentary Environments: Processes, Facies and Stratigraphy. Third edition. Blackwell Science, Oxford, London, pp. 5-36.

Rhoads, D.C., Mulsow, S.G., Gutschick, R., Baldwin, C.T., Stolz, J.F., 1991. The dysaerobic zone revisited: a magnetic facies? In: Tyson, R.V., Pearson, T.H. (Eds.), Modern and Ancient Continental Shelf Anoxia. Geol. Soc. London, Spec. Publ. 58, 187-199.

Robinson, S.G., Sahota, J.T.S., Oldfield, F., 2000. Early diagenesis in North Atlantic abyssal plain sediments characterized by rock-magnetic and geochemical indices. Mar. Geol. 163, 77-107.

Rühlemann, C., Mulitza, S., Müller, P.J., Wefer, G., Zahn, R., 1999a. Warming of the tropical Atlantic Ocean and slowdown of thermohaline circulation during the last deglaciation. Nature 402, 511-514.

Rühlemann, C., Müller, P.J., Schneider, R.R., 1999b. Organic Carbon and Carbonate as Paleoproductivity Proxies: Examples from High and Low Productivity Areas of the Tropical Atlantic. In: Fischer, G., Wefer. G. (Eds.), Use of Proxies in Paleoceanography: Examples from the South Atlantic. Springer-Verlag, Berlin, Heidelberg, pp. 315-344.

Sarnthein, M., Tetzlaff, G., Koopmann, B., Wolter, K., Pflaumann, U., 1981. Glacial and interglacial wind regimes over the eastern subtropical Atlantic and North-West Africa. Nature 293, 193-196.

Shaw, T.J., Gieskes, J.M., Jahnke, R.A., 1990. Early diagenesis in differing depositional environments: The response of transition metals in porewater. Geochim. Cosmochim. Acta 54, 1233-1246.

Tarduno, J.A., Wilkison, S.L., 1996. Non-steady state magnetic mineral reduction, chemical lock-in, and delayed remanence acquisition in pelagic sediments. Earth Planet. Sci. Lett. 144, 315-326.

Thomson, J., Wilson, T.R.S., Culkin, F., Hydes, D.J., 1984. Non-steady state diagenetic record in eastern equatorial Atlantic sediments. Earth Planet. Sci. Lett. 71, 23-30.

Thomson, J., Higgs, N.C., Croudace, I.W., Colley, S., Hydes, D.J., 1993. Redox zonation of elements at an oxic / post-oxic boundary in deep-sea sediments. Geochim. Cosmochim. Acta 57, 579-595.

Thomson, J., Higgs, N.C., Clayton, T., 1995. A geochemical criterion for the recognition of Heinrich events and estimations of their depositional fluxes by the $(^{230}Th_{excess})_0$ profiling method. Earth Planet. Sci. Lett. 135, 41-56.

Thomson, J., Higgs, N.C., Colley, S., 1996. Diagenetic redistributions of redox-sensitive elements in northeast Atlantic glacial/interglacial transition sediments. Earth Planet. Sci. Lett. 139, 365-377.

Thomson, J., Jarvis, I., Green, D.R.H., Green, D.A., Clayton, T., 1998. Mobility and immobility of redox-sensitive elements in deep-sea turbidites during shallow burial. Geochim. Cosmochim. Acta 62, 643-656.

Tyson, R.V., Pearson, T.H., 1991. Modern and ancient continental shelf anoxia: an overview. In: Tyson, R.V., Pearson, T.H. (Ed.), Modern and Ancient Continental Shelf Anoxia. Geol. Soc. London, Spec. Publ. 58, 1-24.

van Hoof, A.A.M., van Os, B.J.H., Rademakers, J.G., Langereis, C.G., de Lange, G.J., 1993. A paleomagnetic and geochemical record of the upper Cochiti reversal and two subsequent precessional cycles from Southern Sicily (Italy). Earth Planet. Sci. Lett. 117, 235-250.

van Santvoort, P.J.M., de Lange, G.J., Thomson, J., Cussen, H., Wilson, T.R.S., Krom, M.D., Ströhle, K., 1996. Active post-depositional oxidation of the most recent sapropel (S1) in sediments of the eastern Mediterranean Sea. Geochim. Cosmochim. Acta 60 (21), 4007-4027.

Verardo, D.J., McIntyre, A., 1994. Production and destruction: control of biogenous sedimentation in the tropical Atlantic 0-300,000 years B.P. Paleoceanography 9, 63-86.

von Dobeneck, T., 1996. A systematic analysis of natural magnetic mineral assemblages based on modelling

hysteresis loops with coercivity-related hyperbolic basis functions. Geophys. J. Int. 124, 675-694.

Wagner, T., Klemd, R., 1995. Core Descriptions and Smears Slide Analysis. In: Schulz, H., Bleil, U., Henrich, R., Segl, M. (Eds.), Geo Bremen SOUTH ATLANTIC 1994, Cruise No. 29, 17 Juni – 5 September 1994. METEOR-Berichte, Universität Hamburg, pp. 233-248.

Wagner, T., 1999. Petrology of organic matter in modern and late Quaternary deposits of the Equatorial Atlantic: climatic and oceanographic links. Int. J. of Coal Geology 39, 155-184.

Wallace, H.E., Thomson, J., Wilson, T.R.S., Weaver, P.P.E., Higgs, N.C., Hydes, D.J., 1988. Active diagenetic formation of metal-rich layers in N. E. Atlantic sediments. Geochim. Cosmochim. Acta 52, 1557-1569.

Wenzhöfer, F., Glud, R.N., 2002. Benthic carbon mineralization in the Atlantic: a synthesis based on in situ data from the last decade. Deep-Sea Res. I 49, 1255-1279.

Wilson, T.R.S., Thomson, J., Colley, S., Hydes, D.J., Higgs, N.C., Sørensen, J., 1985. Early organic diagenesis: The significance of progressive subsurface oxidation fronts in pelagic sediments. Geochim. Cosmochim. Acta 49, 811-822.

Summary and perspectives

This study is a substantial contribution to the interpretation of the marine sedimentary record and to the reconstruction of Late Quaternary material budgets and current systems. It delineates the high potential of rock magnetic properties for understanding the marine geochemical cycles of iron and carbon. Responding very susceptible to diagenetic processes the techniques of 'Environmental Magnetism' are powerful tools in developing new proxy parameters for diagenetically induced alterations in marine sedimentary deposits. In this context the multidisciplinary approach of combining rock magnetics with geochemical analytical methods is an important aspect because it provides unique information. Both disciplines make use of logging techniques which excellently complete one another and which enable the fast recording of the required data sets.

Beside the technical progress in analytics this approach provides new insights in paleoceanography and helps to reveal biases or overprints on the primary signal. Thus a stratigraphic network of the Late Quaternary Equatorial Atlantic could be established and new information about the regional distribution of the diagenetic alterations under investigation were achieved. The strategy for combining proxies allowed derivation of new indices which stand in for magnetite depletion, precipitation and iron relocation. For example the ratio of the iron concentration and the magnetic susceptibility, both detected by logging techniques, display magnetite dissolution in a quick and easy manner. Furthermore it exemplifies how multiproxy studies and scanning techniques represent very successful tools for developing new fields in marine geology.

The results identify sediment sequences deposited during cold climates and during transitions from glacial to interglacial conditions as by far the most diagenetically affected. This confirms the significance of these time periods with regard to drastic changes in oceanographic, climatic and depositional conditions. Primary productivity during the glacial intervals must have been a manyfold of what is called 'enhanced productivity' in the modern central Equatorial Atlantic. Significantly more organic carbon was pumped down into the deep ocean during glaciations than today, leaving surface waters with reduced CO_2 levels in comparison with the present. More fine scale events of post depositional alterations during interglacials are also detected by the high resolution records. These horizons are not paralleled by higher concentrations of preserved organic carbon. Possibly rock magnetic parameters may be used in further research as tracers which allow to reconstruct small suboxic or anoxic events in the sediment resulting from short-termed productivity pulses not preserved in organic carbon records. Early diagenesis may not only overprint the pristine sedimentary signal, but can also provide valuable information on kind and origin of the changing processes which in turn are related to climate changes. The study confirms that nearly all proxy parameters are influenced by post depositional alterations and elucidates the need for a better understanding of these processes.

Acknowledgements

I thank Professor Dr. Ulrich Bleil for supervising and supporting my Ph.D. thesis. Also Professor Dr. Tilo von Dobeneck was very helpful and had a lot of good advice. Their arguments and constructive criticism have greatly improved my work, my talks, my posters and the manuscripts. I have to mention Dr. Frank Schmieder who spent several years with me in our office, there is nothing more to say about that. A perpetually perfect running magnetic lab was enabled by Christian Hilgenfeldt and Thomas Frederichs. Also Andreas Steinbach, Liane Brück and Heike Piero were very helpful.

Many thanks to Dr. Sabine Kasten, Dr. Martin Kölling, Dipl.-Geol. Anja Reitz and Dr. Thomas Wagner for many fruitful discussions, valuable information and true interdisciplinary cooperation. I thank Dr. Ulla Röhl for XRF instructions and Alexius Wülbers and Walter Hale from the ODP core repository for a very friendly and helpful support during my weeks in the XRF container. I also thank Prof. Dr. Olaf Brockamp, Dr. Michael Zuther and Mr. Stefan Sopke for good advice on sample preparation of powder tablets and their support in the XRF lab. Sincere thanks are given to PD Dr. Matthias Zabel for his second opinion. Many other people of the Geosciences Department and last but not least Babette and Lennart supported me during my work.

I participated in four Meteor cruises, accordingly I have to thank officers and crews for professional help and support.

This study was funded by the German Science Foundation in the framework of the special research collaboration 261 and Graduiertenkolleg 221 at the University of Bremen.